Universität Bremen

Institut für Theoretische Physik
Electronic Structure and Correlated Nanosystems

Master's thesis

On the scope of McMillan's formula

Über den Geltungsbereich der McMillan-Formel

submitted by Jan Berges

1st supervisor Prof. Dr. Tim Wehling
2nd supervisor Prof. Dr. Gerd Czycholl

October 10, 2016

Last revised on November 23, 2022

Typeset in Iwona and Inconsolata

Contents

Chapter 1

Introduction

Ever since McMillan's formula has been published in 1968 [1], it has been widely used[1] to obtain estimates of the critical temperature of superconductors as a function of three effective material parameters, namely an average phonon frequency $\langle\omega\rangle$, the electron-phonon coupling strength λ and the Coulomb pseudo-potential μ^*, which can be extracted from experiment [3] or first-principles calculations. It constitutes an approximation to the more general Eliashberg theory of superconductivity [4] from which it was derived by fitting analytic approximations of the underlying equations to exact numerical results. Although for the latter the special phononic density of states of niobium has been assumed, which was simply at hand at that time [5], the validity of the resulting formula turned out to be much more general.

The aim of the present work is to trace the steps that lead from the theory of the fundamental interactions between electrons and phonons to the handy formula for the critical temperature and to perform further tests on its scope, many of them, supposedly, have already been carried out somewhere in its past of almost half a century and fallen into oblivion or, more probably, just overlooked this time. Special attention is paid to potential discrepancies emerging from exceptional densities of electronic states and the question if and possibly how the multi-band case with non-scalar coupling strengths can be brought into accordance. Notwithstanding that in the course of the investigations no references to specific materials are made but rather simple models applied, it is intended that the results be of use for the understanding of novel, especially two-dimensional materials.

For this purpose, an appropriate software is developed which may be used not only to obtain electronic self-energies on the imaginary or real frequency axis as solutions of the multi-band Eliashberg equations or analytically continued by means of Padé approximants [6], respectively, but also to solve the linearized critical-state equations for a parameter of choice, which may be either the critical temperature itself, the phonon frequency or any element of the matrices defining the coupling strengths, for the respective other quantities fixed.

To make a start, the following Chapter 2 gives a very brief introduction to the field of superconductivity, including an outline of its early history and the presentation of the prominent BCS theory [7; 8]. Before this subject can be discussed in more detail, it is necessary to extend the theoretical framework by introducing the fundamental concepts of many-body physics such as Green functions and diagrammatical perturbation theory, which will be done in Chapter 3. On this basis, the different formulations and special cases of the Eliashberg theory of superconductivity are dealt with in Chapter 4, which completes the preparative part of the thesis. Subsequently, the actual numerical results are demonstrated in Chapters 5 and 6 which are dedicated to the results for single- and muli-band systems, respectively, where *band* stands in place for any chosen subset of electronic states. Finally, in Chapter. 7 the most important results are summarized and the pending questions brought up for future discussions. A good deal of the work falls within the scope of Appendix B where, following a short formulary on Fourier analysis in Appendix A, the source code of the employed programs is exposed and commented, supplemented with a short user manual.

[1] Today, the American Physical Society alone lists 3203 references to the original paper by McMillan, to be complemented by 1326 citations of a closely related publication by Allen and Dynes [2].

Chapter 2

Superconductivity

This chapter gives an introduction to the field of superconductivity and is not at all intended to be exhaustive. The theory that will actually be applied in this work is presented in the following two chapters.

In the first section the earlier history of superconductivity is briefly reviewed, loosely following a presentation by Fröhlich [9]. Next, a canonical transformation introduced by the latter is performed, which reveals that the interaction between electrons and phonons can lead to an effective attraction between electrons and consequently to the formation of Cooper pairs. Finally, the corresponding microscopic theory of superconductivity by Bardeen, Cooper and Schrieffer is presented.[1]

Throughout this work units are chosen in which the Boltzmann and the reduced Planck constant are unity, i.e. $k_B = \hbar = 1$. Consequently, the same dimension is attributed to energy and both temperature and frequency.

2.1 Early history of superconductivity

In 1911 the dutch physicist Kamerlingh Onnes finds that mercury ceases to resist electric current completely when cooled down below a critical temperature of about 4 K with the help of liquid helium.[2] This is the first time a manifestation of superconductivity is observed. In the years that follow, similar observations are made for other metals and the fundamental properties of the novel state exposed.

The misconception of superconductors which obey Ohm's law is overcome in 1933, when Meissner and Ochsenfeld find them to be perfect diamagnets [13]: Up to a critical strength an external magnetic field is expelled from a superconductor – even if it was already there *before* the critical temperature has been undercut. On the basis of this observation the London brothers formulate a first macroscopic theory of superconductivity in 1935 [14].

However, not only have the characteristics of a phase transition been left out of consideration, but also the underlying physical mechanisms remain unclear. Some of the further are addressed by the phenomenological theory of Ginzburg and Landau published in 1950 [15], which introduces an order parameter for the superconducting state.

An important hint towards the right direction is the discovery of the isotope effect by Maxwell [16] and Reynolds et al. [17] in the same year: The critical temperature depends on the nuclear mass just as the phononic behavior. At that time, Fröhlich starts to successfully use field-theoretical methods to describe the interaction between electrons and phonons, which is gradually accepted as causing superconductivity. In 1952, his electron-phonon Hamilton operator is established and mapped onto an effective interaction between electrons which turns out to be attractive [18].

[1] Both derivations in this chapter are guided by Czycholl [10].

[2] According to Ref. 11, on April 8, 1911 Kamerlingh Onnes writes *"Kwik nagenoeg nul"* in his notebook, which means *"[resistance of] mercury near enough zero"*. In Communication No. 122b from the Physical Laboratory at Leiden he states more precisely: *"At* 3 °K *[sic], the resistance was found to have fallen below [...] one ten-millionth of the value which it would have at* 0 °C*"* [12].

It is not until 1957 that on this basis the first microscopic theory of superconductivity is formulated by Bardeen, Cooper and Schrieffer [7; 8]. The principal idea is the formation of a condensate of Cooper pairs which opens up an energy gap at the Fermi level the width of which assumes the role of the order parameter.

Since the modeled interaction in the BCS theory is instantaneous as opposed to the underlying electron-phonon interaction which is retarded, discrepancies between theory and experiment emerge, especially when the coupling is strong. In 1960, Eliashberg establishes a theory which accounts for this retarded nature of the interaction [4].

2.2 Canonical transformation

It is now shown that the electron-phonon interaction can involve an effective electron-electron interaction which is attractive [18]. To that end the *Fröhlich-Hamilton operator*

$$H = \overbrace{\sum_k \varepsilon_k c_k^+ c_k + \sum_q \omega_q b_q^+ b_q}^{H_0} + \overbrace{\sum_{kq} g_q c_{k+q}^+ c_k [b_q + b_{-q}^+]}^{V}$$

is considered, which describes the interaction between electrons with wave number $\boldsymbol{k}$ and energy ε_k, which are annihilated and created by the Fermi operator c_k and its adjoint, respectively, and longitudinal phonons, where analogous definitions hold for $\boldsymbol{q}$, ω_q and b_q. The strength of the coupling is given by g_q. The spin is of no importance here and thus omitted.

The idea is to apply a canonical transformation to the Hamilton operator by means of the unitary operator e^{iS}, where S is self-adjoint. Expanding the exponential functions,

$$\begin{aligned} H_T = e^{-iS} H e^{iS} &= H + i[H,S] - \frac{1}{2}[[H,S],S] + \dots \\ &= H_0 + V + i[H_0,S] + i[V,S] - \frac{1}{2}[[H_0,S],S] + \dots \\ &\approx H_0 + \frac{i}{2}[V,S] \equiv H_0 + V_T, \end{aligned}$$

where $[H_0, S] = iV$ has been chosen, which implies a linear dependence of S on V. Thus all terms which are at least quadratic in the interaction are neglected. Using the commutators

$$\begin{aligned} \left[b_{q'}^+ b_{q'},\ b_q\ \right] &= -b_q\ \delta_{q'}^q, & \left[c_{k'}^+\ \ c_{k'},\ c_{k+q}^+ c_k\right] &= c_{k+q}^+ c_k \left[\delta_{k'}^{k+q} - \delta_{k'}^k\right], \\ \left[b_{q'}^+ b_{q'},\ b_{-q}^+\right] &= \ \ b_{-q}^+ \delta_{q'}^{-q}, & \left[c_{k'+q'}^+ c_{k'},\ c_{k+q}^+ c_k\right] &= c_{k+q+q'}^+ c_k \delta_{k'}^{k+q} - c_{k+q}^+ c_{k-q'} \delta_{k'}^{k-q'}, \end{aligned}$$

one can verify both that S has the explicit form

$$S = i \sum_{kq} g_q c_{k+q}^+ c_k \left[\frac{b_q}{\varepsilon_{k+q} - \varepsilon_k - \omega_q} + \frac{b_{-q}^+}{\varepsilon_{k+q} - \varepsilon_k + \omega_{-q}} \right]$$

and, assuming $g_q^* = g_{-q}$ and $\omega_q = \omega_{-q}$, that the renormalized interaction is given by

$$\begin{aligned} V_T = &\sum_{kk'q} \frac{|g_q|^2 \omega_q}{(\varepsilon_{k+q} - \varepsilon_k)^2 - \omega_q^2} c_{k+q}^+ c_k c_{k'-q}^+ c_{k'} + \cdots \\ \cdots &- \frac{1}{2} \sum_{kqq'} g_q g_{q'} \left[c_{k+q+q'}^+ c_k - c_{k+q}^+ c_{k-q'}\right] \left[b_{q'} + b_{-q'}^+\right] \left[\frac{b_q}{\varepsilon_{k+q} - \varepsilon_k - \omega_q} + \frac{b_{-q}^+}{\varepsilon_{k+q} - \varepsilon_k + \omega_{-q}} \right]. \end{aligned}$$

The first term describes an effective interaction between electrons which is attractive, i.e. negative, for $|\varepsilon_{k+q} - \varepsilon_k| < \omega_q$. The seconds term describes processes involving two phonons and is disregarded in the following.

Since the energy transfer associated with the attractive interaction is small, only electrons near the Fermi surface are affected, where both free and occupied states are available. Taking

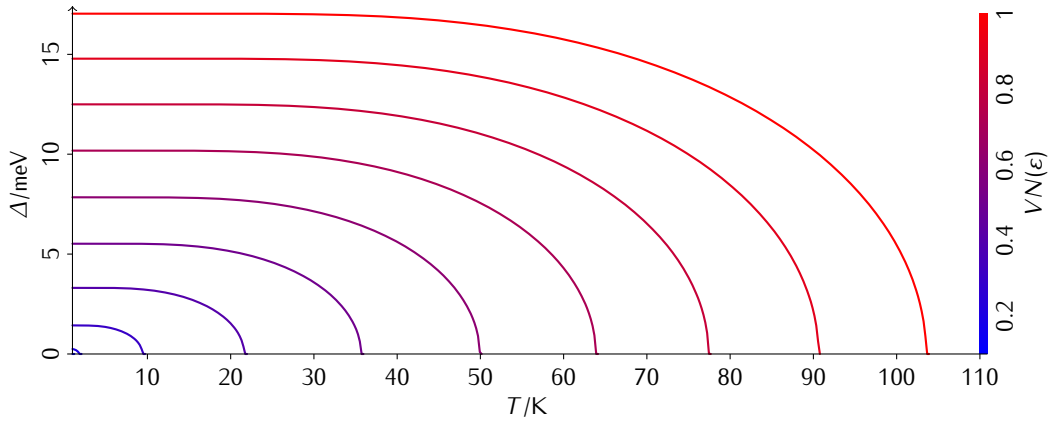

Figure 2.1: Temperature dependence of the BCS gap for different values of the coupling strength $VN(\varepsilon)$. The Debye frequency is assumed to be 20 meV.

further the conservation of momentum into account, the possible momentum transfers are very limited except for the case when the total momentum vanishes. As a consequence, an electron is most susceptible for being effectively attracted to its time-revered counterpart, which has both opposite momentum and spin, whereby the latter prevents local interactions from vanishing. The crucial idea which led to the understanding of superconductivity is that such electrons form so-called *Cooper pairs*, bound by the attractive interaction.

2.3 BCS theory

In 1957, Bardeen, Cooper and Schrieffer developed, on the basis of the results presented in the previous section, a model Hamilton operator to describe superconductivity [7; 8]. It is reduced to the essential, namely an attractive interaction of uniform strength V between electrons which form a Cooper pair and are no further away from the Fermi surface than a typical phonon frequency, typically Debye's ω_D. Since the total momentum of a Cooper pair is zero, the internal momentum transfer corresponds to a rotation in $\boldsymbol{k}$-space. The model reads

$$\mathrm{H} = \sum_{k\sigma} \varepsilon_k \mathrm{n}_{k\sigma} - \sum_{kk'} V_{kk'} \mathrm{C}^+_{k'} \mathrm{C}_k \quad \text{with} \quad \mathrm{n}_{k\sigma} = \mathrm{c}^+_{k\sigma} \mathrm{c}_{k\sigma}.$$

$\mathrm{C}_k = \mathrm{c}_{-k\downarrow} \mathrm{c}_{k\uparrow}$ is a Cooper-pair annihilator, which does *not* satisfy Bose commutation relations:

$$[\mathrm{C}_k, \mathrm{C}^+_{k'}] = (1 - \mathrm{n}_{k\uparrow} - \mathrm{n}_{-k\downarrow}) \delta_{kk'}.$$

Measuring energies relative to the Fermi level, the interaction strength is given by

$$V_{kk'} = \begin{cases} V & \text{if } |\varepsilon_k| < \omega_\mathrm{D} \text{ and } |\varepsilon_{k'}| < \omega_\mathrm{D}, \\ 0 & \text{otherwise.} \end{cases}$$

In order to promote the solution of the Hamilton operator, the interaction term is usually factorized into anomalous expectation values. Hence, in the exact identity [19, Eq. 4.20]

$$\mathrm{C}^+_{k'} \mathrm{C}_k = (\mathrm{C}^+_{k'} - \langle \mathrm{C}^+_{k'} \rangle)(\mathrm{C}_k - \langle \mathrm{C}_k \rangle) + \langle \mathrm{C}^+_{k'} \rangle \mathrm{C}_k + \langle \mathrm{C}_k \rangle \mathrm{C}^+_{k'} - \langle \mathrm{C}^+_{k'} \rangle \langle \mathrm{C}_k \rangle$$

leading and trailing summands, which represent fluctuations of the Cooper pair operators and a constant energy shift, respectively, are neglected from now on. The averages of either two creation or annihilation operator do not vanish, as one might expect, because the Hamilton operator with respect to which they are evaluated no longer conserves the particle number:

$$\mathrm{H} = \sum_{k\sigma} \varepsilon_k \mathrm{n}_{k\sigma} - \sum_k \Delta_k [\mathrm{C}_k + \mathrm{C}^+_k] \quad \text{with} \quad \Delta_k = \sum_{k'} V_{kk'} \langle \mathrm{C}_{k'} \rangle. \tag{2.1}$$

A self-consistently problem has emerged. Δ_k will turn out to be a suitable order parameter for the superconducting state. Being not interested in its phase, which would be important to describe e.g. tunneling effects, it is assumed to be real.

At this point, the HAMILTON operator is still not diagonal. This may be accomplished with the help of the *BOGOLIUBOV quasi-particles* [20, p. 42],

$$\begin{aligned} \alpha_k &= u_k c_{k\uparrow} - v_k c^+_{-k\downarrow}, & c_{k\uparrow} &= u_k \alpha_k + v_k \beta^+_k, \\ \beta_k &= u_k c_{-k\downarrow} + v_k c^+_{k\uparrow}, & c_{-k\downarrow} &= u_k \beta_k - v_k \alpha^+_k, \end{aligned}$$

where the coefficients u_k and v_k may also chosen to be real. It is desirable that the new operators obey FERMI commutation relations. Except with their own adjoints they already anti-commute so that the only further requirement is

$$\{\alpha_k, \alpha^+_k\} = \{\beta_k, \beta^+_k\} = u_k^2 + v_k^2 \equiv 1.$$

A choice of u_k and v_k which both satisfies the above relation and diagonalizes the HAMILTON operator is given by [20, Eq. 7]

$$\left\{ \begin{matrix} u_k^2 \\ v_k^2 \end{matrix} \right\} = \frac{1}{2}\left[1 \pm \frac{\varepsilon_k}{E_k}\right] \quad \text{with} \quad E_k = \sqrt{\varepsilon_k^2 + \Delta_k^2},$$

where braces enclose alternatives. Therewith, the free and interacting parts are found to be

$$\begin{aligned} \sum_{k\sigma} \varepsilon_k n_{k\sigma} &= \sum_k \left[\frac{\varepsilon_k^2}{E_k}(\alpha^+_k \alpha_k + \beta^+_k \beta_k - 1) + \frac{\Delta_k \varepsilon_k}{E_k}(\alpha^+_k \beta^+_k + \beta_k \alpha_k) + \varepsilon_k \right], \\ -\sum_k \Delta_k [C_k + C^+_k] &= \sum_k \left[\frac{\Delta_k^2}{E_k}(\alpha^+_k \alpha_k + \beta^+_k \beta_k - 1) - \frac{\Delta_k \varepsilon_k}{E_k}(\alpha^+_k \beta^+_k + \beta_k \alpha_k) \right], \end{aligned}$$

of which constants will again be neglected. Altogether, the diagonal HAMILTON operator reads

$$H = \sum_k E_k (\alpha^+_k \alpha_k + \beta^+_k \beta_k).$$

This identifies E_k as the new single-particle energy and Δ_k as half of a band gap which has opened up in the spectrum. The latter remains to be determined self-consistently:

$$\begin{aligned} \Delta_k &= \sum_{k'} V_{kk'} [u^2_{k'} \langle \beta_{k'} \alpha_{k'} \rangle - v^2_{k'} \langle \alpha^+_{k'} \beta^+_{k'} \rangle + u_{k'} v_{k'} (1 - \langle \alpha^+_{k'} \alpha_{k'} \rangle - \langle \beta^+_{k'} \beta_{k'} \rangle)] \\ &= \frac{1}{2} \sum_k V_{kk'} \frac{\Delta_{k'}}{E_{k'}} [1 - 2 f_+(E_{k'})] = \frac{1}{2} \sum_k V_{kk'} \frac{\Delta_{k'}}{E_{k'}} \tanh \frac{E_{k'}}{2T}. \end{aligned}$$

Above, averages of operators which do not conserve the number of BOGOLIUBOV quasi-particles vanish, while the average occupation numbers are given by FERMI functions $f_+(E_k)$ as will be derived in Section 3.3. The trivial solution $\Delta_k = 0$ to the above equation exists for all temperatures T and represents the normal state. The presence of a non-zero solution characterizes the superconducting state.

From the definition of $V_{kk'}$ it follows that also Δ_k is a constant Δ for $\boldsymbol{k}$ within the FERMI shell and zero otherwise. Hence, dividing by $\Delta \neq 0$,

$$1 = \frac{V}{2} \sum_k^{|\varepsilon_k < \omega_D|} \frac{\tanh \frac{\sqrt{\varepsilon_k^2 + \Delta^2}}{2T}}{\sqrt{\varepsilon_k^2 + \Delta^2}} = \frac{V}{2} \int_{-\omega_D}^{\omega_D} \mathrm{d}\varepsilon \, N(\varepsilon) \frac{\tanh \frac{\sqrt{\varepsilon^2 + \Delta^2}}{2T}}{\sqrt{\varepsilon^2 + \Delta^2}},$$

where $N(\varepsilon)$ is the density of states, usually assumed to be constant over the range of integration. This is the famous *BCS gap equation*. The resulting temperature dependence of the order parameter for different coupling strengths is displayed in Fig. 2.1.

Chapter 3

Many-body physics

Superconductivity results from the interaction of a huge number of particles and quasiparticles, conventionally electrons and phonons, and depends strongly on temperature. A prominent approach to such problems is the Green-function method of statistical physics, which emerged in the middle of the 20th century as a side product of quantum electrodynamics.[1] Since the equations which make up Eliashberg theory, namely Eqs. 4.5 on page 23, are only meaningful within this framework, a review of the relevant aspects is given in this chapter.[2]

Initially, the possible ways of handling time dependence in quantum mechanics are presented, focussing on the interaction picture. On this basis Green functions are defined, including their imaginary-axis formulation. Next, not only to exemplify what has been stated so far but also because it will provide the fundamental building block for what follows, the special case of non-interacting particles is discussed. Subsequently, the perturbation series and Wick's theorem for non-zero temperatures are derived, which prepare the ground for Feynman's diagrammatical perturbation theory. For some model interactions the most important diagrams are deduced explicitly. Finally, the self-energy and its most common approximations are introduced.

In some places where no ambiguity arises, different quantities are represented by the same symbol and only distinguished by the name or presence of a formal argument. This concerns e.g. mutual Fourier transforms as well as functions of real and imaginary time.

3.1 Dynamical pictures

It is convenient to present time dependence in quantum mechanics on the basis of expectation values. Let the Hamilton operator of the system be $H = H_0 + V$ with H_0 diagonal and V an interaction. At time t, the expectation value of the observable X in the state $|\psi\rangle$ reads

$$\langle\psi|\, e^{iHt}\, X\, e^{-iHt}\, |\psi\rangle = \langle\psi|\, e^{iHt}\, e^{-iH_0t}\, e^{iH_0t}\, X\, e^{-iH_0t}\, e^{iH_0t}\, e^{-iHt}\, |\psi\rangle.$$

So far, both observables and states are assumed to be independent of time. In practice however, they are usually associated with the adjacent exponential functions, which can be done in different ways, each of which corresponds to a so-called *dynamical picture*.

In the *Schrödinger picture* the full time dependency is ascribed to the states. Differentiation with respect to time yields the Schrödinger equation. Formally,

$$|\psi(t)\rangle = e^{-iHt}\, |\psi\rangle \quad \Rightarrow \quad i\frac{d}{dt}|\psi(t)\rangle = H|\psi(t)\rangle.$$

[1] In 1949 Dyson publishes an attempt to unify *"The radiation theories of Tomonaga, Schwinger, and Feynman"* [21] together with an early Feynman diagram. Six years later Matsubara applies the new methods to the calculation of the grand-canonical partition function [22].

[2] Physical concepts that are very well established nowadays will be stated without reference to their specific origins. They are covered in most textbooks on this subject such as the one by Mahan [23].

As opposed to this, in the *Heisenberg picture* only the observables depend on time. In this case differentiation using the product rule yields Heisenberg's equation of motion. Thus

$$X(t) = e^{iHt}\, X\, e^{-iHt} \quad \Rightarrow \quad i\frac{d}{dt}X(t) = [X(t), H].$$

A useful compromise is provided by the *Dirac picture*, also known as *interaction picture*, where the time dependence is shared among observables and states. The former evolve according to the unperturbed part of the Hamilton operator while the latter are governed by the interaction.

To be able to distinguish between the different pictures, time arguments will be enclosed in square brackets $[\dots]$. Formally, both a Heisenberg- and a Schrödinger-like equation of motion emerge for observables and states, respectively:

$$X[t] = e^{iH_0 t}\, X\, e^{-iH_0 t} \quad \Rightarrow \quad i\frac{d}{dt}X[t] = [X[t], H_0], \tag{3.1a}$$

$$|\psi[t]\rangle = e^{iH_0 t}\, e^{-iHt}\, |\psi\rangle \quad \Rightarrow \quad i\frac{d}{dt}|\psi[t]\rangle = V[t]|\psi[t]\rangle. \tag{3.1b}$$

3.1.1 Dyson series

According to Eq. 3.1b, the unitary *time-evolution operator* $S(t, t_0)$ for arbitrary initial times t_0,[3] precisely the one defined by $|\psi[t]\rangle = S(t, t_0)|\psi[t_0]\rangle$, has to satisfy the differential equation

$$\frac{d}{dt}S(t, t_0) = -iV[t]\, S(t, t_0) \quad \text{with} \quad S(t_0, t_0) = 1.$$

Integration followed by a fixed-point iteration, which is expected to converge, yields

$$S(t, t_0) = 1 - i\int_{t_0}^{t} dt'\, V[t]\, S(t, t_0) = \sum_{n=0}^{\infty} (-i)^n \int_{t_0}^{t} dt_1 \int_{t_0}^{t_1} dt_2 \cdots \int_{t_0}^{t_{n-1}} dt_n\, V[t_1] \dots V[t_n].$$

With S_n being the group of all $n!$ permutations of $1 \dots n$ one can just as well write

$$S(t, t_0) = \sum_{n=0}^{\infty} \frac{(-i)^n}{n!} \sum_{P \in S_n} \int_{t_0}^{t} dt_{P(1)} \int_{t_0}^{t_{P(1)}} dt_{P(2)} \cdots \int_{t_0}^{t_{P(n-1)}} dt_{P(n)}\, V[t_{P(1)}] \dots V[t_{P(n)}]$$

since a permutation of the dummy variables does not alter the value of the integral. For $t > t_0$, which will be assumed from now on, the domain of integration is always an n-simplex defined by $t_0 < t_{P(n)} < \cdots < t_{P(1)} < t$. Noting that the n-simplices for all permutations add up to the n-dimensional hypercube defined by $t_0 < t_i < t$ for all $i \in \{0 \dots n\}$,[4] one finds most beneficial formulation of the *Dyson series*[5]

$$S(t, t_0) = \sum_{n=0}^{\infty} \frac{(-i)^n}{n!} \int_{t_0}^{t} dt_1 \cdots \int_{t_0}^{t} dt_n\, T\, V[t_1] \dots V[t_n], \tag{3.2}$$

where T is a *time-ordering operator*, which sorts the factors of a product of operators chronologically with the result that their actual time arguments ascend from right to left.

If the time dependence of the perturbation operator does not involve any non-commuting quantities, the time-ordering operator is no longer needed and Eq. 3.2 can be written as

$$S(t, t_0) = \exp\left[-i\int_{t_0}^{t} dt'\, V[t']\right].$$

But even if the operators do not commute it is common practice to use a symbolic exponential function with the time-ordering operator placed in front.

[3] Dirac introduces this operator in § 44 *"The perturbation considered as causing transitions"* of his textbook on quantum mechanics [24].

[4] The idea of speaking of *'simplices'* and *'hypercubes'* in this context is taken from lecture notes by V. Kaplunovsky.

[5] See Eq. 32 in Dyson's paper [21] for an analogous formula, which he further discusses in Ref. 25.

3.2 Green functions

Gathering complete information about an interacting many-body system is a hard, if not impossible task. However, much can be learned from studying the behavior of single test particles within this system.

To that end *correlation functions* like $\langle \mathrm{A}(t)\,\mathrm{B}(t')\rangle$ are considered, where A and B are either fermionic or bosonic ladder operators. They describe how the presence or absence of a certain particle at one time correlates with an analogous occurrence at another time.

To take an equilibrium temperature β^{-1} into account, $\langle \dots \rangle$ shall denote an ensemble average. For brevity, a canonical ensemble with the partition function $Z = \operatorname{Tr} \mathrm{e}^{-\beta \mathrm{H}}$ is assumed; associating the Hamilton operator H with $\mathrm{H} - \mu \mathrm{N}$, where μ is the chemical potential and N the particle-number operator, yields the grand canonical ensemble.

$$\begin{aligned} \langle \mathrm{A}(t)\,\mathrm{B}(t')\rangle &= \frac{1}{Z} \operatorname{Tr}\left[\mathrm{e}^{-\beta \mathrm{H}}\, \mathrm{e}^{\mathrm{i}\mathrm{H}t}\, \mathrm{A}\, \mathrm{e}^{-\mathrm{i}\mathrm{H}t}\, \mathrm{e}^{\mathrm{i}\mathrm{H}t'}\, \mathrm{B}\, \mathrm{e}^{-\mathrm{i}\mathrm{H}t'}\right] \\ &= \frac{1}{Z} \operatorname{Tr}\left[\mathrm{e}^{-\beta \mathrm{H}}\, \mathrm{e}^{\mathrm{i}\mathrm{H}(t-t')}\, \mathrm{A}\, \mathrm{e}^{-\mathrm{i}\mathrm{H}(t-t')}\, \mathrm{B}\right] = \langle \mathrm{A}(t-t')\,\mathrm{B}\rangle \equiv C(t-t') \end{aligned} \tag{3.3}$$

depends on time differences only, since the trace of a product is invariant under cyclic permutations of the factors. With the energy eigenstates $|n\rangle$ and -values E_n,

$$C(t) = \frac{1}{Z} \sum_{nm} \langle n|\mathrm{e}^{-\beta \mathrm{H}}\, \mathrm{e}^{\mathrm{i}\mathrm{H}t}\, \mathrm{A}\, \mathrm{e}^{-\mathrm{i}\mathrm{H}t}|m\rangle\langle m|\mathrm{B}|n\rangle = \frac{1}{Z} \sum_{nm} \mathrm{e}^{-\beta E_n} \underbrace{\langle n|\mathrm{A}|m\rangle}_{A_{nm}} \underbrace{\langle m|\mathrm{B}|n\rangle}_{B_{mn}} \mathrm{e}^{\mathrm{i}(E_n - E_m)t}. \tag{3.4}$$

A Fourier transform using Eq. A.3c reveals a weighted excitation spectrum:

$$C(\omega) = \frac{1}{2\pi} \int_{-\infty}^{\infty} \mathrm{d}t\, C(t)\, \mathrm{e}^{\mathrm{i}\omega t} = \frac{1}{Z} \sum_{nm} \mathrm{e}^{-\beta E_n} A_{nm} B_{mn}\, \delta[\omega - (E_m - E_n)]. \tag{3.5}$$

At temperature β^{-1}, the probability that a many-particle state $|n\rangle$ with energy E_n is realized reads $\mathrm{e}^{-\beta E_n}/Z$ and the average occupation number of a single-particle state with energy ε is given by $f_\pm(\varepsilon) = [\mathrm{e}^{\beta\varepsilon} \pm 1]^{-1}$ as derived in Section 3.3. From now on upper and lower signs hold for fermions and bosons, respectively. One can easily verify that

$$\mathrm{e}^{-\beta E_n} = \left[1 \mp f_\pm(E_m - E_n)\right]\left[\mathrm{e}^{-\beta E_n} \pm \mathrm{e}^{-\beta E_m}\right]$$

and write Eq. 3.5 as $C(\omega) = [1 \mp f_\pm(\omega)]A(\omega)$ with the *spectral function*

$$A(\omega) = \frac{1}{Z} \sum_{nm} \left[\mathrm{e}^{-\beta E_n} \pm \mathrm{e}^{-\beta E_m}\right] A_{nm} B_{mn}\, \delta[\omega - (E_m - E_n)]. \tag{3.6}$$

It is straightforward to reverse the steps that led from Eq. 3.3 to Eq. 3.5 and apply them to Eq. 3.6. The Fourier transform of the spectral function turns out to be the expectation value of the (anti-) commutator of the respective operators:

$$A(t) = \int_{-\infty}^{\infty} \mathrm{d}\omega\, A(\omega)\, \mathrm{e}^{-\mathrm{i}\omega t} = \langle [\mathrm{A}(t), \mathrm{B}]_\pm \rangle. \tag{3.7}$$

Causality forbids the present to affect the past. This may be implemented into the theory by nullifying the correlation for negative time differences. Together with a factor $-\mathrm{i}$, which is solely introduced for convenience, this yields the *retarded Green function*

$$G_{\mathrm{ret.}}(t) = -\mathrm{i}\Theta(t)\, A(t) = -\mathrm{i}\Theta(t)\, \langle [\mathrm{A}(t), \mathrm{B}]_\pm \rangle. \tag{3.8}$$

With the help of Eqs. 3.7 and A.3a, yet another Fourier transform back to the energy domain, by convention without a factor of $(2\pi)^{-1}$, yields

$$G_{\mathrm{ret.}}(\omega) = \int_{-\infty}^{\infty} \mathrm{d}t\, G_{\mathrm{ret.}}(t)\, \mathrm{e}^{\mathrm{i}\omega t} = -\mathrm{i} \int_{-\infty}^{\infty} \mathrm{d}\omega'\, A(\omega') \int_0^{\infty} \mathrm{d}t\, \mathrm{e}^{\mathrm{i}(\omega - \omega')t} = \int_{-\infty}^{\infty} \mathrm{d}\omega'\, \frac{A(\omega')}{\omega - \omega' + \mathrm{i}0^+}. \tag{3.9}$$

The Sokhotski–Plemelj theorem leads to a useful expression for the spectral function:

$$\operatorname{Im} \frac{1}{\omega + \mathrm{i}0^+} = -\pi\delta(\omega) \quad \Rightarrow \quad A(\omega) = -\frac{1}{\pi} \operatorname{Im} G_{\mathrm{ret.}}(\omega). \tag{3.10}$$

3.2.1 Imaginary-time formalism

The retarded GREEN function as defined in Eq. 3.8 contains two different types of exponential functions: the ensemble weight which decays with increasing energy, and the ones oscillating with time. It would be convenient to be able to treat both in one go which can be accomplished by assuming the time to be purely imaginary. Introducing a real parameter $\tau = \mathrm{i}t$ and writing

$$\mathrm{X}(\tau) = \mathrm{e}^{\mathrm{H}\tau}\,\mathrm{X}\,\mathrm{e}^{-\mathrm{H}\tau}$$

as in Eq. 2.6 of Ref. 22, the theory as been formally freed from the periodic terms.

The *MATSUBARA-GREEN function* is preliminary defined as

$$G(\tau) = -\langle \mathrm{T}\,\mathrm{A}(\tau)\,\mathrm{B}\rangle,$$

where T acts as in Eq. 3.2, except that is sorts with respect to the parameter τ and induces a change of sign each time two fermion operator are transposed.

Using the cyclic property of the trace and introducing unity, one finds the property

$$\begin{aligned}\langle \mathrm{A}(\tau)\,\mathrm{B}\rangle &= \frac{1}{Z}\,\mathrm{Tr}\left[\mathrm{e}^{-\beta\mathrm{H}}\,\mathrm{e}^{\mathrm{H}\tau}\,\mathrm{A}\,\mathrm{e}^{-\mathrm{H}\tau}\,\mathrm{e}^{\beta\mathrm{H}}\,\mathrm{e}^{-\beta\mathrm{H}}\,\mathrm{B}\right]\\ &= \frac{1}{Z}\,\mathrm{Tr}\left[\mathrm{e}^{-\beta\mathrm{H}}\,\mathrm{B}\,\mathrm{e}^{\mathrm{H}(\tau-\beta)}\,\mathrm{A}\,\mathrm{e}^{-\mathrm{H}(\tau-\beta)}\right] = \langle \mathrm{B}\,\mathrm{A}(\tau-\beta)\rangle\end{aligned}$$

and as a consequence for $0 < \tau < \beta$

$$G(\tau) = -\langle \mathrm{B}\,\mathrm{A}(\tau-\beta)\rangle = \pm\langle \mathrm{T}\,\mathrm{A}(\tau-\beta)\,\mathrm{B}\rangle = \mp G(\tau-\beta). \tag{3.11}$$

Being only interested in the interval $(-\beta, \beta)$ one can just as well consider a modified GREEN function which continues periodically beyond this domain, namely

$$\widetilde{G}(\tau) = \frac{1}{\beta}\sum_{n\in\mathbb{Z}} \mathrm{e}^{-\mathrm{i}\pi n\tau/\beta} G_n \quad \text{with} \quad G_n = \frac{1}{2}\int_{-\beta}^{\beta} \mathrm{d}\tau\, \mathrm{e}^{\mathrm{i}\pi n\tau/\beta} G(\tau).$$

Because of the (anti-) periodicity found in Eq. 3.11 one has

$$\int_{-\beta}^{0} \mathrm{d}\tau\, \mathrm{e}^{\mathrm{i}\pi n\tau/\beta}\, G(\tau) = \mp\int_{-\beta}^{0} \mathrm{d}\tau\, \mathrm{e}^{\mathrm{i}\pi n\tau/\beta} G(\tau+\beta) = \mp \mathrm{e}^{-\mathrm{i}\pi n}\int_{0}^{\beta} \mathrm{d}\tau\, \mathrm{e}^{\mathrm{i}\pi n\tau/\beta} G(\tau),$$

which causes every other series coefficient to vanish, thus

$$G_n = \begin{cases} \int_0^\beta \mathrm{d}\tau\, \mathrm{e}^{\mathrm{i}\pi n\tau/\beta}\, G(\tau) & \text{for fermions (bosons) if } n \text{ is odd (even),}\\ 0 & \text{otherwise.}\end{cases}$$

So one redefines the *MATSUBARA-Green function* and its imaginary-axis representation:

$$G(\tau) = \frac{1}{\beta}\sum_{n\in\mathbb{Z}} \mathrm{e}^{-\mathrm{i}\omega_n\tau} G(\mathrm{i}\omega_n) \quad \text{and} \quad G(\mathrm{i}\omega_n) = \int_0^\beta \mathrm{d}\tau\, \mathrm{e}^{\mathrm{i}\omega_n\tau} G(\tau) = -\int_0^\beta \mathrm{d}\tau\, \mathrm{e}^{\mathrm{i}\omega_n\tau}\langle \mathrm{A}(\tau)\mathrm{B}\rangle \tag{3.12}$$

with the *MATSUBARA frequencies*

$$\omega_n = \begin{cases} \frac{(2n+1)\pi}{\beta} & \text{for fermions,}\\ \frac{2n\pi}{\beta} & \text{for bosons.}\end{cases}$$

The latter are denoted ν_n in the future. Using Eq. 3.4 and comparing with Eqs. 3.9 one finds that $G_{\mathrm{ret.}}(\omega)$ can be obtained from $G(\mathrm{i}\omega)$ through *analytic continuation* $\mathrm{i}\omega \to \omega + \mathrm{i}0^+$, since

$$\begin{aligned} G(\mathrm{i}\omega_n) &= -\frac{1}{Z}\sum_{nm} \mathrm{e}^{-\beta E_n} A_{nm} B_{mn} \int_0^\beta \mathrm{d}\tau\, \mathrm{e}^{\mathrm{i}\omega_n\tau}\mathrm{e}^{(E_n-E_m)\tau}\\ &= \frac{1}{Z}\sum_{nm} A_{nm} B_{mn}\frac{\mathrm{e}^{-\beta E_n} \pm \mathrm{e}^{-E_m\beta}}{\mathrm{i}\omega_n - (E_m - E_n)} = \int_{-\infty}^{\infty}\mathrm{d}\omega \frac{A(\omega)}{\mathrm{i}\omega_n - \omega}.\end{aligned} \tag{3.13}$$

3.3 Free particles

The theory presented in the preceding sections will now be exemplified by means of the special case of free particles, which will turn out to be fundamental in the following section. In this context *'free'* shall not be understood as *'free from any forces'* but rather as *'non-interacting'* since independent Bloch electrons in a fixed lattice are very well considered free, just as every quasi-particle which diagonalizes a single-particle Hamilton operator. In second quantization the latter is quadratic in the particle operators and diagonalized it reads

$$\mathrm{H}_0 = \sum_k \varepsilon_k \mathrm{n}_k \quad \text{with} \quad \mathrm{n}_k = \mathrm{a}_k^+ \mathrm{a}_k .$$

where a_k annihilates a fermion or boson with arbitrary, possibly combined, quantum number k, while ε_k and the operator n_k represent the corresponding energy and occupation number.

First, the time-dependence of the creation and annihilation operators is presented. Using Eq. 3.1a as well as the canonical (anti-) commutation relations one finds

$$\begin{aligned} \mathrm{a}_k[t] &= \mathrm{e}^{-\mathrm{i}\varepsilon_k t}\,\mathrm{a}_k, \quad \mathrm{a}_k^+[t] = \mathrm{e}^{\mathrm{i}\varepsilon_k t}\,\mathrm{a}_k^+, \\ \mathrm{a}_k[\tau] &= \mathrm{e}^{-\varepsilon_k \tau}\,\mathrm{a}_k, \quad \mathrm{a}_k^+[\tau] = \mathrm{e}^{\varepsilon_k \tau}\,\mathrm{a}_k^+ . \end{aligned} \tag{3.14}$$

The Dirac picture is used to allow for a perturbation V to be added without having to update these equations. If H_0 is already the full Hamilton operator, they are equally valid in the Heisenberg picture.

Next, the *Fermi-Dirac* and the *Bose-Einstein distribution* $f_\pm$ are derived, which give the average number of fermions and bosons, respectively, with the same quantum number as a function of their energy. Each eigenstate $|n\rangle$ of the free Hamilton operator H_0 is a Fock state, thus an (anti-) symmetric product of the occupied single-particle states, and the corresponding energy $E_n = \sum_k \varepsilon_k n_k$, where n_k are occupation numbers, is a sum of single-particle energies.

$$f_\pm(\varepsilon_k) = \langle \mathrm{n}_k \rangle_0 = \frac{\sum_n \langle n|\mathrm{n}_k|n\rangle \mathrm{e}^{-\beta E_n}}{\sum_n \mathrm{e}^{-\beta E_n}} = \frac{\sum_{n_k=0}^{N} n_k \mathrm{e}^{-\beta \varepsilon_k n_k}}{\sum_{n_k=0}^{N} \mathrm{e}^{-\beta \varepsilon_k n_k}},$$

where N is the maximum number of particles allowed to occupy the same state and $\langle \dots \rangle_0$ denotes an average with respect to a diagonal Hamilton operator. In the last step the fraction has been reduced through division by the partial sum of the denominator for which $\langle n|\mathrm{n}_k|n\rangle = 0$.

For fermions $N = 1$ and thus

$$f_+(\varepsilon_k) = \frac{\mathrm{e}^{-\beta\varepsilon_k}}{1+\mathrm{e}^{-\beta\varepsilon_k}} = \frac{1}{\mathrm{e}^{\beta\varepsilon_k}+1}.$$

For bosons $N = \infty$ and, recognizing that $0+(n_k-1)+1, 1+(n_k-2)+1 \dots (n_k-1)+0+1$ are n_k ways to express n_k as well as a geometric series, one finds

$$f_-(\varepsilon_k) = \frac{\sum_{n=0}^{\infty}\sum_{m=0}^{\infty} \mathrm{e}^{-\beta\varepsilon_k(n+m+1)}}{\sum_{n=0}^{\infty} \mathrm{e}^{-\beta\varepsilon_k n}} = \sum_{m=0}^{\infty} \mathrm{e}^{-\beta\varepsilon_k(m+1)} = \frac{\mathrm{e}^{-\beta\varepsilon_k}}{1-\mathrm{e}^{-\beta\varepsilon_k}} = \frac{1}{\mathrm{e}^{\beta\varepsilon_k}-1}.$$

Finally, the Green functions on the imaginary-axis as defined in Eq. 3.12 are determined.

For electrons, the operators A and B are simply $\mathrm{c}_{k\sigma}$ and $\mathrm{c}_{k\sigma}^+$. One can formulate correlation functions $\langle \mathrm{c}_{k\sigma}[\tau]\,\mathrm{c}_{k\sigma}^+\rangle_0 = \mathrm{e}^{-\varepsilon_k\tau}[1-f_+(\varepsilon_k)]$ and therewith

$$G^0_{k\sigma}(\mathrm{i}\omega_n) = -\int_0^\beta \mathrm{d}\tau\, \mathrm{e}^{\mathrm{i}\omega_n\tau}\langle \mathrm{c}_{k\sigma}[\tau]\,\mathrm{c}_{k\sigma}^+\rangle_0 = \frac{1+\mathrm{e}^{-\beta\varepsilon_k}}{\mathrm{i}\omega_n-\varepsilon_k}[1-f_+(\varepsilon_k)] = \frac{1}{\mathrm{i}\omega_n-\varepsilon_k}, \tag{3.15}$$

which corresponds to a spectral function $A(\omega) = \delta(\omega-\varepsilon_k)$ as follows from Eq. 3.13.

For phonons one usually applies a different notation with symmetric operators $\varphi_q = \mathrm{b}_q + \mathrm{b}_{-q}^+$. Analogously, this yields $\langle \varphi_q[\tau]\,\varphi_q^+\rangle_0 = \mathrm{e}^{-\omega_q\tau}[1+f_-(\omega_q)] + \mathrm{e}^{\omega_{-q}\tau} f_-(\omega_{-q})$ and thus

$$D^0_q(\mathrm{i}\nu_n) = -\int_0^\beta \mathrm{d}\tau\, \mathrm{e}^{\mathrm{i}\nu_n\tau}\langle \varphi_q[\tau]\,\varphi_q^+\rangle_0 = \frac{1}{\mathrm{i}\nu_n-\omega_q} - \frac{1}{\mathrm{i}\nu_n+\omega_{-q}} \overset{\omega_q=\omega_{-q}}{=} -\frac{2\omega_q}{\nu_n^2+\omega_q^2} \tag{3.16}$$

as well as the spectral function $B(\omega) = \delta(\omega-\omega_q) - \delta(\omega+\omega_{-q})$.

3.4 Perturbation series

It is yet to be clarified how the full Green function for arbitrary interactions can be calculated. The basis idea is to build it iteratively from what is already known, namely the Green functions of free particles.

The first step is to rewrite the Green function in a way that both the ensemble average and the time dependence of the operators refer to the unperturbed part H_0 of the Hamilton operator.

In the imaginary-time formalism, the time-evolution operator according to Eq. 3.2 reads

$$S(\tau, \tau_0) = \sum_{n=0}^{\infty} \frac{(-1)^n}{n!} \int_{\tau_0}^{\tau} d\tau_1 \cdots \int_{\tau_0}^{\tau} d\tau_n \, T\, V[\tau_1] \ldots V[\tau_n]. \tag{3.17}$$

For brevity, let $S(\tau) = S(\tau, 0) = e^{H_0 \tau} e^{-H\tau}$. Inserting unities it can be shown that

$$\langle \ldots \rangle = \frac{1}{Z} \operatorname{Tr}\left[e^{-\beta H} \ldots\right] = \frac{1}{Z} \operatorname{Tr}\left[e^{-\beta H_0} e^{\beta H_0} e^{-\beta H} \ldots\right] = \frac{\langle S(\beta) \ldots \rangle_0}{\langle S(\beta) \rangle_0},$$
$$A(\tau) = e^{H\tau} A\, e^{-H\tau} = e^{H\tau} e^{-H_0\tau} e^{H_0\tau} A\, e^{-H_0\tau} e^{H_0\tau} e^{-H\tau} = S^{-1}(\tau) A[\tau] S(\tau).$$

The Matsubara-Green function defined in Eq. 3.12 may thus be written as

$$\begin{aligned} G(\tau) &= -\langle T\, A(\tau) B(0) \rangle = -\Theta(\tau) \langle A(\tau) B(0) \rangle \pm \Theta(-\tau) \langle B(-\tau) A(0) \rangle \\ &= \frac{1}{\langle S(\beta) \rangle_0} \begin{cases} -\langle S(\beta) \quad S^{-1}(\tau) \quad A[\tau] \quad S(\tau) \quad B[0] \rangle_0 & \text{for } 0 < \tau < \beta, \\ \pm\langle S(\beta) \quad S^{-1}(-\tau) \quad B[-\tau] \quad S(-\tau) \quad A[0] \rangle_0 & \text{for } -\beta < \tau < 0. \end{cases} \end{aligned}$$

Since $S(\beta) S^{-1}(\pm\tau) = S(\beta, \pm\tau)$, in both cases the expectation value is fully time-ordered from right to left. Consequently, it makes no difference if one introduces a time-ordering operator for the Dirac picture that acts *after* the time-evolution operators have been expanded up to the level of creation and annihilation operators. Then the factors may be freely permuted, except that sign changes have to taken into account. However, the latter does not apply to the time-evolution operators since the interaction usually contains an even number of fermion operators. Mutual inverses cancel each other and the final expression reads

$$G(\tau) = -\frac{\langle T\, A[\tau] S(\beta) B[0] \rangle_0}{\langle S(\beta) \rangle_0}. \tag{3.18}$$

Using the above formula, the Matsubara-Green function may be calculated to an arbitrary order of accuracy by simply truncating the Taylor series in Eq. 3.17 after the corresponding number of terms.

As an example, a perturbation of the form $V = \sum_{kk'} v_{kk'} a^+_{k'} a_k$ is considered. As a single-particle operator it describes the interaction of a particle with some scattering potential rather than with other particles. The first terms of the enumerator in Eq. 3.18 read

$$\begin{aligned} \langle T\, A[\tau] S(\beta) B[0] \rangle_0 &= \langle T\, A[\tau] B[0] \rangle_0 - \int_0^\beta d\tau_1 \sum_{k,k'} v_{kk'} \langle T\, A[\tau] a^+_{k'}[\tau_1] a_k[\tau_1] B[0] \rangle_0 \\ &+ \frac{1}{2} \int_0^\beta d\tau_1 \int_0^\beta d\tau_2 \sum_{k,k',q,q'} v_{kk'} v_{qq'} \langle T\, A[\tau] a^+_{k'}[\tau_1] a_k[\tau_1] a^+_{q'}[\tau_2] a_q[\tau_2] B[0] \rangle_0 + \cdots \end{aligned}$$

Continuing in this way, expectation values of products of a growing number of creation and annihilation operators will emerge. Fortunately, these can be factorized into free-particle Green functions with the help of Wick's theorem, which is presented in the following section.

This is the last step to be taken on the way to Feynman's diagrammatical perturbation theory, which will be outlined afterwards during the analysis of some model interactions.

3.4.1 Wick's theorem

For an even number of fermion or any number of boson operators A_i with $i \in \{1 \dots n\}$ one has

$$[A_1, A_2 \dots A_n]_\pm = \sum_{i=2}^{n} (\mp 1)^i A_2 \dots A_{i-1} [A_1, A_i]_\pm A_{i+1} \dots A_n, \tag{3.19}$$

where $i \dots j$ is an empty sequence for $i > j$. For example, the special case of six operators reads

$$[A, BCDEF]_\pm = [A, B]_\pm CDEF \mp B[A, C]_\pm DEF + BC[A, D]_\pm EF \mp BCD[A, E]_\pm F + BCDE[A, F]_\pm.$$

Taking the average of the left-hand side of Eq. 3.19 with respect to H_0 yields

$$\langle [A_1, A_2 \dots A_n]_\pm \rangle_0 = \frac{1}{Z} \operatorname{Tr}\{e^{-\beta H_0} [A_1, A_2 \dots A_n]_\pm\} = \frac{1}{Z} \operatorname{Tr}\{[e^{-\beta H_0}, A_1]_\pm A_2 \dots A_n]\},$$

where the cyclic property of the trace has been used. With the help of Eq. 3.14 one finds

$$[e^{-\beta H_0}, A_1]_\pm = e^{-\beta H_0} e^{\beta H_0} [e^{-\beta H_0}, A_1]_\pm = e^{-\beta H_0} \left[1 \pm e^{\varepsilon(A_1)\beta}\right] A_1 = \frac{e^{-\beta H_0} A_1}{\pm f_\pm[\varepsilon(A_1)]},$$

where $\varepsilon(A)$ is the energy change caused by applying A to the state of the unperturbed system.

The right-hand side of Eq. 3.19 is averaged as well. A comparison,

$$\langle [A_1, A_2 \dots A_n]_\pm \rangle_0 = \frac{\langle A_1 \dots A_n \rangle_0}{\pm f_\pm[\varepsilon(A_1)]} = \sum_{i=2}^{n} (\mp 1)^i [A_1, A_i]_\pm \langle A_2 \dots A_{i-1} A_{i+1} \dots A_n \rangle_0,$$

considering $\langle AB \rangle_0 = \pm f_\pm[\varepsilon(A)][A, B]_\pm$ yields *Wick's theorem*[6] for non-zero temperatures:

$$\begin{aligned} \langle A_1 \dots A_n \rangle_0 &= \sum_{i=2}^{n} (\mp 1)^i \langle A_1 A_i \rangle_0 \langle A_2 \dots A_{i-1} A_{i+1} \dots A_n \rangle_0 \\ &= \sum_{P \in P_n} (\mp 1)^{T(P)} \langle A_{P(1)} A_{P(2)} \rangle_0 \langle A_{P(3)} A_{P(4)} \rangle_0 \dots \langle A_{P(n-1)} A_{P(n)} \rangle_0, \end{aligned}$$

where $T(P)$ is the number of transpositions the permutation P consists of and

$$P_n = \{P \in S_n \mid P(1) < P(3) < \dots < P(n-1) \text{ and } P(i) < P(i+1) \text{ for all } i \in \{1, 3 \dots n-1\}\}$$

is the group of all possible pairings. Since within each pair of operators the original order is preserved, the theorem holds for time-ordered expectation values as well, thus

$$\langle \mathrm{T}\, A_1[\tau_1] \dots A_n[\tau_n] \rangle_0 = \sum_{P \in P_n} (\mp 1)^{T(P)} \langle \mathrm{T}\, A_{P(1)}[\tau_{P(1)}] A_{P(2)}[\tau_{P(2)}] \rangle_0 \dots \langle \mathrm{T}\, A_{P(n-1)}[\tau_{P(n-1)}] A_{P(n)}[\tau_{P(n)}] \rangle_0. \tag{3.20}$$

3.5 Model interactions

For a satisfactory description of superconductivity, not only the *'normal'* Green function

$$G_{k\sigma}(\tau) = -\langle \mathrm{T}\, c_{k\sigma}(\tau)\, c^+_{k\sigma}(0) \rangle \in \mathbb{R}, \tag{3.21a}$$

which describes a propagating electron, but also the *anomalous Gor'kov-Green function* [29]

$$F_{k\sigma}(\tau) = -\langle \mathrm{T}\, c_{k\sigma}(\tau)\, c_{-k-\sigma}(0) \rangle \in \mathbb{C}, \tag{3.21b}$$

which indicates the existence of Cooper pairs in analogy to the BCS gap in Eq. 2.1, is needed. Solely for convenience, one introduces two additional functions

$$\widetilde{G}_{k\sigma}(\tau) = -\langle \mathrm{T}\, c^+_{-k-\sigma}(\tau)\, c_{-k-\sigma}(0) \rangle = -G_{-k-\sigma}(-\tau), \tag{3.21c}$$

$$\widetilde{F}_{k\sigma}(\tau) = -\langle \mathrm{T}\, c^+_{-k-\sigma}(\tau)\, c^+_{k\sigma}(0) \rangle = [F_{k\sigma}(\tau)]^* \tag{3.21d}$$

[6] The theorem is named in honor of Ref. 26. The generalization to non-zero temperatures was first carried out by Matsubara [22] and shown to be exact by Thouless [27]. The derivation at hand is due to Gaudin [28].

as well as the phonon GREEN function

$$D_q(\tau) = -\langle \mathrm{T}\, \varphi_q(\tau)\, \varphi_q^+(0)\rangle = D_{-q}(-\tau) \in \mathbb{R}. \tag{3.21e}$$

In the following, leading terms of the electronic GREEN functions are calculated explicitly for some model interactions. First, the perturbation series for the electron-phonon interaction as described by the HOLSTEIN-HAMILTON operator is analyzed up the second order. As will be shown, the latter bears a close resemblance to the first order terms of the homogeneous electron gas and the simpler HUBBARD model of interacting electrons.

For HAMILTON operators which conserve the number of electrons, by which e.g. free electrons but also all of the following models are described, the GOR'KOV-GREEN functions vanish. Nevertheless, in subsequent applications of WICK's theorem, unperturbed expectation values of COOPER-pair creation and annihilation operators *which originate from the interaction* terms are kept, since in a further step they will be redefined with respect to the interacting system, in which the strict conservation of particles is dropped.

3.5.1 HOLSTEIN model

In real space, the interaction term of the *HOLSTEIN-HAMILTON operator* reads [30]

$$V = g \sum_{R\sigma} c^+_{R\sigma} c_{R\sigma} [b_R + b^+_R],$$

where g is the local electron-phonon coupling strength and $c_{R\sigma}$ and b_R annihilate electronic and phononic excitations, respectively, localized at the lattice sites $\boldsymbol{R}$.

A discrete FOURIER transform of the creation and annihilation operators with the help of Eq. A.1 yields the momentum-space representation

$$V = \frac{g}{\sqrt{N}} \sum_{kk'\sigma q} \frac{1}{N} \sum_R e^{i(k'-k)R} c^+_{k'\sigma} c_{k\sigma} [e^{-iqR} b_q + e^{iqR} b^+_q] = \frac{g}{\sqrt{N}} \sum_{k\sigma q} c^+_{k+q\sigma} c_{k\sigma} \varphi_q.$$

Normal GREEN function

First, $G_{k\sigma}(\tau)$ is evaluated. The zeroth term is just the GREEN function of non-interacting electrons, the MATSUBARA representation of which is given in Eq. 3.15. First-order terms vanish because φ_q does not conserve the particle number, unlike the unperturbed HAMILTON operator with respect to which the averages are taken. Eventually, in second order one finds

$$\begin{aligned} G^{2\mathrm{nd}}_{k\sigma}(\tau) &\propto \sum_{k'k''\sigma\sigma' qq'} \int_0^\beta \mathrm{d}\tau' \int_0^\beta \mathrm{d}\tau'' \, \langle \dots \rangle_0, \qquad (3.22)\\ \langle \dots \rangle_0 &= \langle \mathrm{T}\, c_{k\sigma}[\tau] c^+_{k'+q\sigma'}[\tau'] c_{k'\sigma'}[\tau'] \varphi_q[\tau'] c^+_{k''+q'\sigma''}[\tau''] c_{k''\sigma''}[\tau''] \varphi_{q'}[\tau''] c^+_{k\sigma}[0]\rangle_0 \\ &= \underbrace{\langle \mathrm{T}\, c_{k\sigma}[\tau] c^+_{k'+q\sigma'}[\tau'] c_{k'\sigma'}[\tau'] c^+_{k''+q'\sigma''}[\tau''] c_{k''\sigma''}[\tau''] c^+_{k\sigma}[0]\rangle_0}_{\langle \mathrm{el.}\rangle_0} \underbrace{\langle \mathrm{T}\, \varphi_q[\tau'] \varphi_{q'}[\tau'']\rangle_0}_{-D^0_q(\tau'-\tau'')\,\delta^{-q}_{q'}}, \end{aligned}$$

where the GREEN function $D^0_q(\tau)$ of free phonons can be transformed into Eq. 3.16. Further application of WICK's theorem as stated in Eq. 3.20 to the electronic part $\langle \mathrm{el.}\rangle_0$ yields

$$\begin{array}{llllll}
- \langle \mathrm{T}\, c_{k\sigma}[\tau] c^+_{k''+q'\sigma''}[\tau'']\rangle_0 & \langle \mathrm{T}\, c_{k'\sigma'}[\tau'] c^+_{k'+q\sigma'}[\tau']\rangle_0 & \langle \mathrm{T}\, c_{k''\sigma''}[\tau''] c^+_{k\sigma}[0]\rangle_0 & \delta^0_q \delta^0_{q'} & \delta^\sigma_{\sigma''} & \delta^k_{k''} \\
- \langle \mathrm{T}\, c_{k\sigma}[\tau] c^+_{k'+q\sigma'}[\tau']\rangle_0 & \langle \mathrm{T}\, c_{k''\sigma''}[\tau''] c^+_{k''+q'\sigma''}[\tau'']\rangle_0 & \langle \mathrm{T}\, c_{k'\sigma'}[\tau'] c^+_{k\sigma}[0]\rangle_0 & \delta^0_q \delta^0_{q'} & \delta^\sigma_{\sigma'} & \delta^k_{k'} \\
+ \langle \mathrm{T}\, c_{k\sigma}[\tau] c^+_{k'+q\sigma'}[\tau']\rangle_0 & \langle \mathrm{T}\, c_{k'\sigma'}[\tau'] c^+_{k''+q'\sigma''}[\tau'']\rangle_0 & \langle \mathrm{T}\, c_{k''\sigma''}[\tau''] c^+_{k\sigma}[0]\rangle_0 & \delta^{-q}_{q'} & \delta^\sigma_{\sigma'} \delta^\sigma_{\sigma''} & \delta^k_{k''} \delta^{k-q}_{k'} \\
+ \langle \mathrm{T}\, c_{k\sigma}[\tau] c^+_{k''+q'\sigma''}[\tau'']\rangle_0 & \langle \mathrm{T}\, c_{k''\sigma''}[\tau''] c^+_{k'+q\sigma'}[\tau']\rangle_0 & \langle \mathrm{T}\, c_{k'\sigma'}[\tau'] c^+_{k\sigma}[0]\rangle_0 & \delta^{-q}_{q'} & \delta^\sigma_{\sigma'} \delta^\sigma_{\sigma''} & \delta^k_{k'} \delta^{k+q}_{k''} \\
+ \langle \mathrm{T}\, c_{k'\sigma'}[\tau'] c^+_{k'+q\sigma'}[\tau']\rangle_0 & \langle \mathrm{T}\, c_{k''\sigma''}[\tau''] c^+_{k''+q'\sigma''}[\tau'']\rangle_0 & \langle \mathrm{T}\, c_{k\sigma}[\tau] c^+_{k\sigma}[0]\rangle_0 & \delta^0_q \delta^0_{q'} & & \\
- \langle \mathrm{T}\, c_{k'\sigma'}[\tau'] c^+_{k''+q'\sigma''}[\tau'']\rangle_0 & \langle \mathrm{T}\, c_{k''\sigma''}[\tau''] c^+_{k'+q\sigma'}[\tau']\rangle_0 & \langle \mathrm{T}\, c_{k\sigma}[\tau] c^+_{k\sigma}[0]\rangle_0 & \delta^{-q}_{q'} & \delta^{\sigma'}_{\sigma''} & \delta^{k'+q}_{k''} \\
+ \langle \mathrm{T}\, c_{k'\sigma'}[\tau'] c_{k''\sigma''}[\tau'']\rangle_0 & \langle \mathrm{T}\, c^+_{k''+q'\sigma''}[\tau''] c^+_{k'+q\sigma'}[\tau']\rangle_0 & \langle \mathrm{T}\, c_{k\sigma}[\tau] c^+_{k\sigma}[0]\rangle_0 & \delta^{-q}_{q'} & \delta^{-\sigma'}_{\sigma''} & \delta^{-k'}_{k''}.
\end{array}$$

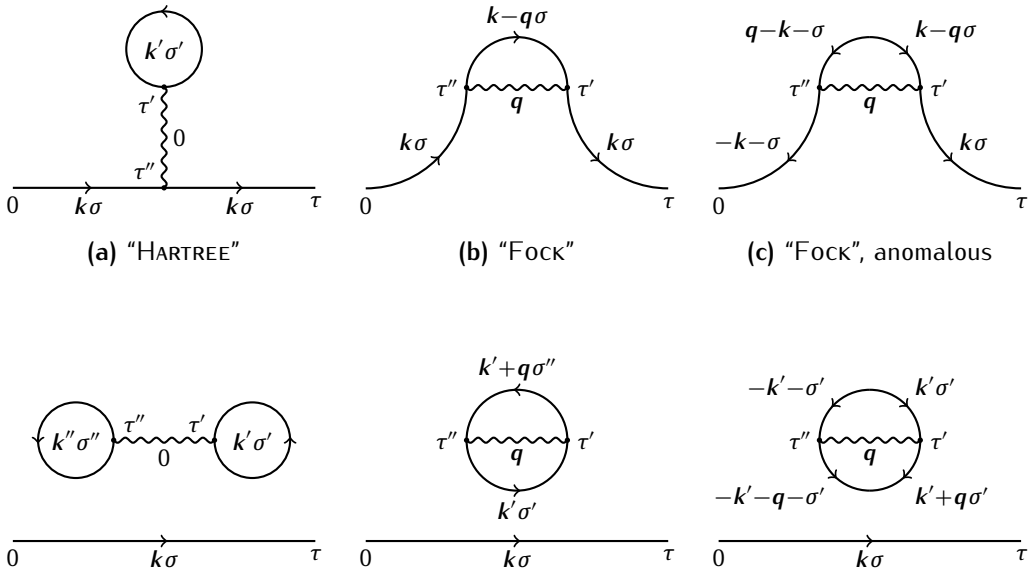

(a) "Hartree" **(b)** "Fock" **(c)** "Fock", anomalous

(d) "glasses" **(e)** "porthole" **(f)** "porthole", anomalous

Figure 3.1: Second-order processes that occur in the Feynman-Dyson perturbation series of $G_{k\sigma}$ and $F_{k\sigma}$ in the Holstein model. The quantum numbers $\boldsymbol{k}'$, $\boldsymbol{k}''$, σ', σ'' and $\boldsymbol{q}$ of internal lines are summed, time parameters τ' and τ'' of internal vertices integrated over. Solid and wavy lines represent electrons and phonons, respectively. The convention is followed that arrows point from creation towards annihilation. Thus out- or inward double arrows stand for Cooper pairs of unspecified origin or destiny.

Substituting the corresponding non-interacting Matsubara-Green functions and performing the summation to eliminate the Kronecker deltas, one obtains

$$\begin{aligned}
\sum_{\substack{k' \, k'' \\ \sigma' \, \sigma'' \\ q \;\; q'}} \langle \dots \rangle_0 = \; & - \sum_{k'\sigma'} && G^0_{k\sigma}(\tau - \tau'') && G^0_{k'\sigma'}(0) && G^0_{k\sigma}(\tau'') && D^0_0(\tau' - \tau'') && \text{(3.1a)} \\
& - \sum_{k''\sigma''} && G^0_{k\sigma}(\tau - \tau') && G^0_{k''\sigma''}(0) && G^0_{k\sigma}(\tau') && D^0_0(\tau' - \tau'') && \\
& + \sum_{q} && G^0_{k\sigma}(\tau - \tau') && G^0_{k-q\sigma}(\tau' - \tau'') && G^0_{k\sigma}(\tau'') && D^0_q(\tau' - \tau'') && \text{(3.1b)} \\
& + \sum_{q} && G^0_{k\sigma}(\tau - \tau'') && G^0_{k+q\sigma}(\tau'' - \tau') && G^0_{k\sigma}(\tau') && D^0_q(\tau' - \tau'') && \\
& + \sum_{k'k''\sigma'\sigma''} && G^0_{k'\sigma'}(0) && G^0_{k''\sigma''}(0) && G^0_{k\sigma}(\tau) && D^0_0(\tau' - \tau'') && \text{(3.1d)} \\
& - \sum_{k'\sigma' q} && G^0_{k'\sigma'}(\tau' - \tau'') && G^0_{k'+q\sigma'}(\tau'' - \tau') && G^0_{k\sigma}(\tau) && D^0_q(\tau' - \tau'') && \text{(3.1e)} \\
& + \sum_{k'\sigma' q} && F^0_{k'\sigma'}(\tau' - \tau'') && \widetilde{F}^0_{k'+q\sigma'}(\tau'' - \tau') && G^0_{k\sigma}(\tau) && D^0_q(\tau' - \tau''). && \text{(3.1f)}
\end{aligned}$$

The corresponding *Feynman diagrams* are depicted in Fig. 3.1.

The last three terms represent *disconnected diagrams*. Calculating the second order of $\langle S(\beta) \rangle_0$, which has been ignored so far, yields these very diagrams, except that the in- and outgoing electron lines are missing. It turns out that every diagram part contained in the denominator $\langle S(\beta) \rangle_0$ of Eq. 3.18 will reappear in the nominator in a way that

$$\langle \mathrm{T}\, \mathrm{A}[\tau]\, \mathrm{S}(\beta)\, \mathrm{B}[0] \rangle_0 = \langle \mathrm{S}(\beta) \rangle_0 \langle \mathrm{T}\, \mathrm{A}[\tau]\, \mathrm{S}(\beta)\, \mathrm{B}[0] \rangle_0^{\mathrm{c}},$$

where $\langle \dots \rangle_0^{\mathrm{c}}$ is $\langle \dots \rangle_0$ less all terms corresponding to disconnected diagrams. Hence,

$$G(\tau) = -\langle \mathrm{T}\, \mathrm{A}[\tau]\, \mathrm{S}(\beta)\, \mathrm{B}[0] \rangle_0^{\mathrm{c}}.$$

In the following, all terms with $D^0_0(\tau' - \tau'')$ are neglected since phonons with $\boldsymbol{q} = 0$ are no actual phonons but rather translations of the crystal as a whole or permanent strains [23, p. 82], which shall not be considered.

Performing the integrals, the remaining two terms turn out to be equivalent since τ' and τ'' occur in exchangeable positions. Transforming to MATSUBARA frequencies as per Eq. 3.12 yields

$$\begin{aligned} G^{\text{2nd}}_{k\sigma}(\mathrm{i}\omega_n) &= \int_0^\beta \mathrm{d}\tau\, \mathrm{e}^{\mathrm{i}\omega_n\tau} G^{\text{2nd}}_{k\sigma}(\tau) \\ &= -\frac{g^2}{N}\sum_{q}\int_0^\beta \mathrm{d}\tau \int_0^\beta \mathrm{d}\tau' \int_0^\beta \mathrm{d}\tau''\, \mathrm{e}^{\mathrm{i}\omega_n\tau} G^0_{k\sigma}(\tau-\tau')\, G^0_{k-q\sigma}(\tau'-\tau'')\, G^0_{k\sigma}(\tau'')\, D^0_q(\tau'-\tau'') \\ &= -\frac{g^2}{N\beta}\sum_{q}\sum_{ijkm} G^0_{k\sigma}(\mathrm{i}\omega_i)\, G^0_{k-q\sigma}(\mathrm{i}\omega_m)\, G^0_{k\sigma}(\mathrm{i}\omega_j)\, D^0_q(\mathrm{i}\nu_k) \times \cdots \\ \cdots \times \frac{1}{\beta}\int_0^\beta \mathrm{d}\tau\, \mathrm{e}^{\mathrm{i}(\omega_n-\omega_i)\tau} &\frac{1}{\beta}\int_0^\beta \mathrm{d}\tau'\, \mathrm{e}^{\mathrm{i}(\omega_i-\omega_m-\nu_k)\tau'} \frac{1}{\beta}\int_0^\beta \mathrm{d}\tau''\, \mathrm{e}^{\mathrm{i}(\omega_m-\omega_j+\nu_k)\tau''}. \end{aligned}$$

Noting that differences of MATSUBARA frequencies of mixed and equal type are fermionic and bosonic, respectively, and that for bosons the MATSUBARA-FOURIER series is defined as an ordinary FOURIER series, one can apply the orthogonality relation given in Eq. A.2a. Thus

$$G^{\text{2nd}}_{k\sigma}(\mathrm{i}\omega_n) = G^0_{k\sigma}(\mathrm{i}\omega_n)\, \Sigma^0_{k\sigma}(\mathrm{i}\omega_n)\, G^0_{k\sigma}(\mathrm{i}\omega_n),$$

where the part in between is a *self-energy contribution* and given by

$$\Sigma^0_{k\sigma}(\mathrm{i}\omega_n) = -\frac{g^2}{N\beta}\sum_{qm} G^0_{k-q\sigma}(\mathrm{i}\omega_m)\, D^0_q(\mathrm{i}\omega_n-\mathrm{i}\omega_m) = -\frac{g^2}{N\beta}\sum_{qm} G^0_{q\sigma}(\mathrm{i}\omega_m)\, D^0_{k-q}(\mathrm{i}\omega_n-\mathrm{i}\omega_m).$$

GOR'KOV-GREEN function

Next, $F_{k\sigma}(\tau)$ is analyzed. The procedure is as above except that

$$\langle \text{el.}\rangle_0 = \langle \mathrm{T}\, \mathrm{c}_{k\sigma}[\tau]\, \mathrm{c}^+_{k'+q\sigma'}[\tau']\, \mathrm{c}_{k'\sigma'}[\tau']\, \mathrm{c}^+_{k''+q'\sigma''}[\tau'']\, \mathrm{c}_{k''\sigma''}[\tau'']\, \mathrm{c}_{-k-\sigma}[0]\rangle_0$$

has to be considered. With the help of WICK's theorem this reduces to

$$\begin{aligned} &-\langle \mathrm{T}\, \mathrm{c}_{k\sigma}[\tau]\, \mathrm{c}^+_{k'+q\sigma'}[\tau']\rangle_0 \quad \langle \mathrm{T}\, \mathrm{c}_{k'\sigma'}[\tau']\, \mathrm{c}_{k''\sigma''}[\tau'']\rangle_0\, \langle \mathrm{T}\, \mathrm{c}^+_{k''+q'\sigma''}[\tau'']\, \mathrm{c}_{-k-\sigma}[0]\rangle_0\, \delta^{-q}_{q'}\, \delta^{\sigma}_{\sigma'}\delta^{-\sigma}_{\sigma''}\, \delta^{k-q}_{k'}\delta^{q-k}_{k''} \\ &-\langle \mathrm{T}\, \mathrm{c}_{k\sigma}[\tau]\, \mathrm{c}^+_{k''+q'\sigma''}[\tau'']\rangle_0\, \langle \mathrm{T}\, \mathrm{c}_{k''\sigma''}[\tau'']\, \mathrm{c}_{k'\sigma'}[\tau']\rangle_0\, \langle \mathrm{T}\, \mathrm{c}^+_{k'+q\sigma'}[\tau']\, \mathrm{c}_{-k-\sigma}[0]\rangle_0 \quad \delta^{-q}_{q'}\, \delta^{-\sigma}_{\sigma'}\delta^{\sigma}_{\sigma''}\, \delta^{-k-q}_{k'}\delta^{k+q}_{k''}. \end{aligned}$$

Substituting GREEN's functions, one finds two contributions which again will prove equivalent:

$$\begin{aligned} \sum_{k'k''\sigma'\sigma''qq'}\langle\ldots\rangle_0 = \; &-\sum_q \quad G^0_{k\sigma}(\tau-\tau') \quad F^0_{k-q\sigma}(\tau'-\tau'') \quad \widetilde{G}^0_{k\sigma}(\tau'') \quad D^0_q(\tau'-\tau'') \quad \text{(Fig. 3.1c)} \\ &-\sum_q \quad G^0_{k\sigma}(\tau-\tau'') \quad F^0_{k+q\sigma}(\tau''-\tau') \quad \widetilde{G}^0_{k\sigma}(\tau') \quad D^0_q(\tau'-\tau''). \end{aligned}$$

Bar the sign, the final result formally resembles the one for $G^{\text{2nd}}_{k\sigma}(\mathrm{i}\omega_n)$:

$$F^{\text{2nd}}_{k\sigma}(\mathrm{i}\omega_n) = G^0_{k\sigma}(\mathrm{i}\omega_n)\, \Sigma^0_{k\sigma}(\mathrm{i}\omega_n)\, \widetilde{G}^0_{k\sigma}(\mathrm{i}\omega_n) \quad \text{with} \quad \Sigma^0_{k\sigma}(\mathrm{i}\omega_n) = \frac{g^2}{N\beta}\sum_{qm} F^0_{q\sigma}(\mathrm{i}\omega_m)\, D^0_{k-q}(\mathrm{i}\omega_n-\mathrm{i}\omega_m).$$

Auxiliary GREEN functions

For completeness, the corresponding results for $\widetilde{G}_{k\sigma}(\mathrm{i}\omega_n)$ and $\widetilde{F}_{k\sigma}(\mathrm{i}\omega_n)$ shall be derived as well. From the properties given in Eqs. 3.21 it follows that $\widetilde{G}_{k\sigma}(\mathrm{i}\omega_n) = -G_{-k-\sigma}(-\mathrm{i}\omega_n)$, $[G_{k\sigma}(\mathrm{i}\omega_n)]^* = G_{k\sigma}(-\mathrm{i}\omega_n)$ and $[F_{k\sigma}(\mathrm{i}\omega_n)]^* = \widetilde{F}_{k\sigma}(-\mathrm{i}\omega_n)$ as well as $D_q(\mathrm{i}\omega_n) = D_{-q}(-\mathrm{i}\omega_n)$. Thus

$$\begin{aligned} \widetilde{G}^{\text{2nd}}_{k\sigma}(\mathrm{i}\omega_n) &= -G^{\text{2nd}}_{-k-\sigma}(-\mathrm{i}\omega_n) \\ &= \widetilde{G}^0_{k\sigma}(\mathrm{i}\omega_n)\, \Sigma^0_{k\sigma}(\mathrm{i}\omega_n)\, \widetilde{G}^0_{k\sigma}(\mathrm{i}\omega_n), \quad \Sigma^0_{k\sigma}(\mathrm{i}\omega_n) = -\frac{g^2}{N\beta}\sum_{qm}\widetilde{G}^0_{q\sigma}(\mathrm{i}\omega_m)\, D^0_{k-q}(\mathrm{i}\omega_n-\mathrm{i}\omega_m), \\ \widetilde{F}^{\text{2nd}}_{k\sigma}(\mathrm{i}\omega_n) &= [F^{\text{2nd}}_{k\sigma}(-\mathrm{i}\omega_n)]^* \\ &= \widetilde{G}^0_{k\sigma}(\mathrm{i}\omega_n)\, \Sigma^0_{k\sigma}(\mathrm{i}\omega_n)\, G^0_{k\sigma}(\mathrm{i}\omega_n), \quad \Sigma^0_{k\sigma}(\mathrm{i}\omega_n) = +\frac{g^2}{N\beta}\sum_{qm}\widetilde{F}^0_{q\sigma}(\mathrm{i}\omega_m)\, D^0_{k-q}(\mathrm{i}\omega_n-\mathrm{i}\omega_m). \end{aligned}$$

3.5.2 Homogeneous electron gas

The interaction within an *homogenous electron gas* reads [10, p. 165]

$$\mathrm{V} = \frac{1}{2} \sum_{kk'\sigma\sigma'q} U_q \, \mathrm{c}^+_{k+q\sigma} \mathrm{c}^+_{k'-q\sigma'} \mathrm{c}_{k'\sigma'} \mathrm{c}_{k\sigma} \quad \text{with} \quad U_q = \frac{e^2}{V} \frac{4\pi}{q^2}.$$

Normal Green function

The first-order term of the Feynman-Dyson perturbation series for $G_{k\sigma}(\tau)$ is thus

$$\begin{aligned} G^{1\mathrm{st}}_{k\sigma}(\tau) &= \frac{1}{2} \sum_{k'k''\sigma'\sigma''q} U_q \int_0^\beta \mathrm{d}\tau' \, \langle \ldots \rangle^{\mathrm{c.}}_0, \\ \langle \ldots \rangle_0 &= \langle \mathrm{T} \, \mathrm{c}_{k\sigma}[\tau] \, \mathrm{c}^+_{k'+q\sigma'}[\tau'] \, \mathrm{c}^+_{k''-q\sigma''}[\tau'] \, \mathrm{c}_{k''\sigma''}[\tau'] \, \mathrm{c}_{k'\sigma'}[\tau'] \, \mathrm{c}^+_{k\sigma}[0] \rangle_0 \\ &= \langle \mathrm{T} \, \mathrm{c}_{k\sigma}[\tau] \, \mathrm{c}^+_{k'+q\sigma'}[\tau'] \, \mathrm{c}_{k'\sigma'}[\tau'] \, \mathrm{c}^+_{k''-q\sigma''}[\tau'] \, \mathrm{c}_{k''\sigma''}[\tau'] \, \mathrm{c}^+_{k\sigma}[0] \rangle_0. \end{aligned}$$

A comparison with Eq. 3.22, the corresponding formula for the Holstein model, reveals that

$$\langle \ldots \rangle_0 = \sum_{q'} \delta^{-q}_{q'} \int_0^\beta \mathrm{d}\tau'' \, \delta(\tau'' - \tau'_+) \, \langle \mathrm{el.} \rangle_0,$$

where τ'_+ corresponds to a time infinitesimally later than τ' in order to ensure a causal time-ordering. The Kronecker delta is actually superflous for being contained in each term of $\langle \mathrm{el.} \rangle_0$ anyway. Once the factorized expression has been rewritten in terms of Green functions, the subscript plus sign can be dropped again. One finds

$$\sum_{k'k''\sigma'\sigma''q} U_q \langle \ldots \rangle^{\mathrm{c.}}_0 = 2 G^0_{k\sigma}(\tau - \tau') \overbrace{\left[U_0 \sum_{k'\sigma'} G^0_{k'\sigma'}(0) - \sum_q U_q \, G^0_{k-q\sigma}(0) \right]}^{\equiv \Lambda_{k\sigma}(0)} G^0_{k\sigma}(\tau').$$

As a function of Matsubara frequencies one has

$$\begin{aligned} G^{1\mathrm{st}}_{k\sigma}(\mathrm{i}\omega_n) &= \int_0^\beta \mathrm{d}\tau \, \mathrm{e}^{\mathrm{i}\omega_n \tau} G^{1\mathrm{st}}_{k\sigma}(\tau) = \int_0^\beta \mathrm{d}\tau \int_0^\beta \mathrm{d}\tau' \, \mathrm{e}^{\mathrm{i}\omega_n \tau} G^0_{k\sigma}(\tau - \tau') \, \Lambda_{k\sigma}(0) \, G^0_{k\sigma}(\tau') \\ &= \frac{1}{\beta} \sum_{ijm} G^0_{k\sigma}(\mathrm{i}\omega_i) \, \Lambda_{k\sigma}(\mathrm{i}\omega_m) \, G^0_{k\sigma}(\mathrm{i}\omega_j) \, \frac{1}{\beta} \int_0^\beta \mathrm{d}\tau \, \mathrm{e}^{\mathrm{i}(\omega_n - \omega_i)\tau} \, \frac{1}{\beta} \int_0^\beta \mathrm{d}\tau' \, \mathrm{e}^{\mathrm{i}(\omega_i - \omega_j)\tau'} \\ &= G^0_{k\sigma}(\mathrm{i}\omega_n) \, \Sigma^0_{k\sigma} \, G^0_{k\sigma}(\mathrm{i}\omega_n) \quad \text{with} \quad \Sigma^0_{k\sigma} = \frac{U_0}{\beta} \sum_{k'\sigma' m} G^0_{k'\sigma'}(\mathrm{i}\omega_m) - \frac{1}{\beta} \sum_{qm} U_{k-q} G^0_{q\sigma}(\mathrm{i}\omega_m). \end{aligned}$$

The two terms in $\Sigma^0_{k\sigma}$, which is independent of frequency because the Coulomb interaction is unscreened and assumed to be instantaneous, are the leading Hartree and Fock self-energy contributions. The former may be compensated exactly by a homogenous positive background, which is done in the so-called *jellium model* [10, p. 182].

Gor'kov-Green function

Analogously, during the calculation of $F^0_{k\sigma}(\tau)$ one obtains

$$\sum_{k'k''\sigma'\sigma''q} \langle \ldots \rangle^{\mathrm{c.}}_0 = 2 \sum_q U_q \, G^0_{k\sigma}(\tau - \tau') \, F^0_{k-q\sigma}(0) \, \widetilde{G}^0_{k\sigma}(\tau').$$

As in the case of the Holstein interaction, there is no anomalous Hartree contribution and, apart from the sign the anomalous Fock contribution formally resembles the normal one:

$$F^{1\mathrm{st}}_{k\sigma}(\mathrm{i}\omega_n) = G^0_{k\sigma}(\mathrm{i}\omega_n) \, \Sigma^0_{k\sigma} \, \widetilde{G}^0_{k\sigma}(\mathrm{i}\omega_n) \quad \text{with} \quad \Sigma^0_{k\sigma} = \frac{1}{\beta} \sum_{qm} U_{k-q} F^0_{q\sigma}(\mathrm{i}\omega_m).$$

3.5.3 Hubbard model

The *Hubbard model* further restricts the Coulomb interaction to occur only between electrons at the same site, which must consequently have opposite spins because of the Pauli principle. With the on-site Coulomb repulsion U, the corresponding operator in real space reads [30]

$$V = U \sum_{R} c^{+}_{R\uparrow} c^{+}_{R\downarrow} c_{R\downarrow} c_{R\uparrow}.$$

As for the Holstein model, a discrete Fourier transform using Eq. A.1 is applied, yielding

$$\begin{aligned} V &= \frac{U}{N} \sum_{kk'qq'} \frac{1}{N} \sum_{R} e^{i(q+q'-k-k')R} c^{+}_{q'\uparrow} c^{+}_{q\downarrow} c_{k'\downarrow} c_{k\uparrow} \\ &= \frac{U}{N} \sum_{kk'q} c^{+}_{k+k'-q\uparrow} c^{+}_{q\downarrow} c_{k'\downarrow} c_{k\uparrow} = \frac{U}{N} \sum_{kk'q} c^{+}_{k+q\uparrow} c^{+}_{k'-q\downarrow} c_{k'\downarrow} c_{k\uparrow}. \end{aligned}$$

Normal Green function

In terms of $\langle \text{el.} \rangle_0$ from Eq. 3.22, the first order of the perturbation series for $G_{k\sigma}(\tau)$ reads

$$G^{1st}_{k\sigma}(\tau) = \frac{U}{N} \sum_{k'k''\sigma'\sigma''qq'} \delta^{\uparrow}_{\sigma'} \delta^{\downarrow}_{\sigma''} \delta^{-q}_{q'} \int_0^\beta d\tau' \int_0^\beta d\tau'' \, \delta(\tau'' - \tau'_+) \langle \text{el.} \rangle^{c}_{0}.$$

Since interactions between electrons with the same spin are not considered in this model, an electron cannot interact with itself and thus there is no Fock contribution. The Hartree part is

$$G^{1st}_{k\sigma}(i\omega_n) = G^{0}_{k\sigma}(i\omega_n) \, \Sigma^{0}_{\sigma} \, G^{0}_{k\sigma}(i\omega_n) \quad \text{with} \quad \Sigma^{0}_{\sigma} = \frac{U}{N\beta} \sum_{k'm} G^{0}_{k'-\sigma}(i\omega_m).$$

Gor'kov-Green function

Nevertheless, the analogous calculation of $F_{k\sigma}(\tau)$ yields the usual anomalous Fock contribution

$$F^{1st}_{k\sigma}(i\omega_n) = G^{0}_{k\sigma}(i\omega_n) \, \Sigma^{0}_{\sigma} \, \widetilde{G}^{0}_{k\sigma}(i\omega_n) \quad \text{with} \quad \Sigma^{0}_{\sigma} = \frac{U}{N\beta} \sum_{qm} F^{0}_{q\sigma}(i\omega_m).$$

3.6 Self-energy

The full Green function is found by adding *all* diagrams, that are properly connected. But which are valid connections? In Fig. 3.1, each diagram features three fermion lines, a single boson line and two vertices at each of which one fermion is annihilated and another created under the influence of one boson. This process is simultaneous and conserves both momentum and spin. Leaving the anomalous lines $\rightarrow\!\leftarrow$ and $\leftarrow\!\rightarrow$ out of account for the moment, a general diagram for this type of interaction contains

$n \times$, $(2n+1) \times$ and $2n \times$  with $n \in \mathbb{N}$,

where the gray lines define the *'contacts'*. As a consequence, there is always one in- and one outgoing side of a fermion line, which is not connected to a vertex.

It is convenient to define the *self-energy* $\Sigma = \sum_i \Sigma_i$ as the sum of all *irreducible* diagram parts Σ_i, i.e. such which can not be split into two disconnected parts by *'cutting'* one fermion line, because a way to generate all diagrams is to take all permutations of all possible subsets of all irreducible parts and join them with fermion lines:

$$\begin{aligned} G &= G_0 + G_0 \Sigma G_0 + G_0 \Sigma G_0 \Sigma G_0 + \dots \\ &= G_0 + G_0 \Sigma (G_0 + G_0 \Sigma G_0 + \dots) \\ &= G_0 + G_0 \Sigma G. \end{aligned}$$

This is knows as the *Dyson equation* which can also be formulated diagrammatically as

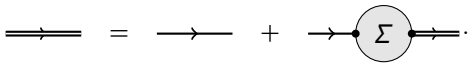

(3.23a)

Since the *'dressed'* G appears on both sides of the equation, the latter defines a self-consistency problem. It can be solved iteratively, i.e. by calculating $G_{n+1} = G_0 + G_0 \Sigma G_n$ with the *'bare'* G_0 as the initial value. At each step a higher number of diagrams is considered. Multiplication with G_0^{-1} from the left and G^{-1} from the right side yields

$$G^{-1} = G_0^{-1} - \Sigma.$$

The denominators of G and G_0 contain the excitation energies of the full and the unperturbed system, as can be seen in Eq. 3.13 and Eq. 3.15, respectively. Thus Σ acts as an energy *renormalization*.

How can the full self-energy be obtained? It turns out that it can be derived from the leading self-energy contributions, calculated in the previous section and shown in Fig. 3.1a and 3.1b, through renormalization of selected lines and even one vertex. This yields

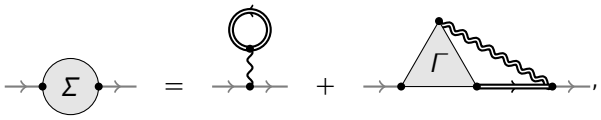

(3.23b)

where the *full vertex* Γ has been introduced. The Hartree term on the left can be either neglected, as in the phonon case, or incorporated into the single-particle dispersion relation.

The dressed boson Green function, D say, obeys another Dyson equation,

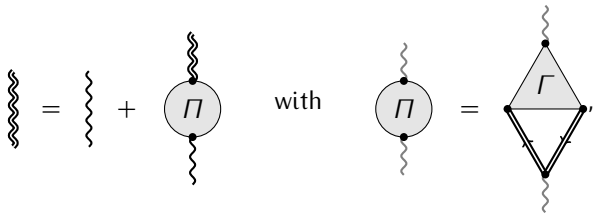

(3.23c)

where the corresponding self-energy Π is referred to as the *polarization*.

Finally, the full vertex is given by the plain vertex together with vertex corrections, i.e. by all diagram parts with can mediate a boson-induced fermionic transition:

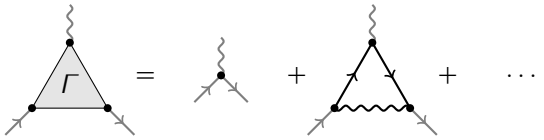

Unfortunately, there is no integral equation for Γ that could be formulated diagrammatically with nothing but the building blocks introduced so far, since the vertex corrections involve a functional derivative of the self-energy with respect to the dressed Green function. Representing this part with a trapezoidal shape, one can write

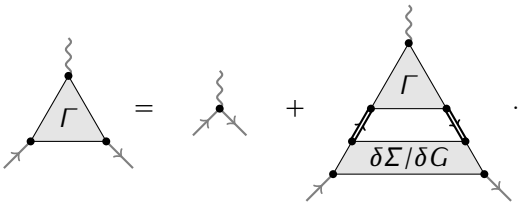

(3.23d)

Eqs. 3.23, known as *Hedin's equations* [31, Appendix A; 32, Eqs. 13.19], are all coupled among themselves, which makes their solution a non-trivial task. In practice one often applies certain approximations, which are presented in the following.

3.6.1 GW approximation

A considable simplification consists in neglecting all vertex corrections, i.e. replacing Γ with the bare vertex [31, Eq. A27, A28; 32, Eqs. 13.20, 13.21]. The corresponding diagram reads:

(3.24)

Since the dressed boson line is often denoted as W, this is known as the *GW approximation* with reference to the resulting formula for the Fock part of Σ. With focus on Π and for historical reasons it is also referred to as the *random-phase approximation* (RPA).

3.6.2 HF approximation

The self-energy can be further simplified by neglecting the polarization and thus replacing all dressed boson lines with simple ones. This yields the *Hartree-Fock approximation* (HF):

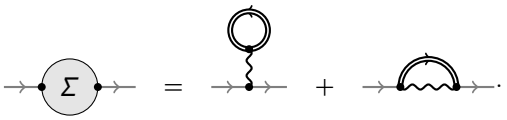

(3.25)

Within HF, many-body problems can always be mapped onto effective single-particle problems.

Chapter 4

Eliashberg theory

Based on the results presented in the previous chapter, one can formulate a set of equations, namely the Eliashberg equations, which determine self-energies for both normal and anomalous Green functions, the latter being suitable order parameters for the superconducting state.

To that end it is convenient to combine the Green functions of interest into a 2×2 matrix, i.e. to use the Nambu formalism, which is presented in the first section.[1] With that, the general form of the Eliashberg equations on the imaginary frequency axis is derived, followed by two common approximations which assume (1) a local self-energy and (2) a constant density of states. Next, it is shown how the corresponding real-axis equations can be obtained through analytic continuation. On this basis McMillan's formula for the critical temperature is derived, whereby the Coulomb pseudo-potential is introduced. This requires a more detailed discussion of rescaling of the Coulomb interaction, leading to results which are also useful in dealing with the chemical potential. After that, the whole formalism is generalized to multiple electronic bands. The penultimate section is dedicated to the determination of the critical temperature via linearized Eliashberg equations. Finally, it is demonstrated how imaginary-axis results can be continued to the real axis by means of Padé approximants.

4.1 Nambu formalism

As found by Nambu [33], the Dyson equations for all four electronic Green functions introduced at the beginning of Section 3.5 can be compactly formulated as a single matrix equation. Diagrammatically, within the GW approximation and without Hartree contributions, it reads

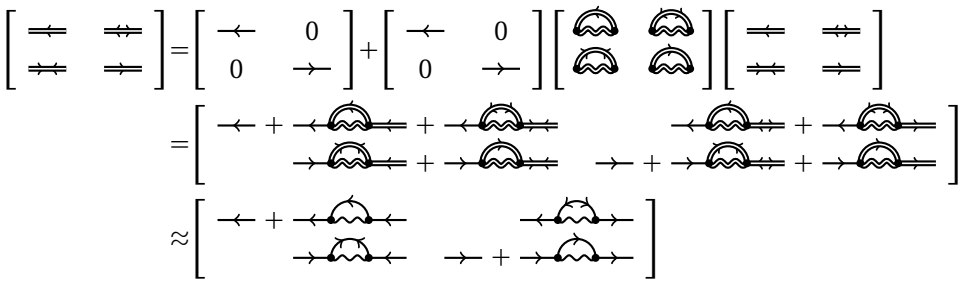

and formally, where quantum numbers and frequency arguments have been suppressed,

$$\begin{aligned}
\begin{bmatrix} G & F \\ \widetilde{F} & \widetilde{G} \end{bmatrix} &= \begin{bmatrix} G_0 & 0 \\ 0 & \widetilde{G}_0 \end{bmatrix} + \begin{bmatrix} G_0 & 0 \\ 0 & \widetilde{G}_0 \end{bmatrix} \begin{bmatrix} \Sigma^G & \Sigma^F \\ \Sigma^{\widetilde{F}} & \Sigma^{\widetilde{G}} \end{bmatrix} \begin{bmatrix} G & F \\ \widetilde{F} & \widetilde{G} \end{bmatrix} \\
&= \begin{bmatrix} G_0 + G_0\Sigma^G G + G_0\Sigma^F \widetilde{F} & G_0\Sigma^G F + G_0\Sigma^F \widetilde{G} \\ \widetilde{G}_0\Sigma^{\widetilde{F}} G + \widetilde{G}_0\Sigma^{\widetilde{G}} \widetilde{F} & \widetilde{G}_0 + \widetilde{G}_0\Sigma^{\widetilde{F}} F + \widetilde{G}_0\Sigma^{\widetilde{G}} \widetilde{G} \end{bmatrix} \\
&\approx \begin{bmatrix} G_0 + G_0\Sigma_0^G G_0 & G_0\Sigma_0^F \widetilde{G}_0 \\ \widetilde{G}_0\Sigma_0^{\widetilde{F}} G_0 & \widetilde{G}_0 + \widetilde{G}_0\Sigma_0^{\widetilde{G}} \widetilde{G}_0 \end{bmatrix}.
\end{aligned} \tag{4.1}$$

$\rightarrow\!\leftarrow$ and $\leftarrow\!\rightarrow$ vanish, so does each term of the perturbation series of $\rightrightarrows\!\leftleftarrows$ and $\leftrightarrows$. However, a non-zero self-consistent solution of the above integral equations may still exist [33, before Eq. 2.14], which is exactly the case in the superconducting state. It implies that the number of electrons is not necessarily conserved, but this becomes insignificant in the macroscopic limit [10, p. 423]. The critical temperature may be defined as the highest temperature which allows the off-diagonal components to be non-zero [34, p. 37].

Giving names to the involved matrices, the Dyson equation may be written as $\boldsymbol{G} = \boldsymbol{G}_0 + \boldsymbol{G}_0\boldsymbol{\Sigma}\boldsymbol{G}$ or $\boldsymbol{G}^{-1} = \boldsymbol{G}_0^{-1} - \boldsymbol{\Sigma}$, using inverse matrices. With the help of the two-component operators

$$\Psi_k = \begin{bmatrix} c_{k\uparrow} \\ c^+_{-k\downarrow} \end{bmatrix} \quad \text{and} \quad \Psi_k^+ = \begin{bmatrix} a^+_{k\uparrow} & a_{-k\downarrow} \end{bmatrix}$$

the dressed (bare) Green function matrix is concisely defined as

$$\boldsymbol{G}_k^{(0)}(i\omega_n) = -\int_0^\beta d\tau\, e^{i\omega_n\tau}\langle \Psi_k(\tau)\, \Psi_k^+(0)\rangle_{(0)}.$$

Introducing unit and Pauli matrices

$$\boldsymbol{\sigma}_0 = \begin{bmatrix} 1 & 0 \\ 0 & 1 \end{bmatrix}, \quad \boldsymbol{\sigma}_1 = \begin{bmatrix} 0 & 1 \\ 1 & 0 \end{bmatrix}, \quad \boldsymbol{\sigma}_2 = \begin{bmatrix} 0 & -i \\ i & 0 \end{bmatrix}, \quad \boldsymbol{\sigma}_3 = \begin{bmatrix} 1 & 0 \\ 0 & -1 \end{bmatrix}$$

and the real scalar functions $Z_k(i\omega_n)$, $\phi_k^{(\prime)}(i\omega_n)$ and $\chi_k(i\omega_n)$, the self-energy matrix is written as

$$\begin{aligned} \boldsymbol{\Sigma}_k(i\omega_n) &= i\omega_n[1 - Z_k(i\omega_n)]\boldsymbol{\sigma}_0 + \phi_k(i\omega_n)\boldsymbol{\sigma}_1 + \phi'_k(i\omega_n)\boldsymbol{\sigma}_2 + \chi_k(i\omega_n)\boldsymbol{\sigma}_3 \\ &= \begin{bmatrix} i\omega_n[1 - Z_k(i\omega_n)] + \chi_k(i\omega_n) & \phi_k(i\omega_n) - i\phi'_k(i\omega_n) \\ \phi_k(i\omega_n) + i\phi'_k(i\omega_n) & i\omega_n[1 - Z_k(i\omega_n)] - \chi_k(i\omega_n) \end{bmatrix}. \end{aligned} \tag{4.2}$$

With $[\boldsymbol{G}_k^0(i\omega_n)]^{-1} = i\omega_n\boldsymbol{\sigma}_0 - (\varepsilon_k - \mu)\boldsymbol{\sigma}_3$, where μ is the chemical potential which for simplicity has been dropped in the derivations of Section 3.2, the Dyson equation reads

$$\begin{aligned} \boldsymbol{G}_k^{-1}(i\omega_n) &= [\boldsymbol{G}_k^0(i\omega_n)]^{-1} - \boldsymbol{\Sigma}_k(i\omega_n) \\ &= i\omega_n Z_k(i\omega_n)\boldsymbol{\sigma}_0 - \phi_k(i\omega_n)\boldsymbol{\sigma}_1 - \phi'_k(i\omega_n)\boldsymbol{\sigma}_2 - [\varepsilon_k - \mu + \chi_k(i\omega_n)]\boldsymbol{\sigma}_3 \\ &= \begin{bmatrix} i\omega_n Z_k(i\omega_n) - \varepsilon_k + \mu - \chi_k(i\omega_n) & -\phi_k(i\omega_n) + i\phi'_k(i\omega_n) \\ -\phi_k(i\omega_n) - i\phi'_k(i\omega_n) & i\omega_n Z_k(i\omega_n) + \varepsilon_k - \mu + \chi_k(i\omega_n) \end{bmatrix}. \end{aligned}$$

Inversion yields

$$\begin{aligned} \boldsymbol{G}_k(i\omega_n) &= -\Theta_k^{-1}(n)\{i\omega_n Z_k(i\omega_n)\boldsymbol{\sigma}_0 + \phi_k(i\omega_n)\boldsymbol{\sigma}_1 + \phi'_k(i\omega_n)\boldsymbol{\sigma}_2 + [\varepsilon_k - \mu + \chi_k(i\omega_n)]\boldsymbol{\sigma}_3\} \\ &= -\frac{1}{\Theta_k(n)}\begin{bmatrix} i\omega_n Z_k(i\omega_n) + \varepsilon_k - \mu + \chi_k(i\omega_n) & \phi_k(i\omega_n) - i\phi'_k(i\omega_n) \\ \phi_k(i\omega_n) + i\phi'_k(i\omega_n) & i\omega_n Z_k(i\omega_n) - \varepsilon_k + \mu - \chi_k(i\omega_n) \end{bmatrix}, \end{aligned}$$

where the denominator is given by

$$\Theta_k(n) = -\det \boldsymbol{G}_k^{-1}(i\omega_n) = [\omega_n Z_k(i\omega_n)]^2 + [\varepsilon_k - \mu + \chi_k(i\omega_n)]^2 + \phi_k^2(i\omega_n) + \phi_k'^2(i\omega_n).$$

The excitation energies are the poles of $\boldsymbol{G}_k(i\omega_n)$, i.e. the zeros of $\Theta_k(n)$, which satisfy

$$(i\omega_n)^2 = \left[\frac{\varepsilon_k - \mu + \chi_k(i\omega_n)}{Z_k(i\omega_n)}\right]^2 + \frac{\phi_k^2(i\omega_n) + \phi_k'^2(i\omega_n)}{Z_k^2(i\omega_n)} \equiv \widetilde{\varepsilon}_k^2(i\omega_n) + |\Delta_k(i\omega_n)|^2.$$

This identifies $Z_k(i\omega_n)$ as a renormalization function, $\chi_k(i\omega_n)$ as an energy shift and $\phi_k^{(\prime)}(i\omega_n)$ as an order parameter for the superconducting state just like the energy gap which turns out to be

$$\Delta_k(i\omega_n) = \frac{\phi_k(i\omega_n) - i\phi'_k(i\omega_n)}{Z_k(i\omega_n)}.$$

[1] These derivations are guided by Section 3.2 of Ref. 35 and Section II of Ref. 36.

4.2 General equations

Considering the HUBBARD (HOLSTEIN) model, the approximation made in Eq. 4.1 is correct up to the first (second) order of the perturbation series. From the analytic expressions derived in Section 3.5.3 (3.5.1) on can thus derive the self-energy for the *HUBBARD-HOLSTEIN model*,

$$\boldsymbol{\Sigma}_k(\mathrm{i}\omega_n) = \boldsymbol{\Sigma}_k^{\text{el.}} + \boldsymbol{\Sigma}_k^{\text{ph.}}(\mathrm{i}\omega_n).$$

Within the HF approximation defined in Eq. 3.25 one can include any contribution from the COULOMB interaction into the single-particle energies ε_k and therewith into the bare GREEN function matrix $\boldsymbol{G}_0$. In doing so for the normal state [34, p. 37], the electronic part reads

$$\begin{aligned}\boldsymbol{\Sigma}_k^{\text{el.}} = \frac{U}{N\beta}\sum_{qm}[\boldsymbol{G}_q(\mathrm{i}\omega_m) - \boldsymbol{G}_q^{\text{n.}}(\mathrm{i}\omega_m)] &\approx \frac{U}{N\beta}\sum_{qm}\boldsymbol{G}_q^{\text{od.}}(\mathrm{i}\omega_m) \\ &= -\frac{U}{N\beta}\sum_{qm}\frac{\phi_q(\mathrm{i}\omega_m)\boldsymbol{\sigma}_1 + \phi'_q(\mathrm{i}\omega_m)\boldsymbol{\sigma}_2}{\Theta_q(m)},\end{aligned}$$

where *'n.'* denotes the normal-state GREEN function and *'od.'* indicates that components which are not *'off-diagonal'* have been nullified. The above approximation becomes exact at the critical temperature and is also valid below [34, p. 38] since the diagonal components are not very sensitive to changes in temperature.

For the phononic part the GW approximation defined in Eq. 3.24 is used. In the case of the electron-phonon interaction this is a rather good approximation since vertex corrections can be neglected according to MIGDAL's theorem [37]. Thus

$$\begin{aligned}\boldsymbol{\Sigma}_k^{\text{ph.}}(\mathrm{i}\omega_n) &= -\frac{g^2}{N\beta}\sum_{qm}\boldsymbol{\sigma}_3\,\boldsymbol{G}_q(\mathrm{i}\omega_m)\,\boldsymbol{\sigma}_3\,D_{k-q}(\mathrm{i}\omega_n - \mathrm{i}\omega_m) \\ &= \frac{g^2}{N\beta}\sum_{qm}\frac{\mathrm{i}\omega_m Z_q(\mathrm{i}\omega_m)\boldsymbol{\sigma}_0 - \phi_q(\mathrm{i}\omega_m)\boldsymbol{\sigma}_1 - \phi'_q(\mathrm{i}\omega_m)\boldsymbol{\sigma}_2 + [\varepsilon_q - \mu + \chi_q(\mathrm{i}\omega_m)]\boldsymbol{\sigma}_3}{\Theta_q(m)}D_{k-q}(\mathrm{i}\omega_n - \mathrm{i}\omega_m),\end{aligned}$$

where the PAULI matrices in the first line swap the sign of the off-diagonal components.

From now on, $T = \beta^{-1}$ is used rather than β. A coefficient comparison with Eq. 4.2 yields the *ELIASHBERG equations* [4] for the HUBBARD-HOLSTEIN model:

$$\mathrm{i}\omega_n[1 - Z_k(\mathrm{i}\omega_n)] = \frac{T}{N}\sum_{qm}\frac{\mathrm{i}\omega_m Z_q(\mathrm{i}\omega_m)}{\Theta_q(m)}g^2 D_{k-q}(\mathrm{i}\omega_n - \mathrm{i}\omega_m), \tag{4.3a}$$

$$\phi_k^{(\prime)}(\mathrm{i}\omega_n) = -\frac{T}{N}\sum_{qm}\frac{\phi_q^{(\prime)}(\mathrm{i}\omega_m)}{\Theta_q(m)}\big[g^2 D_{k-q}(\mathrm{i}\omega_n - \mathrm{i}\omega_m) + U\big], \tag{4.3b}$$

$$\chi_k(\mathrm{i}\omega_n) = \frac{T}{N}\sum_{qm}\frac{\varepsilon_q - \mu + \chi_q(\mathrm{i}\omega_m)}{\Theta_q(m)}g^2 D_{k-q}(\mathrm{i}\omega_n - \mathrm{i}\omega_m). \tag{4.3c}$$

Since $\phi_k(\mathrm{i}\omega_n)$ and $\phi'_k(\mathrm{i}\omega_n)$ obey identical equations and enter the common denominator $\Theta_q(\mathrm{i}\omega_m)$ only in form of the absolute value $|\phi_k(\mathrm{i}\omega) - \mathrm{i}\phi'_k(\mathrm{i}\omega_n)|^2$, the phase of $\phi_k(\mathrm{i}\omega) - \mathrm{i}\phi'_k(\mathrm{i}\omega_n)$ is left undetermined. This gauge invariance allows to set $\phi'_k(\mathrm{i}\omega_n) = 0$ [34, p. 37; 33, around Eq. 2.20].

Using the definitions

$$\mu_C = n(\mu_0)\,U, \quad \lambda_q(n) = -n(\mu_0)\,g^2 D_q(\mathrm{i}\nu_n), \quad n(\varepsilon) = \frac{N(\varepsilon)}{N}, \quad N(\varepsilon) = \sum_k \delta(\varepsilon - \varepsilon_k), \tag{4.4}$$

where $n(\varepsilon)$ is the density of states per spin and unit cell and μ_0 is the free-particle chemical potential, one can equivalently write

$$\begin{aligned}\boldsymbol{\Sigma}_k(\mathrm{i}\omega_n) = \frac{T}{N(\mu_0)}\sum_{qm}\Theta_q^{-1}(m)\big\{&\cdots \\ \cdots\{-\mathrm{i}\omega_m Z_q(\mathrm{i}\omega_m)\boldsymbol{\sigma}_0 + \phi_q(\mathrm{i}\omega_m)\boldsymbol{\sigma}_1 - [\varepsilon_q - \mu + \chi_q(\mathrm{i}\omega_m)]\boldsymbol{\sigma}_3\}\lambda_{k-q}(n-m) - \phi_q(\mathrm{i}\omega_m)\boldsymbol{\sigma}_1\mu_C\big\},&\end{aligned}$$

which yields a more common formulation of the ELIASHBERG equations:

$$Z_{\boldsymbol{k}}(\mathrm{i}\omega_n) = 1 + \frac{T}{N(\mu_0)}\frac{1}{\omega_n}\sum_{\boldsymbol{q}m}\frac{\omega_m Z_{\boldsymbol{q}}(\mathrm{i}\omega_m)}{\Theta_{\boldsymbol{q}}(m)}\lambda_{\boldsymbol{k}-\boldsymbol{q}}(n-m), \tag{4.5a}$$

$$\phi_{\boldsymbol{k}}(\mathrm{i}\omega_n) = \frac{T}{N(\mu_0)}\sum_{\boldsymbol{q}m}\frac{\phi_{\boldsymbol{q}}(\mathrm{i}\omega_m)}{\Theta_{\boldsymbol{q}}(m)}\big[\lambda_{\boldsymbol{k}-\boldsymbol{q}}(n-m) - \mu_{\mathrm{C}}\big], \tag{4.5b}$$

$$\chi_{\boldsymbol{k}}(\mathrm{i}\omega_n) = -\frac{T}{N(\mu_0)}\sum_{\boldsymbol{q}m}\frac{\varepsilon_{\boldsymbol{q}} - \mu + \chi_{\boldsymbol{q}}(\mathrm{i}\omega_m)}{\Theta_{\boldsymbol{q}}(m)}\lambda_{\boldsymbol{k}-\boldsymbol{q}}(n-m). \tag{4.5c}$$

It is often convenient to work with the spectral representations

$$D_{\boldsymbol{q}}(\mathrm{i}\nu_n) = -\int_0^\infty \mathrm{d}\omega\,\frac{2\omega\,B_{\boldsymbol{q}}(\omega)}{\nu_n^2+\omega^2},$$
$$\lambda_{\boldsymbol{q}}(n) = \int_0^\infty \mathrm{d}\omega\,\frac{2\omega\,\alpha^2F_{\boldsymbol{q}}(\omega)}{\nu_n^2+\omega^2} \quad \text{with} \quad \alpha^2F_{\boldsymbol{q}}(\omega) = n(\mu_0)\,g^2B_{\boldsymbol{q}}(\omega).$$

$B_{\boldsymbol{q}}(\omega)$ and $\alpha^2F_{\boldsymbol{q}}(\omega)$ are *phonon* and *electron-phonon spectral functions*, respectively. The name of the latter is composed of the traditional names α for the matrix element g of the electron-phonon coupling [37, Eq. 1, e.g.] and $F(\omega)$ for the phonon density of states [34, p. 16], which is basically the $\boldsymbol{q}$-average of the spectral function $B_{\boldsymbol{q}}(\omega)$.

In order to conserve the particle number, the chemical potential μ has to be determined self-consistently alongside the self-energy components. This is discussed in detail in Section 4.7.

4.3 Common approximations

The numerical solution of the ELIASHBERG equations in the form presented in Eq. 4.5 involves a high computational workload, especially because of the summations over the BRILLOUIN zone. It is therefore common to apply certain approximations.

4.3.1 Local self-energy

If the electron-phonon coupling strength $\lambda_{\boldsymbol{q}}(n) \equiv \lambda(n)$ is independent of $\boldsymbol{q}$, the self-energy $\boldsymbol{\Sigma}_{\boldsymbol{k}}(\mathrm{i}\omega_n) \equiv \boldsymbol{\Sigma}(\mathrm{i}\omega_n)$ and its components Z, ϕ and χ are independent of $\boldsymbol{k}$, i.e. *local*. This is achieved, say, by taking a FERMI-surface average $\langle\langle\alpha^2F\rangle_{\varepsilon_{\boldsymbol{k}}=\mu}\rangle_{\varepsilon_{\boldsymbol{k}+\boldsymbol{q}}=\mu}$ [34, Eqs. 3.23, 3.24], where

$$\langle f_{\boldsymbol{k}}\rangle_{\varepsilon_{\boldsymbol{k}}=\mu} = \frac{\sum_{\boldsymbol{k}}\delta(\varepsilon_{\boldsymbol{k}}-\mu)\,f_{\boldsymbol{k}}}{\sum_{\boldsymbol{k}}\delta(\varepsilon_{\boldsymbol{k}}-\mu)},$$

or by assuming the simplest spectral function $B(\omega) = \delta(\omega-\omega_{\mathrm{E}}) - \delta(\omega+\omega_{\mathrm{E}})$, where ω_{E} is a single EINSTEIN frequency which is already renormalized. In the latter case,

$$D(\mathrm{i}\nu_n) = -\frac{2\omega_{\mathrm{E}}}{\nu_n^2+\omega_{\mathrm{E}}^2} \quad \text{and} \quad \lambda(n) = \frac{2\omega_{\mathrm{E}}\,n(\mu_0)\,g^2}{\nu_n^2+\omega_{\mathrm{E}}^2} \equiv \frac{\lambda}{1+\left[\frac{\nu_n}{\omega_{\mathrm{E}}}\right]^2},$$

where $\lambda \equiv \lambda(0) = 2n(\mu_0)\,g^2/\omega_{\mathrm{E}}$ is the parameter which will subsequently be used to define the electron-phonon coupling strength and $D(\mathrm{i}\nu_n)$ resembles the bare phonon GREEN function $D_0(\mathrm{i}\nu_n)$ for the HAMILTON operator

$$\mathrm{H}_0 = \omega_{\mathrm{E}}\sum_{\boldsymbol{R}}\mathrm{b}^+_{\boldsymbol{R}}\mathrm{b}_{\boldsymbol{R}} = \omega_{\mathrm{E}}\sum_{\boldsymbol{q}\boldsymbol{q}'}\frac{1}{N}\sum_{\boldsymbol{R}}\mathrm{e}^{\mathrm{i}(\boldsymbol{q}'-\boldsymbol{q})\boldsymbol{R}}\mathrm{b}^+_{\boldsymbol{q}'}\mathrm{b}_{\boldsymbol{q}} = \omega_{\mathrm{E}}\sum_{\boldsymbol{q}}\mathrm{b}^+_{\boldsymbol{q}}\mathrm{b}_{\boldsymbol{q}}.$$

It is now possible to replace the $\boldsymbol{q}$-summation by an energy integral:

$$\boldsymbol{\Sigma}(\mathrm{i}\omega_n) = T\sum_m\int_{-\infty}^{\infty}\mathrm{d}\varepsilon\,\frac{N(\varepsilon)}{N(\mu_0)}\Theta^{-1}(\varepsilon,m)\big\{\cdots$$
$$\cdots\{-\mathrm{i}\omega_m Z(\mathrm{i}\omega_m)\boldsymbol{\sigma}_0 + \phi(\mathrm{i}\omega_m)\boldsymbol{\sigma}_1 - [\varepsilon-\mu+\chi(\mathrm{i}\omega_m)]\boldsymbol{\sigma}_3\}\lambda(n-m) - \phi(\mathrm{i}\omega_m)\boldsymbol{\sigma}_1\mu_{\mathrm{C}}\big\} \tag{4.6}$$

with $\Theta(\varepsilon, n) = [\omega_n Z(\mathrm{i}\omega_n)]^2 + \phi^2(\mathrm{i}\omega_n) + [\varepsilon - \mu + \chi(\mathrm{i}\omega_n)]^2$. The *local* Eliashberg *equations* read

$$Z(\mathrm{i}\omega_n) = 1 + \frac{T}{\omega_n} \sum_m \int_{-\infty}^{\infty} \mathrm{d}\varepsilon \frac{N(\varepsilon)}{N(\mu_0)} \frac{\omega_m Z(\mathrm{i}\omega_m)}{\Theta(\varepsilon, m)} \lambda(n-m), \tag{4.7a}$$

$$\phi(\mathrm{i}\omega_n) = T \sum_m \int_{-\infty}^{\infty} \mathrm{d}\varepsilon \frac{N(\varepsilon)}{N(\mu_0)} \frac{\phi(\mathrm{i}\omega_m)}{\Theta(\varepsilon, m)} [\lambda(n-m) - \mu_\mathrm{C}], \tag{4.7b}$$

$$\chi(\mathrm{i}\omega_n) = -T \sum_m \int_{-\infty}^{\infty} \mathrm{d}\varepsilon \frac{N(\varepsilon)}{N(\mu_0)} \frac{\varepsilon - \mu + \chi(\mathrm{i}\omega_m)}{\Theta(\varepsilon, m)} \lambda(n-m). \tag{4.7c}$$

4.3.2 Constant density of states

Save for the factor $N(\varepsilon)$, which is unspecified at this point, the integrands in Eq. 4.6 converge towards zero as ε diverges from $\mu - \chi(\mathrm{i}\omega_m) \approx \mu_0$. Therefore it may be acceptable to approximate $N(\varepsilon)$ by a constant $N(\mu_0)$ [38, below Eq. 26; 34, p. 17; 36, Section II.B], which is visualized in Fig. 4.1, so that the integration can be performed analytically. With the help of

$$\frac{1}{\pi} \int_{-\infty}^{\infty} \mathrm{d}x \frac{z}{x^2 + z^2} = \operatorname{sgn} \operatorname{Re} z \quad \text{and} \quad \int_{-\infty}^{\infty} \mathrm{d}x \frac{x}{x^2 + z^2} = 0, \tag{4.8}$$

where vanishing and non-vanishing integrals are understood as Cauchy principal values or follow from the residue theorem, respectively, and writing $\Delta(\mathrm{i}\omega_n) = \phi(\mathrm{i}\omega_n)/Z(\mathrm{i}\omega_n)$, this yields

$$\boldsymbol{\Sigma}(\mathrm{i}\omega_n) = \pi T \sum_m \frac{\{-\mathrm{i}\omega_m \boldsymbol{\sigma}_0 + \Delta(\mathrm{i}\omega_m)\boldsymbol{\sigma}_1\}\lambda(n-m) - \Delta(\mathrm{i}\omega_m)\boldsymbol{\sigma}_1 \mu_\mathrm{C}}{\sqrt{\omega_m^2 + \Delta^2(\mathrm{i}\omega_m)}}$$

and thus the *CDOS* Eliashberg *equations*

$$Z(\mathrm{i}\omega_n) = 1 + \frac{\pi T}{\omega_n} \sum_m \frac{\omega_m}{\sqrt{\omega_m^2 + \Delta^2(\mathrm{i}\omega_m)}} \lambda(n-m), \tag{4.9a}$$

$$\Delta(\mathrm{i}\omega_n) = \frac{\pi T}{Z(\mathrm{i}\omega_n)} \sum_m \frac{\Delta(\mathrm{i}\omega_m)}{\sqrt{\omega_m^2 + \Delta^2(\mathrm{i}\omega_m)}} [\lambda(n-m) - \mu_\mathrm{C}]. \tag{4.9b}$$

The chemical potential and the energy shift have disappeared from the equations and the density of states only enters through the coupling strengths.

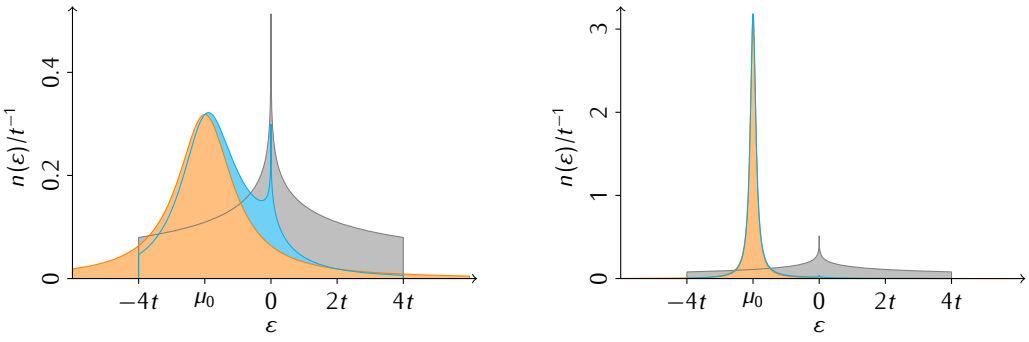

(a) $\omega = t$. At higher frequencies, exact and approximate integrand may differ considerably.

(b) $\omega = t/10$. At lower frequencies, points for numerical integration must be chosen carefully.

Figure 4.1: The CDOS approximation is exemplified by its application to the scalar product of the density of states $n(\varepsilon)$ of a square tight-binding lattice, to be discussed in Section 5.1.2, and a Lorentz function:

$$\frac{1}{\pi} \int_{-\infty}^{\infty} \mathrm{d}\varepsilon \frac{n(\varepsilon)}{n(\mu_0)} \frac{\omega}{\omega^2 + \varepsilon^2} \quad (\text{⬬}) \quad \approx \quad \frac{1}{\pi} \int_{-\infty}^{\infty} \mathrm{d}\varepsilon \frac{\omega}{\omega^2 + \varepsilon^2} \quad (\text{⬬}) \,.$$

The exact integral bears a close resemblance to those which occur in the local self energy in Eq. 4.6.

4.4 Real-axis equations

In this section the analytic continuation of the self-energy and the corresponding ELIASHBERG equations, which is complicated by the summation over MATSUBARA frequencies, is performed within the CDOS approximation.

The first step is to withdraw the dependence on MATSUBARA frequencies from the GREEN function using a spectral representation. Undoing the energy integration and applying Eq. 3.10,

$$\int_{-\infty}^{\infty} \mathrm{d}\varepsilon\, \boldsymbol{G}_\varepsilon(\mathrm{i}\omega_n) = -\frac{1}{\pi} \int_{-\infty}^{\infty} \mathrm{d}\omega' \, \frac{1}{\mathrm{i}\omega_n - \omega'} \, \mathrm{Im} \int_{-\infty}^{\infty} \mathrm{d}\varepsilon\, \boldsymbol{G}_\varepsilon(\omega'_+),$$

where $\omega'_+ = \omega' + \mathrm{i}0^+$. The GREEN function matrix, analytically continued to arbitrary frequency arguments ω and dependent on energy $\varepsilon_{\boldsymbol{k}}$ rather than wave number $\boldsymbol{k}$, reads

$$\boldsymbol{G}_\varepsilon(\omega) = \frac{\omega Z(\omega)\boldsymbol{\sigma}_0 + \phi(\omega)\boldsymbol{\sigma}_1 + \varepsilon\boldsymbol{\sigma}_3}{\omega^2 Z^2(\omega) - \phi^2(\omega) - \varepsilon^2}.$$

Using Eqs. 4.8 one finds, in accordance with Eq. 2.19a of Ref. 39,

$$-\frac{1}{\pi} \int_{-\infty}^{\infty} \mathrm{d}\varepsilon\, \boldsymbol{G}_\varepsilon(\omega) = \frac{\omega Z(\omega)\boldsymbol{\sigma}_0 + \phi(\omega)\boldsymbol{\sigma}_1}{\sqrt{-\omega^2 Z^2(\omega) + \phi^2(\omega)}} = \mathrm{i}\frac{\omega Z(\omega)\boldsymbol{\sigma}_0 + \phi(\omega)\boldsymbol{\sigma}_1}{\sqrt[+]{\omega^2 Z^2(\omega) - \phi^2(\omega)}} = \mathrm{i}\frac{\omega\boldsymbol{\sigma}_0 + \Delta(\omega)\boldsymbol{\sigma}_1}{\sqrt[*]{\omega^2 - \Delta^2(\omega)}}.$$

For the integral to be correct, the first square must have a positive real part. Since a multiplication with i corresponds to a rotation by $\frac{\pi}{2}$ in the complex plane, the second square root must be taken from the upper half-plane [39, Eq. 2.19b]. Accordingly the domain of the third square root is the upper half-plane rotated clockwise by the complex argument of $Z(\omega)$.

Using $\mathrm{Im}[\mathrm{i}\ldots] = \mathrm{Re}[\ldots]$, the phononic part of the self-energy reads

$$\begin{aligned}\boldsymbol{\Sigma}^{\mathrm{ph.}}(\mathrm{i}\omega_n) &= T\sum_m \int_{-\infty}^{\infty} \mathrm{d}\varepsilon\, \boldsymbol{\sigma}_3\, \boldsymbol{G}_\varepsilon(\mathrm{i}\omega_m)\, \boldsymbol{\sigma}_3\, \lambda(n-m) \\ &= T\int_{-\infty}^{\infty} \mathrm{d}\omega' \, \mathrm{Re}\left[\frac{\omega'_+\boldsymbol{\sigma}_0 - \Delta(\omega'_+)\boldsymbol{\sigma}_1}{\sqrt[*]{\omega'^2_+ - \Delta^2(\omega'_+)}}\right] \int_0^{\infty} \mathrm{d}\omega''\, \alpha^2F(\omega'') \sum_m \frac{1}{\mathrm{i}\omega_m - \omega'} \frac{2\omega''}{(\omega_n - \omega_m)^2 + \omega''^2}.\end{aligned}$$

It is now possible to eliminate the summation over MATSUBARA frequencies [34, Eqs. 3.40, 3.41],

$$T\sum_m \frac{1}{\mathrm{i}\omega_m - \omega'} \frac{2\omega''}{(\omega_n - \omega_m)^2 + \omega''^2} = \frac{f_+(-\omega') + f_-(\omega'')}{\mathrm{i}\omega_n - \omega' - \omega''} + \frac{f_+(\omega') + f_-(\omega'')}{\mathrm{i}\omega_n - \omega' + \omega''} \equiv \Omega(\mathrm{i}\omega_n, \omega', \omega''),$$

and to analytically continue the self-energy, which yields

$$\boldsymbol{\Sigma}^{\mathrm{ph.}}(\omega) = \int_{-\infty}^{\infty} \mathrm{d}\omega' \, \mathrm{Re}\left[\frac{\omega'_+\boldsymbol{\sigma}_0 - \Delta(\omega'_+)\boldsymbol{\sigma}_1}{\sqrt[*]{\omega'^2_+ - \Delta^2(\omega'_+)}}\right] \int_0^{\infty} \mathrm{d}\omega''\, \alpha^2F(\omega'')\, \Omega(\omega, \omega', \omega'').$$

With the identity [34, Eq. 12.4]

$$T\sum_m \frac{1}{\mathrm{i}\omega_m - \omega'} = -\frac{1}{2}[1 - 2f_+(\omega')] \tag{4.10}$$

the electronic part of the self-energy is analogously found to be

$$\boldsymbol{\Sigma}^{\mathrm{el.}}(\omega) = \mu_C T\sum_m \int_{-\infty}^{\infty} \mathrm{d}\varepsilon\, \boldsymbol{G}^{\mathrm{od.}}_{\boldsymbol{q}}(\omega) = -\frac{\mu_C}{2} \int_{-\infty}^{\infty} \mathrm{d}\omega' \, \mathrm{Re}\left[\frac{\Delta(\omega'_+)\boldsymbol{\sigma}_1}{\sqrt[*]{\omega'^2_+ - \Delta^2(\omega'_+)}}\right][1 - 2f_+(\omega')].$$

Thus for $\boldsymbol{\Sigma}(\omega) = \boldsymbol{\Sigma}^{\mathrm{ph.}}(\omega) + \boldsymbol{\Sigma}^{\mathrm{el.}}(\omega)$ the so-called *real-axis Eliashberg equations*, which are actually defined for the whole complex plane, read

$$\begin{aligned}Z(\omega) &= 1 - \frac{1}{\omega} \int_{-\infty}^{\infty} \mathrm{d}\omega' \, \mathrm{Re}\left[\frac{\omega'_+}{\sqrt[*]{\omega'^2_+ - \Delta^2(\omega'_+)}}\right] \int_0^{\infty} \mathrm{d}\omega''\, \alpha^2F(\omega'')\, \Omega(\omega, \omega', \omega''), \\ \Delta(\omega) &= -\frac{1}{Z(\omega)} \int_{-\infty}^{\infty} \mathrm{d}\omega' \, \mathrm{Re}\left[\frac{\Delta(\omega'_+)}{\sqrt[*]{\omega'^2_+ - \Delta^2(\omega'_+)}}\right] \left\{[1 - 2f_+(\omega')]\,\frac{\mu_C}{2} + \int_0^{\infty} \mathrm{d}\omega''\, \alpha^2F(\omega'')\, \Omega(\omega, \omega', \omega'')\right\}.\end{aligned}$$

Noting that $\lambda(n) = \lambda(-n)$, one can easily verify that even functions $Z(\mathrm{i}\omega_n)$ and $\Delta(\mathrm{i}\omega_n)$ are perfectly compatible with Eqs. 4.9. This property is inherited by the corresponding real-axis quantities. More general: Let $f(\omega)$ represent any of the functions ω^2, $Z(\omega)$ and $\Delta(\omega)$. They all have in common that they turn into their complex conjugate if the sign of either the real or imaginary part of their argument changes [40, Eq. A5]. Formally,

$$f(-\omega) = f(\omega) \quad \text{and} \quad f(\omega^*) = f^*(\omega). \tag{4.11}$$

The same applies to functions which are derived by means of the four basic arithmetical operations, such as $\omega^2 - \Delta^2(\omega)$. Besides, complex conjugation of a number reflects its possible square roots across the axes of the complex plane. As a consequence, if ω is reflected across the real axis, the same is true for the $Z(\omega)$-dependent domain of $\sqrt[*]{\cdots}$ and thus for $\sqrt[*]{\omega^2 - \Delta^2(\omega)}$.

This symmetry is now used to fold the negative half of the range of the ω'-integral onto the positive one, which yields the final form of the real-axis Eliashberg equations [41, Eqs. 2, 3]:

$$Z(\omega) = 1 - \frac{1}{\omega}\int_0^\infty \mathrm{d}\omega'\ \mathrm{Re}\left[\frac{\omega'_+}{\sqrt[*]{\omega'^2_+ - \Delta^2(\omega'_+)}}\right] \times \cdots$$
$$\cdots \times \int_0^\infty \mathrm{d}\omega''\ \alpha^2F(\omega'')[\Omega(\omega,\omega',\omega'') + \Omega(\omega,-\omega',\omega'')], \tag{4.12a}$$

$$\Delta(\omega) = -\frac{1}{Z(\omega)}\int_0^\infty \mathrm{d}\omega'\ \mathrm{Re}\left[\frac{\Delta(\omega'_+)}{\sqrt[*]{\omega'^2_+ - \Delta^2(\omega'_+)}}\right]\Big\{[1-2f_+(\omega')]\,\mu_\mathrm{C} + \cdots$$
$$\cdots + \int_0^\infty \mathrm{d}\omega''\ \alpha^2F(\omega'')[\Omega(\omega,\omega',\omega'') - \Omega(\omega,-\omega',\omega'')]\Big\}. \tag{4.12b}$$

The ω in the denominator of Eq. 4.12a is cancelled since, where braces enclose alternatives,

$$\Omega(\omega,\omega',\omega'') \pm \Omega(\omega,-\omega',\omega'') = \Omega_\pm(\omega,\omega',\omega'') \pm \Omega_\pm(\omega,-\omega',\omega''),$$
$$\Omega_\pm(\omega,\omega',\omega'') = 2\left\{\begin{matrix}\omega\\ \omega'+\omega''\end{matrix}\right\}\frac{f_+(-\omega') + f_-(\omega'')}{\omega^2 - (\omega'+\omega'')^2}.$$

4.5 McMillan's formula

In 1968, William L. McMillan establishes a formula to estimate the transition temperature T_c of superconductors as a function of only three characteristic parameters: an average phonon frequency $\langle\omega\rangle$, the electron-phonon coupling strength λ and the Coulomb pseudo-potential μ^*.[2] This section provides a review of the original work [1].

The starting point is a linearized form of the real-axis Eliashberg equations, which emerges at T_c where $\Delta(\omega)$ is infinitesimal and negligible relative to ω. Introducing two cutoff energies, the maximum phonon frequency ω_0 and the electronic bandwidth E_B, and assuming that $Z(\omega'_+)$ lies in the upper half-plane or on the positive real axis so that $\sqrt[*]{\omega'^2_+} = \omega'_+$, Eq. 4.12 becomes

$$Z(\omega) = 1 - \frac{1}{\omega}\int_0^\infty \mathrm{d}\omega' \int_0^{\omega_0} \mathrm{d}\omega''\ \alpha^2F(\omega'')[\Omega(\omega,\omega',\omega'') + \Omega(\omega,-\omega',\omega'')], \tag{4.13a}$$

$$\Delta(\omega) = -\frac{1}{Z(\omega)}\int_0^\infty \mathrm{d}\omega'\ \frac{\mathrm{Re}[\Delta(\omega')]}{\omega'}\Big\{\Theta(E_\mathrm{B}-\omega')[1-2f_+(\omega')]\,\mu_\mathrm{C} + \cdots \tag{4.13b}$$
$$\cdots + \int_0^{\omega_0} \mathrm{d}\omega''\ \alpha^2F(\omega'')[\Omega(\omega,\omega',\omega'') - \Omega(\omega,-\omega',\omega'')]\Big\}. \tag{4.13c}$$

The idea is to find an analytic expression which roughly approximates T_c and can be used to fit numerical results. To that end, a simple trial function for $\Delta(\omega)$ is introduced, which shall solve the Eliashberg equations, i.e. be self-consistent, at least at low and high frequencies:

$$\Delta(\omega) = \begin{cases}\Delta_0 & \text{for } |\omega| < \omega_0,\\ \Delta_\infty & \text{otherwise,}\end{cases}$$

where $\Delta_0, \Delta_\infty \in \mathbb{R}$. Several approximate contributions to $\Delta(0)$ and $\Delta(\infty)$ are taken into account.

[2] The latter two quantities may be obtained from the density of states measured in a tunneling experiment via the inversion method proposed in Section V of Ref. 3.

1. **Phononic contribution to $\Delta(0)$ for $\omega' < \omega_0$.** Neglecting ω' relative to ω'' yields

$$\Omega(0,\omega',\omega'') - \Omega(0,-\omega',\omega'') \approx -\frac{2}{\omega''}[1-2f_+(\omega')],$$
$$\Delta^{(1)}(0) \approx \frac{\Delta_0}{Z(0)} \underbrace{\int_0^{\omega_0} \frac{\mathrm{d}\omega'}{\omega'}[1-2f_+(\omega')]}_{\approx \ln(\omega_0/T_c)} \underbrace{2\int_0^{\omega_0} \frac{\mathrm{d}\omega''}{\omega''}\alpha^2F(\omega'')}_{\equiv \lambda},$$

   where the *electron-phonon coupling strength* $\lambda \equiv \lambda(0)$ has reappeared. The integral approximation will be justified in Section 4.6.2, observing that $1-2f_+(\omega) = \tanh\frac{\omega}{2T} \approx \frac{2}{\pi}\arctan\frac{\omega}{T}$.

2. **Phononic contribution to $\Delta(0)$ for $\omega' \geq \omega_0$.** Neglecting ω'' relative to ω' yields

$$\Omega(0,\omega',\omega'') - \Omega(0,-\omega',\omega'') \approx -\frac{2}{\omega'}[1+2f_-(\omega'')],$$
$$\Delta^{(2)}(0) \approx \frac{\Delta_\infty\lambda}{Z(0)} \underbrace{\int_{\omega_0}^{\infty} \frac{\mathrm{d}\omega'}{\omega'^2}}_{=1/\omega_0} \underbrace{\frac{2}{\lambda}\int_0^{\omega_0} \mathrm{d}\omega''\,\alpha^2F(\omega'')}_{\equiv\langle\omega\rangle} \underbrace{[1+2f_-(\omega'')]}_{\approx 1},$$

   where an *average phonon frequency* $\langle\omega\rangle$ has been defined.

3. **Phononic contribution to $\Delta(\infty)$.** This part vanishes for $\Omega(\infty,\omega',\omega'') - \Omega(\infty,-\omega',\omega'') = 0$.

4. **Electronic contribution to $\Delta(0)$.** With the same approximations as in $\Delta^{(1)}(0)$ and $\Delta^{(2)}(0)$,

$$\Delta^{(3)}(0) = -\frac{\mu_C}{Z(0)}\left[\Delta_0 \underbrace{\int_0^{\omega_0} \frac{\mathrm{d}\omega'}{\omega'}[1-2f_+(\omega')]}_{\approx \ln(\omega_0/T_c)} + \Delta_\infty \underbrace{\int_{\omega_0}^{E_B} \frac{\mathrm{d}\omega'}{\omega'}}_{=\ln(E_B/\omega_0)} \underbrace{[1-2f_+(\omega')]}_{\approx 1}\right].$$

5. **Electronic contribution to $\Delta(\infty)$.** Analogous to the calculation of $\Delta^{(3)}(0)$,

$$\Delta(\infty) \approx -\frac{\mu_C}{Z(\infty)}\left[\Delta_0 \ln\frac{\omega_0}{T_c} + \Delta_\infty \ln\frac{E_B}{\omega_0}\right].$$

The renormalization at low frequencies is assumed to be $Z(0) = Z(\mathrm{i}\omega_0) = 1+\lambda$, a result which will be derived in Eq. 4.26, whereas for high frequencies one simply has $Z(\infty) = 1$. It is further required that $\Delta(0) \equiv \Delta_0$ and $\Delta(\infty) \equiv \Delta_\infty$. The latter equation may be solved for Δ_∞, which yields

$$\Delta_\infty = -\mu^*\Delta_0 \ln\frac{\omega_0}{T_c} \quad \text{with} \quad \frac{1}{\mu^*} = \frac{1}{\mu_C} + \ln\frac{E_B}{\omega_0}, \tag{4.14}$$

where the *Coulomb pseudo-potential* μ^* has been defined. Hence,

$$\Delta_0 = \Delta^{(1)}(0) + \Delta^{(2)}(0) + \Delta^{(3)}(0) = \frac{\Delta_0}{1+\lambda}[\lambda - \lambda\mu^*\langle\omega\rangle/\omega_0 - \mu^*]\ln\frac{\omega_0}{T_c}.$$

This equation can be solved for T_c. The resulting formula is then generalized by introducing three fit parameters, A, B and C say, in the course of which the the maximum phonon frequency ω_0 is replaced by the, essentially synonymous, Debye frequency Θ:

$$T_c = \omega_0 \exp\left[-\frac{1+\lambda}{\lambda - \lambda\mu^*\langle\omega\rangle/\omega_0 - \mu^*}\right] \to \frac{\Theta}{A}\exp\left[-\frac{B(1+\lambda)}{\lambda - C\lambda\mu^* - \mu^*}\right].$$

For several fixed T_c and μ^* the linearized Eliashberg equations are now solved for λ. De facto, $F(\omega'')$ is chosen to be the phonon density of states of niobium [5] cut off below 100 K and α^2, which determines λ, adjusted to obtain self-consistency.

These results are used to determine A, B and in a second step C via linear regression:

$$\ln\frac{\Theta}{T_c} \overset{\mu^*=0}{=} \ln A + B\frac{1+\lambda}{\lambda} \quad \text{and} \quad \frac{1}{\mu^*}\left[\lambda + \frac{B(1+\lambda)}{\ln(AT_c/\Theta)}\right] = 1 + C\lambda. \tag{4.15}$$

The values found by McMillan read $A = 1.45$, $B = 1.04$ and $C = 0.62$. He also states that for niobium $\Theta = 277$ K and $\langle\omega\rangle = 230$ K, which allows the alternative pre-factor $\langle\omega\rangle/1.20$ in place of $\Theta/1.45$, which should be preferred according to Dynes [42] for a more universal validity.

4.6 Rescaled Coulomb pseudo-potential

The introduction of the Coulomb pseudo-potential[3] in the preceding section requires a more detailed analysis of the Coulomb interaction as occurring in the Eliashberg theory. Before that, however, it is convenient to put the local and CDOS Eliashberg equations (Eqs. 4.7 and 4.9) into a form which is more suitable for both further analysis and computational implementation.

As already stated in Eq. 4.11, one can assume the solutions of the Eliashberg equations to be even function of frequency. Exploiting this symmetry it is possible to fold the negative half of the Matsubara sum onto the positive one, just like it was done with the integrals in Eq. 4.12.

For local self-energies this yields

$$
\begin{aligned}
Z(\mathrm{i}\omega_n) &= 1 + \frac{T}{\omega_n} \sum_{m=0}^{\infty} \int_{-\infty}^{\infty} \mathrm{d}\varepsilon \frac{N(\varepsilon)}{N(\mu_0)} \frac{\omega_m Z(\mathrm{i}\omega_m)}{\Theta(\varepsilon, m)} \Lambda^-(n, m), \\
\phi(\mathrm{i}\omega_n) &= T \sum_{m=0}^{\infty} \int_{-\infty}^{\infty} \mathrm{d}\varepsilon \frac{N(\varepsilon)}{N(\mu_0)} \frac{\phi(\mathrm{i}\omega_m)}{\Theta(\varepsilon, m)} [\Lambda^+(n, m) - 2\mu_C], \\
\chi(\mathrm{i}\omega_n) &= -T \sum_{m=0}^{\infty} \int_{-\infty}^{\infty} \mathrm{d}\varepsilon \frac{N(\varepsilon)}{N(\mu_0)} \frac{\varepsilon - \mu + \chi(\mathrm{i}\omega_m)}{\Theta(\varepsilon, m)} \Lambda^+(n, m)
\end{aligned}
$$

and, under the additional assumption of a constant density of states,

$$
\begin{aligned}
Z(\mathrm{i}\omega_n) &= 1 + \frac{\pi T}{\omega_n} \sum_{m=0}^{\infty} \frac{\omega_m Z(\omega_m)}{\sqrt{[\omega_m Z(\mathrm{i}\omega_m)]^2 + \phi^2(\mathrm{i}\omega_m)}} \Lambda^-(n, m), \\
\phi(\mathrm{i}\omega_n) &= \pi T \sum_{m=0}^{\infty} \frac{\phi(\mathrm{i}\omega_m)}{\sqrt{[\omega_m Z(\mathrm{i}\omega_m)]^2 + \phi^2(\mathrm{i}\omega_m)}} [\Lambda^+(n, m) - 2\mu_C].
\end{aligned}
$$

The occurring electron-phonon coupling matrices are defined as

$$
\Lambda^{\pm}(n, m) = \lambda(n - m) \pm \lambda(n + m + 1).
$$

Solving the above equations on a computer requires a truncation of the infinite summation over Matsubara frequencies. For the phonon part this is unproblematic since it has a natural cutoff through $\lambda(n)$, which decays rapidly with growing magnitude of ν_n. The Coulomb part, however, does not depend on frequency and thus couples terms regardless of the difference of their frequency arguments. As a consequence, the partial sum does converge very slowly – or not at all – with increasing cutoff. The following procedures circumvents this.[4]

4.6.1 Introduction of cutoff frequency

Let $\phi(\mathrm{i}\omega_n) = \phi_{\text{ph.}}(\mathrm{i}\omega_n) + \phi_{\text{el.}}$ and consider the Eliashberg equation for $\phi_{\text{el.}}$,

$$
\phi_{\text{el.}} = -2\mu_C T \sum_{m=0}^{\infty} \int_{-\infty}^{\infty} \mathrm{d}\varepsilon \frac{N(\varepsilon)}{N(\mu_0)} \frac{\phi(\mathrm{i}\omega_m)}{\Theta(\varepsilon, m)}. \tag{4.16}
$$

As will be seen from the results presented in Fig. 5.3, there is a cutoff frequency ω_N above which one can safely assume $\phi_{\text{ph.}}(\mathrm{i}\omega_m) \approx \chi(\mathrm{i}\omega_m) \approx 0$, $\phi_{\text{el.}} \ll \omega_m$ and $Z(\mathrm{i}\omega_m) \approx 1$ such that

$$
-2\mu_C T \sum_{m=N}^{\infty} \int_{-\infty}^{\infty} \mathrm{d}\varepsilon \frac{N(\varepsilon)}{N(\mu_0)} \frac{\phi(\mathrm{i}\omega_m)}{\Theta(\varepsilon, m)} \approx -2\mu_C T \sum_{m=N}^{\infty} \int_{-\infty}^{\infty} \mathrm{d}\varepsilon \frac{N(\varepsilon)}{N(\mu_0)} \frac{\phi_{\text{el.}}}{\omega_m^2 + (\varepsilon - \mu)^2}.
$$

[3] According to Schrieffer [43, p. 187] the formula for μ^* was first given in 1959 by Bogoliubov, Tolmachev and Shirkov [44, p. 83]. Nevertheless, the quantity is sometimes referred to as the *Morel-Anderson pseudo-potential* with reference to Ref. 45 from 1962.

[4] Similar derivations are given by Schrieffer [43, pp. 185–188] and Allen and Mitrović [34, Section 9].

Bringing this part to the left-hand side of Eq. 4.16 yields

$$\left[1 + 2\mu_C T \sum_{m=N}^{\infty} \int_{-\infty}^{\infty} \mathrm{d}\varepsilon \frac{N(\varepsilon)}{N(\mu_0)} \frac{1}{\omega_m^2 + (\varepsilon - \mu)^2}\right] \phi_{\text{el.}} = -2\mu_C T \sum_{m=0}^{N-1} \int_{-\infty}^{\infty} \mathrm{d}\varepsilon \frac{N(\varepsilon)}{N(\mu_0)} \frac{\phi(\mathrm{i}\omega_m)}{\Theta(\varepsilon, m)}$$

or equivalently, introducing a *rescaled Coulomb pseudo-potential* $\mu^*(N)$,

$$\phi_{\text{el.}} = -2\mu^*(N) T \sum_{m=0}^{N-1} \int_{-\infty}^{\infty} \mathrm{d}\varepsilon \frac{N(\varepsilon)}{N(\mu_0)} \frac{\phi(\mathrm{i}\omega_m)}{\Theta(\varepsilon, m)}, \quad \frac{1}{\mu^*(N)} = \frac{1}{\mu_C} + 2T \sum_{m=N}^{\infty} \int_{-\infty}^{\infty} \mathrm{d}\varepsilon \frac{N(\varepsilon)}{N(\mu_0)} \frac{1}{\omega_m^2 + (\varepsilon - \mu)^2}.$$

The truncation of the Matsubara sum has thus been compensated by rescaling the Coulomb interaction. For a computational solution for μ^* it is further convenient to replace the infinite sum by a closed form. This is done by means of the identity [34, Eq. A.14]

$$\sum_{n=0}^{N-1} \frac{x}{(n + \frac{1}{2})^2 + x^2} = \operatorname{Im}[\psi(\tfrac{1}{2} + \mathrm{i}x) - \psi(N + \tfrac{1}{2} + \mathrm{i}x)],$$

where $\psi(x) = \Gamma'(x)/\Gamma(x)$ is the digamma function which asymptotically approaches the natural logarithm for large arguments, as found via the Stirling formula [34, Appendix A]. Consequently,

$$\begin{aligned}
\sum_{n=N}^{\infty} \frac{x}{(n + \frac{1}{2})^2 + x^2} &= \lim_{M\to\infty} \left\{ \operatorname{Im}[\psi(N + \tfrac{1}{2} + \mathrm{i}x) - \psi(M + \tfrac{1}{2} + \mathrm{i}x)] \right\} \\
&\approx \lim_{M\to\infty} \left\{ \operatorname{Im}[\log(N + \tfrac{1}{2} + \mathrm{i}x) - \log(M + \tfrac{1}{2} + \mathrm{i}x)] \right\} \\
&= \lim_{M\to\infty} \Big\{ \arg(N + \tfrac{1}{2} + \mathrm{i}x) - \underbrace{\arg(M + \tfrac{1}{2} + \mathrm{i}x)}_{\to 0} \Big\} = \arctan \frac{x}{N + \frac{1}{2}}
\end{aligned}$$

and thus, removing the singularity at $\varepsilon = \mu$, which is not known in advance and approximated by μ_0 to obtain a formula which can be applied *before* the Eliashberg equations are solved,

$$\frac{1}{\mu^*(N)} = \frac{1}{\mu_C} + \frac{1}{\pi} \int_{-\infty}^{\infty} \mathrm{d}\varepsilon \frac{N(\varepsilon)}{N(\mu_0)} \begin{cases} \frac{1}{\varepsilon - \mu} \arctan \frac{\varepsilon - \mu}{\omega_N} & \text{for } \varepsilon \neq \mu, \\ \frac{1}{\omega_N} & \text{otherwise.} \end{cases} \tag{4.17}$$

4.6.2 Rectangular density of states

For the special case of a density of states which is constant on the interval $[-D, D]$ and zero elsewhere and assuming a chemical potential $\mu = 0$ [34, p. 39], the formula for μ^* reduces to

$$\frac{1}{\mu^*(N)} = \frac{1}{\mu_C} + R(N) \quad \text{with} \quad R(N) = \frac{2}{\pi} \int_0^D \frac{\mathrm{d}\varepsilon}{\varepsilon} \arctan \frac{\varepsilon}{\omega_N}.$$

By means of substitution and partial integration one can further evaluate

$$R(N) = \frac{2}{\pi} \int_0^{\frac{D}{\omega_N}} \frac{\mathrm{d}x}{x} \arctan x = \frac{\arctan \frac{D}{\omega_N}}{\pi/2} \ln \frac{D}{\omega_N} - \underbrace{\frac{2}{\pi} \int_0^{\frac{D}{\omega_N}} \frac{\mathrm{d}x \, \ln x}{1 + x^2}}_{\frac{2}{\pi} \int_{-\infty}^{\ln \frac{D}{\omega_N}} \frac{x \, \mathrm{d}x}{\mathrm{e}^{-x} + \mathrm{e}^{x}} = -\frac{1}{\pi} \int_{\ln \frac{D}{\omega_N}}^{\infty} \frac{x \, \mathrm{d}x}{\cosh x}}.$$

Since the hyperbolic cosine growths exponentially with the magnitude of its arguments while the arc tangent approaches $\pi/2$, for the reasonable assumption that $D \gg \omega_N$ one finds

$$R(N) = \frac{\overbrace{\arctan \frac{D}{\omega_N}}^{\approx 1}}{\pi/2} \ln \frac{D}{\omega_N} + \overbrace{\frac{1}{\pi} \int_{\ln \frac{D}{\omega_N}}^{\infty} \frac{x \, \mathrm{d}x}{\cosh x}}^{\approx 0} \quad \text{so that} \quad \frac{1}{\mu^*(N)} = \frac{1}{\mu_C} + \ln \frac{D}{\omega_N}. \tag{4.18}$$

For the sake of completeness it shall also be mentioned that an exact evaluation of $R(N)$ is possible in terms of dilogarithms:

$$R(N) = \frac{1}{\mathrm{i}\pi} \int_0^{\mathrm{i}\frac{D}{\omega_N}} \frac{\mathrm{d}x}{x} [\ln(1 + x) - \ln(1 - x)] \equiv \frac{\operatorname{Li}_2\left(\mathrm{i}\frac{D}{\omega_N}\right) - \operatorname{Li}_2\left(-\mathrm{i}\frac{D}{\omega_N}\right)}{\mathrm{i}\pi}.$$

4.6.3 Constant density of states

One ought to think that the latest results should be directly applicable to the case of a constant density of states which extends over the whole energy domain. The problem is, however, that within the approximations made μ^* would vanish as $D \to \infty$, regardless of the cutoff chosen.

A well-defined rescaling prescription can be found by applying the steps carried out in Section 4.6.1 directly to the CDOS Eliashberg equation

$$\phi_{\text{el.}} = -2\mu^*(M)\pi T \sum_{m=0}^{M-1} \frac{\phi(\mathrm{i}\omega_m)}{\sqrt{[\omega_m Z(\mathrm{i}\omega_m)]^2 + \phi^2(\mathrm{i}\omega_m)}}, \tag{4.19}$$

where an upper cutoff at ω_M has been introduced in the first place and the appropriate yet unknown $\mu^*(M)$ is used. The idea is to truncate the Coulomb part at a lower frequency ω_N, above which $\phi_{\text{ph.}}(\mathrm{i}\omega_m) \approx 0$, $\phi_{\text{el.}} \ll \omega_m$ and $Z(\mathrm{i}\omega_m) \approx 1$ is still a valid assumption. One has

$$-2\mu^*(M)\pi T \sum_{m=N}^{M-1} \frac{\phi(\mathrm{i}\omega_m)}{\sqrt{[\omega_m Z(\mathrm{i}\omega_m)]^2 + \phi^2(\mathrm{i}\omega_m)}} \approx -2\mu^*(M)\pi T \sum_{m=N}^{M-1} \frac{\phi_{\text{el.}}}{\omega_m}$$

which leads to

$$\phi_{\text{el.}} = -2\mu^*(N)\pi T \sum_{m=0}^{N-1} \frac{\phi(\mathrm{i}\omega_m)}{\sqrt{[\omega_m Z(\mathrm{i}\omega_m)]^2 + \phi^2(\mathrm{i}\omega_m)}}, \quad \mu^*(N) = \frac{\mu^*(M)}{1 + 2\mu^*(M)\pi T \sum_{m=N}^{M-1} \omega_m^{-1}}.$$

As above, one can further simplify

$$2\pi T \sum_{m=N}^{M-1} |\omega_m|^{-1} = \sum_{m=N}^{M-1} \frac{1}{m + \frac{1}{2}} = \psi(M + \tfrac{1}{2}) - \psi(N + \tfrac{1}{2}) \approx \log \frac{M + \frac{1}{2}}{N + \frac{1}{2}} = \ln \frac{\omega_M}{\omega_N},$$

where Eq. A.7 of Ref. 34 has been used. Hence [34, Eq. 9.14],

$$\frac{1}{\mu^*(N)} = \frac{1}{\mu^*(M)} + \ln \frac{\omega_M}{\omega_N}.$$

From comparison with Eq. 4.18 it follows that the CDOS approach reproduces the expected results if the non-rescaled μ_C is used in combination with a cutoff frequency equal to the virtual band-width D. The CDOS approximation thus *requires* a frequency cutoff.

Since D is theoretically infinite and practically unknown it is eliminated by the assumption that it be equal to the band-width E_B in the derivation of McMillan's equation. Combination of the results from Eqs. 4.14 and 4.18 yields the formula to be used within the imaginary-axis CDOS Eliashberg equations [2, Eq. 13]:

$$\frac{1}{\mu^*(N)} = \frac{1}{\mu^*} + \ln \frac{\omega_0}{\omega_N}. \tag{4.20}$$

4.7 Chemical potential

If the chemical potential in the Eliashberg equations is assumed to be constant, the particle number is not necessarily conserved. Following Ref. 46, with the help of Dirichlet's theorem for Fourier series and Eq. 3.12 one finds

$$\begin{aligned}\langle c_k^+ c_k \rangle = 1 - \langle c_k c_k^+ \rangle &= \frac{1 + \langle c_k^+ c_k \rangle - \langle c_k c_k^+ \rangle}{2} \\ &= \frac{1 + G_k(0^-) + G_k(0^+)}{2} = \frac{1}{2} + G_k(0) = \frac{1}{2} + \frac{1}{\beta} \sum_{n \in \mathbb{Z}} G_k(\mathrm{i}\omega_n)\end{aligned}$$

and thus the *particle density* or *occupation number* per unit cell

$$n = \frac{1}{N} \sum_{k\sigma} \langle c_k^+ c_k \rangle = 1 + \frac{2}{\beta N} \sum_{kn} G_k(\mathrm{i}\omega_n) = 1 - \frac{2}{\beta N} \sum_{kn} \frac{\varepsilon_k - \mu + \chi_k(\mathrm{i}\omega_n)}{\Theta_k(n)},$$

not to be confused with the summation index, where terms with $\mathrm{i}\omega_n Z_k(\mathrm{i}\omega_n)$ have cancelled.

4.7.1 Free particles

Using Eq. 4.10 it can be shown that for $Z_{\boldsymbol{k}}(\mathrm{i}\omega_n) = 1$ and $\phi_{\boldsymbol{k}}(\mathrm{i}\omega_n) = \chi_{\boldsymbol{k}}(\mathrm{i}\omega_n) = 0$ the free-particle occupation number is reproduced:

$$n = 1 - \frac{2}{\beta N}\sum_{\boldsymbol{k}n}\frac{\mathrm{i}\omega_n + \varepsilon_{\boldsymbol{k}} - \mu}{\omega_n^2 + (\varepsilon_{\boldsymbol{k}} - \mu)^2} = 1 - \frac{2}{\beta N}\sum_{\boldsymbol{k}n}\frac{1}{\varepsilon_{\boldsymbol{k}} - \mu - \mathrm{i}\omega_n} = \frac{2}{N}\sum_{\boldsymbol{k}} f_+(\varepsilon_{\boldsymbol{k}})$$
$$= 2\int_{-\infty}^{\infty}\mathrm{d}\varepsilon\, n(\varepsilon)\, f_+(\varepsilon) = 1 - \int_{-\infty}^{\infty}\mathrm{d}\varepsilon\, n(\varepsilon)\tanh\frac{\varepsilon - \mu}{2T}.$$

This equation could be solved for μ using a bisection method or the fixed-point equation

$$\mu = \frac{n - 1 + \int_{-\infty}^{\infty}\mathrm{d}\varepsilon\,\varepsilon\, w(\varepsilon)}{\int_{-\infty}^{\infty}\mathrm{d}\varepsilon\, w(\varepsilon)} \quad \text{with} \quad w(\varepsilon) = n(\varepsilon)\begin{cases}\frac{1}{\varepsilon-\mu}\tanh\frac{\varepsilon-\mu}{2T} & \text{for } \varepsilon \neq \mu,\\ \frac{1}{2T} & \text{otherwise.}\end{cases} \tag{4.21}$$

For half-filling, i.e. $n = 1$, this gives simply the *center of mass* of the weight function $w(\varepsilon)$.

4.7.2 Interacting particles

The calculation of the occupation number from the results of the imaginary-axis Eliashberg equations is complicated by the cutoff of the Matsubara sums. A reasonable approximation consists in replacing the unknown part by the corresponding free-particle expression:

$$n \approx 1 - 4T\int_{-\infty}^{\infty}\mathrm{d}\varepsilon\, n(\varepsilon)\Bigg[\sum_{n=0}^{N-1}\frac{\varepsilon - \mu + \chi(\mathrm{i}\omega_n)}{\Theta(\varepsilon, n)} + \underbrace{\sum_{n=N}^{\infty}\frac{\varepsilon - \mu}{\omega_n^2 + (\varepsilon - \mu)^2}}_{\approx \frac{1}{2\pi T}\arctan\frac{\varepsilon-\mu}{\omega_N}}\Bigg],$$

where the intermediate result from Section 4.6.1 has been used. Solving this equation for the left appearance of μ yields a manageable fixed-point equation, namely

$$\mu \approx \frac{\frac{n-1}{4T} + \int_{-\infty}^{\infty}\mathrm{d}\varepsilon\, n(\varepsilon)\big[\sum_{n=0}^{N-1}\frac{\varepsilon+\chi(\mathrm{i}\omega_n)}{\Theta(\varepsilon,n)} + \frac{1}{2\pi T}\arctan\frac{\varepsilon-\mu}{\omega_N}\big]}{\int_{-\infty}^{\infty}\mathrm{d}\varepsilon\, n(\varepsilon)\sum_{n=0}^{N-1}\frac{1}{\Theta(\varepsilon,n)}}. \tag{4.22}$$

Within this work it shall not be resolved if Eqs. 4.21 and 4.22 guarantee convergence for all possible densities of states, self-energies and starting points. However, in all cases studied convergence at a sufficient rate has been observed.

4.8 Multi-band equations

At this point the most important aspects of Eliashberg theory for local self-energies at arbitrary temperatures have been introduced. A straightforward generalization of the involved equations is with respect to multiple electronic bands which will turn out to be equivalent to allowing for Fermi-pocket resolved anisotropy.

Since a band index is a quantum number just as the wave number, both can be treated on the same footing. Thus, in Eqs. 4.5 one simply has to complement the natural occurrences of the wave numbers $\boldsymbol{k}$ and $\boldsymbol{q}$, even though they have been averaged out as in the case of the Coulomb interaction, with band indices i and j, respectively. In doing so, the self-energy components searched for are defined for each band separately and scalar coupling strengths become matrices describing intra- and inter-band interactions.

The corresponding local Eliashberg equations read

$$Z_i(\mathrm{i}\omega_n) = 1 + \frac{T}{\omega_n}\sum_j\sum_{m=0}^{N-1}\int_{-\infty}^{\infty}\mathrm{d}\varepsilon\frac{n_j(\varepsilon)}{n_j(\mu_0)}\frac{\omega_m Z_j(\mathrm{i}\omega_m)}{\Theta_j(\varepsilon,m)}\Lambda_{ij}^{-}(n,m), \tag{4.23a}$$

$$\phi_i(\mathrm{i}\omega_n) = T\sum_j\sum_{m=0}^{N-1}\int_{-\infty}^{\infty}\mathrm{d}\varepsilon\frac{n_j(\varepsilon)}{n_j(\mu_0)}\frac{\phi_j(\mathrm{i}\omega_m)}{\Theta_j(\varepsilon,m)}[\Lambda_{ij}^{+}(n,m) - 2\mu_{ij}^{*}(N)], \tag{4.23b}$$

$$\chi_i(\mathrm{i}\omega_n) = -T\sum_j\sum_{m=0}^{N-1}\int_{-\infty}^{\infty}\mathrm{d}\varepsilon\frac{n_j(\varepsilon)}{n_j(\mu_0)}\frac{\varepsilon-\mu+\chi_j(\mathrm{i}\omega_m)}{\Theta_j(\varepsilon,m)}\Lambda_{ij}^{+}(n,m). \tag{4.23c}$$

The common denominator and the electron-phonon coupling matrices are defined as

$$\Theta_i(\varepsilon,n) = [\omega_n Z_i(\mathrm{i}\omega_n)]^2 + \phi_i^2(\mathrm{i}\omega_n) + [\varepsilon-\mu+\chi_i(\mathrm{i}\omega_n)]^2,$$
$$\Lambda_{ij}^{\pm}(n,m) = \lambda_{ij}(n-m) \pm \lambda_{ij}(n+m+1).$$

$n_j(\varepsilon)$ denotes the density of states for the j-th band, normalized with respect to integration over ε and summation over j to obtain an occupation number $n \in [0,2]$ defined for $N\to\infty$ as

$$n = 1 - 4T\sum_i\sum_{n=0}^{N-1}\int_{-\infty}^{\infty}\mathrm{d}\varepsilon\, n_i(\varepsilon)\frac{\varepsilon-\mu+\chi_i(\mathrm{i}\omega_n)}{\Theta_i(\varepsilon,n)}.$$

Again, the density of states is also part of the definition of the electron-phonon coupling strength $\lambda_{ij} \equiv \lambda_{ij}(0) = -n_j(\mu_0)\, g_{ij}^2\, D(0)$. For symmetric electron-phonon matrix elements $g_{ij} = g_{ji}$, which can be taken for granted, it follows that $\lambda_{ij}/\lambda_{ji} = n_j(\mu_0)/n_i(\mu_0)$ [35, Eq. 3.64].

Analogously, for constant band densities of states one finds [47, Eqs. 1, 2]

$$Z_i(\mathrm{i}\omega_n) = 1 + \frac{\pi T}{\omega_n}\sum_j\sum_{m=0}^{N-1}\frac{\omega_m}{\sqrt{\omega_m^2+\Delta_j^2(\mathrm{i}\omega_m)}}\Lambda_{ij}^{-}(n,m), \tag{4.24a}$$

$$\Delta_i(\mathrm{i}\omega_n) = \frac{\pi T}{Z_i(\mathrm{i}\omega_n)}\sum_j\sum_{m=0}^{N-1}\frac{\Delta_j(\mathrm{i}\omega_m)}{\sqrt{\omega_m^2+\Delta_j^2(\mathrm{i}\omega_m)}}[\Lambda_{ij}^{+}(n,m) - 2\mu_{ij}^{*}(N)]. \tag{4.24b}$$

$\mu_{ij}^{*}(N)$ is assumed to be rescaled appropriately for the respective set of equations.

4.8.1 Alternate interpretation

In the multi-band case the summations over band indices are already part of the underlying interaction Hamilton operators and find their way through the Feynman-Dyson perturbation theory into the Eliashberg equations. However, it is also possible to yield formally identical equations within the single-band formalism.

The basic idea of the local approximation is to reduce the dependence on wave numbers to a mere energy-dependence. Essentially,

$$\sum_{\boldsymbol{k}} f(\boldsymbol{k}) \approx \int_{-\infty}^{\infty}\mathrm{d}\varepsilon\,\overbrace{\sum_{\boldsymbol{k}}\delta(\varepsilon-\varepsilon_{\boldsymbol{k}})}^{N(\varepsilon)}\, f(\varepsilon).$$

In the special case where $f(\boldsymbol{k})$ is a function of $\varepsilon_{\boldsymbol{k}}$ only, the above equation becomes exact. Otherwise $f(\varepsilon)$ must be an appropriate constant-energy average. The alternate idea is now to split the domain of the band-structure, e.g. the first Brillouin zone, into subdomains for which separate densities of states are determined [48; 49] and the corresponding averages taken:

$$\sum_{\boldsymbol{k}} f(\boldsymbol{k}) \approx \sum_i\int_{-\infty}^{\infty}\mathrm{d}\varepsilon\,\overbrace{\sum_{\boldsymbol{k}\in D_i}\delta(\varepsilon-\varepsilon_{\boldsymbol{k}})}^{N_i(\varepsilon)}\, f_i(\varepsilon) \quad \text{where} \quad \bigcup_i D_i = \text{Brillouin zone}.$$

In this case, i indicates subdomains of the reciprocal space rather than bands. This procedure may in turn be generalized with respect to further quantum numbers such as *real* band indices. Most generally, the indices i number arbitrary disjoint subsets of electronic states.

4.9 Linearized equations

At T_c, where the order parameter $\Delta(i\omega_m)$ is infinitesimal, and in the normal state, where it is zero, it can be neglected relative to ω_m. Analogous to Eqs. 4.13, the real-axis equations used by McMillan, the CDOS Eliashberg equations on the imaginary axis and for multiple electronic bands, as given in Eqs. 4.24, assume the following linear form:

$$Z_i(i\omega_n) = 1 + \frac{1}{2n+1}\sum_j \sum_{m=0}^{N-1} \Lambda^-_{ij}(n,m), \tag{4.25a}$$

$$\Delta_i(i\omega_n) = \frac{1}{Z_i(i\omega_n)}\sum_j \sum_{m=0}^{N-1} \frac{\Delta_j(i\omega_m)}{2m+1}[\Lambda^+_{ij}(n,m) - 2\mu^*_{ij}(N)]. \tag{4.25b}$$

At this point the equation for $Z_i(i\omega_n)$ is neither coupled to the equation of $\Delta_i(i\omega)$ nor must it be solved self-consistently. For $N \to \infty$ one can further evaluate

$$Z_i(i\omega_n) = 1 + \frac{1}{2n+1}\sum_j \sum_{m=-n}^{n} \lambda_{ij}(m) = 1 + \frac{1}{2n+1}\sum_j \Big[\lambda_{ij} + 2\sum_{m=1}^{n} \lambda_{ij}(m)\Big]. \tag{4.26}$$

This yields the matrix equation $\boldsymbol{\Delta}\cdot\boldsymbol{K} = \boldsymbol{\Delta}$, component-wise written as [34, Eq. 11.10]

$$\begin{aligned}
\Delta_i(i\omega_n) &= \sum_j \sum_{m=0}^{N-1} K_{ij}(n,m)\,\Delta_j(i\omega_m),\\
K_{ij}(n,m) &= \frac{1}{2m+1}[\Lambda^+_{ij}(n,m) - \delta_{ij}\delta_{nm}D^N_i(n) - 2\mu^*_{ij}(N)],\\
D^N_i(n) &= \sum_j \sum_{m=0}^{N-1} \Lambda^-_{ij}(n,m) \overset{N=\infty}{=} \sum_j \Big[\lambda_{ij} + 2\sum_{m=1}^{n}\lambda_{ij}(m)\Big].
\end{aligned} \tag{4.27}$$

Since at temperatures greater than, equal to or less than T_c multiplication with the *kernel* $\boldsymbol{K}$ ought to or diminish, maintain or amplify the magnitude of the order parameter $\boldsymbol{\Delta}$, respectively, T_c is defined as the temperature at which the greatest eigenvalue of $\boldsymbol{K}$ crosses unity [34, p. 47].

Before the analysis can go more into detail, it is necessary to introduce the direct matrix product and its spectral properties, which will be done in the following section.

4.9.1 Direct product

The *direct product* or *Kronecker product* $\boldsymbol{A}\otimes\boldsymbol{B}$ of the $r\times c$ matrix $\boldsymbol{A}$ and the $R\times C$ matrix $\boldsymbol{B}$ is the $rc\times RC$ matrix defined by

$$(\boldsymbol{A}\otimes\boldsymbol{B})_{ij,nm} = A_{in}B_{jm},$$

where ij, nm can be interpreted e.g. as $iR+j, nC+m$ if all indices are zero-based. This definition also holds for column vectors if these are considered as, say, $N\times 1$ matrices.

With the help of the identity

$$(\boldsymbol{A}\otimes\boldsymbol{B})\cdot(\boldsymbol{C}\otimes\boldsymbol{D}) = (\boldsymbol{A}\cdot\boldsymbol{C})\otimes(\boldsymbol{B}\cdot\boldsymbol{D})$$

which is easily proved component-wise,

$$\begin{aligned}
[(\boldsymbol{A}\otimes\boldsymbol{B})\cdot(\boldsymbol{C}\otimes\boldsymbol{D})]_{ij,pq} &= \sum_{nm}(\boldsymbol{A}\otimes\boldsymbol{B})_{ij,nm}\,(\boldsymbol{C}\otimes\boldsymbol{D})_{nm,pq} = \sum_{nm} A_{in}B_{jm}C_{np}D_{mq}\\
&= \sum_n A_{in}C_{np}\sum_m B_{jm}D_{mq} = (\boldsymbol{A}\cdot\boldsymbol{C})_{ip}\,(\boldsymbol{B}\cdot\boldsymbol{D})_{jq} = [(\boldsymbol{A}\cdot\boldsymbol{C})\otimes(\boldsymbol{B}\cdot\boldsymbol{D})]_{ij,pq},
\end{aligned}$$

one can show that, if the eigenvalue equations $\boldsymbol{A}\cdot\boldsymbol{\alpha} = a\boldsymbol{\alpha}$ and $\boldsymbol{B}\cdot\boldsymbol{\beta} = b\boldsymbol{\beta}$ hold,

$$(\boldsymbol{A}\otimes\boldsymbol{B})\cdot(\boldsymbol{\alpha}\otimes\boldsymbol{\beta}) = (\boldsymbol{A}\cdot\boldsymbol{\alpha})\otimes(\boldsymbol{B}\cdot\boldsymbol{\beta}) = (a\boldsymbol{\alpha})\otimes(b\boldsymbol{\beta}) = ab(\boldsymbol{\alpha}\otimes\boldsymbol{\beta}). \tag{4.28}$$

The eigenvectors and -values of the direct product of two matrices are thus the direct and normal products of the respective eigenvectors and -values of the individual matrices.

4.9.2 Effective scalar coupling strengths

Below, two approximations are presented which allow to map the matrices describing multi-band coupling strengths onto scalar values which lead to similar critical temperatures and, above all, may also be inserted into McMillan's equation. It shall be noted that for all non-scalar couplings there are always innumerable sets of effective scalar parameters which yield exactly the same critical temperature – it is just that there are no simple rules to generate them.

Non-renormalized

Supposing that there is no energy renormalization, i.e. $Z_i(\mathrm{i}\omega_n) = 1$ for all bands and frequencies, which constitutes a very rough approximation, the kernel reduces to

$$K_{ij}(n,m) = \frac{1}{2m+1}[\Lambda^+_{ij}(n,m) - 2\mu^*_{ij}(N)].$$

Assuming further that the matrices $\boldsymbol{\lambda}$ and $\boldsymbol{\mu}^*(N)$ describing the intra- and inter-band electron-phonon coupling strengths and rescaled Coulomb pseudo-potentials are proportional, i.e. $\mu^*_{ij}(N) = c\,\lambda_{ij}$ with $c \geq 0$, one can write $K_{ij}(n,m) = \lambda_{ij} Q(n,m)$ with $Q(n,m)$ independent of band indices. This is nothing but a direct matrix product:

$$\boldsymbol{K} = \boldsymbol{\lambda} \otimes \boldsymbol{Q}.$$

Hence, applying Eq. 4.28, the largest eigenvalue of $\boldsymbol{K}$ is the product of the largest eigenvalues of $\boldsymbol{Q}$ and $\boldsymbol{\lambda}$ (in magnitude). As a consequence, if there exists a single-band system with positive coupling strengths λ and $\mu^*(N)$ which exhibits the same critical temperature as a multi-band system with coupling matrices $\boldsymbol{\lambda}$ and $\boldsymbol{\mu}^*(N)$, then the further would be given by the greatest eigenvalues of the latter if the renormalization were unity. For two bands and $\mu^*(N) = 0$,

$$\lambda = \frac{1}{2}\Big[\lambda_{11} + \lambda_{22} + \sqrt{(\lambda_{11} - \lambda_{22})^2 + 4\lambda_{12}\lambda_{21}}\Big].$$

Cutoff-independent

Another approach takes the mapping searched for as independent of the cutoff frequency ω_N. This allows to derive it for the most simple case where $N = 1$. Consequently, $n = m = 1$ and

$$K_{ij} = 2\lambda_{ij} - \delta_{ij}\sum_k \lambda_{ik} - 2\mu^*_{ij}(N),$$

where $\lambda_{ij}(1) \approx \lambda_{ij}$ has been assumed in addition. For two bands and $\mu^*_{ij}(N) = 0$,

$$\boldsymbol{K} = \begin{bmatrix} \lambda_{11} - \lambda_{12} & 2\lambda_{12} \\ 2\lambda_{21} & \lambda_{22} - \lambda_{21} \end{bmatrix}$$

the greatest eigenvalue of which gives the desired approximate effective coupling strength:

$$\lambda = \frac{1}{2}\Big[\lambda_{11} - \lambda_{12} - \lambda_{21} + \lambda_{22} + \sqrt{(\lambda_{11} - \lambda_{12} + \lambda_{21} - \lambda_{22})^2 + 16\lambda_{12}\lambda_{21}}\Big].$$

4.9.3 Beyond CDOS

If the band densities of states are not considered to be constant, Eqs. 4.23 have to be solved. The only simplification emerging at T_c is that the order parameter can be neglected in the common denominator which becomes $\Theta_i(\varepsilon, n) = [\omega_n Z_i(\mathrm{i}\omega_n)]^2 + [\varepsilon - \mu + \chi_i(\mathrm{i}\omega_n)]^2$. As a consequence, renormalization function and energy shift are decoupled from the order parameter and may thus be determined independently. Having done so, these normal-state properties, together with the self-consistent chemical potential, are inserted into the remaining equation which yields

$$\begin{aligned} \phi_i(\mathrm{i}\omega_n) &= \sum_j \sum_{m=0}^{N-1} K_{ij}(n,m)\,\phi_j(\mathrm{i}\omega_m), \\ K_{ij}(n,m) &= T_c \int_{-\infty}^{\infty} \mathrm{d}\varepsilon \frac{n_j(\varepsilon)}{n_j(\mu_0)} \frac{\Lambda^+_{ij}(n,m) - 2\mu^*_{ij}(N)}{[\omega_m Z_j(\mathrm{i}\omega_m)]^2 + [\varepsilon - \mu + \chi_j(\mathrm{i}\omega_m)]^2}. \end{aligned} \tag{4.29}$$

4.10 Padé approximants

The imaginary-axis Eliashberg equations are more convenient for a computational implementation than their real-axis counterparts since they involve sums over already discrete Matsubara frequencies rather than integrals the domains of which are yet to be discretized, which is always accompanied by some loss of accuracy. In addition, no complex quantities are involved.

Because real-axis results can be obtained from imaginary-axis results via analytic continuation as per Eq. 3.13, being interested in the former it may still be worth it to take a detour via the latter. Hereby the problem arises, that an *analytic* continuation can only be applied to some analytic expression, whereas the numerical results are generally just a finite set of sample points. In the following, a solution proposed by Vidberg and Serene in 1977 [6] is presented.

Let $\Sigma(\mathrm{i}\omega_n)$ with $n \in \{0 \dots N-1\}$ act as a placeholder for any of the self-energy components resulting from the Eliashberg equations and derived quantities. The idea is to interpolate this numerical result by a rational function to which the analytic continuation can then be applied. This *Padé approximant* may be written as a continued fraction

$$\Sigma(\omega) = \cfrac{c_0}{1 + \cfrac{c_1\,(\omega - \mathrm{i}\omega_0)}{1 + \cfrac{c_2\,(\omega - \mathrm{i}\omega_1)}{\dots}}} \quad \text{with} \quad c_n = 0 \quad \text{for} \quad n \geq N, \tag{4.30}$$

where the non-zero coefficients have to be determined so that all imaginary-axis results are reproduced. For this purpose, Vidberg and Serene propose the following algorithm:

$g_0(\mathrm{i}\omega_m) \leftarrow \Sigma(\mathrm{i}\omega_m)$ for all m.

For $n = 0 \dots N-2$:

$$g_{n+1}(\mathrm{i}\omega_m) \leftarrow \frac{g_n(\mathrm{i}\omega_n) - g_n(\mathrm{i}\omega_m)}{(\mathrm{i}\omega_m - \mathrm{i}\omega_n) g_n(\mathrm{i}\omega_m)} \quad \text{for } m > n.$$

$c_n \leftarrow g_n(\mathrm{i}\omega_n)$ for all n.

For each $\omega \in \mathbb{R}$ of interest:

$\boldsymbol{x}_0(\omega) \leftarrow (0 \quad 1)$.

$\boldsymbol{x}_1(\omega) \leftarrow (c_0 \;\; 1)$.

For $n = 1 \dots N-1$:

$$\boldsymbol{x}_{n+1}(\omega) \leftarrow \boldsymbol{x}_n(\omega) + c_n(\omega - \mathrm{i}\omega_{n-1})\,\boldsymbol{x}_{n-1}(\omega).$$

$$\Sigma(\omega) \leftarrow \frac{[\boldsymbol{x}_N(\omega)]_1}{[\boldsymbol{x}_N(\omega)]_2}.$$

Having determined the coefficients, this algorithm does not calculate the continued fraction as stated in Eq. 4.30 but rather its representation as a fraction of two polynomials via a forward-recurrence formula. This would be favorable if not only the final but also intermediate approximants $[\boldsymbol{x}_n(\omega)]_1/[\boldsymbol{x}_n(\omega)]_2$ taking only $n < N$ points into account were needed. However, being only interested in the N-point Padé approximant, a backward-recurrence algorithm which simply calculates the continued fraction successively from *'tail to head'* is preferable for both requiring less operations and being numerically more stable [50]:

For each $\omega \in \mathbb{R}$ of interest:

$\Sigma(\omega) \leftarrow 1$.

For $n = 1 \dots N-1$ in reversed order:

$$\Sigma(\omega) \leftarrow 1 + \frac{c_n\,(\omega - \mathrm{i}\omega_{n-1})}{\Sigma(\omega)}.$$

$$\Sigma(\omega) \leftarrow \frac{c_0}{\Sigma(\omega)}.$$

The actual implementation for this work can be consulted in Section B.4.

Chapter 5

Single-band results

Having presented most of the analytic framework, the following chapters will be dedicated to the presentation of more specific, mostly numerical results. For now, only a single electronic band is taken into account.

To make a start, the self-energy components which constitute the solution of the Eliashberg equations will be presented as functions of both Matsubara and real frequencies. Before that, however, the analytic continuation by means of Padé approximants shall be validated and an exemplary density of states to work with introduced. Next, several convergence tests are performed which guarantee the accuracy of the following results: McMillan's equation is adapted to the special case of Einstein phonon spectra and subsequently tested as part of a series of critical-temperature benchmarks. Finally, the influence of density of states and particle number is discussed in detail.

5.1 Preliminary considerations

5.1.1 Validation of Padé approximant

In this section the suitability of Padé approximants to perform an analytic continuation of numerical data is tested using the example of the only self-energy component of interest for which an analytic expression is available, namely the renormalization function in the normal state within the CDOS approximation.

With the help of Eq. A.7 of Ref. 34 one can easily extend the domain of Eq. 4.26 from the Matsubara frequencies on the imaginary axis to the whole complex plane. For a single band,

$$Z(\omega) = 1 + \frac{\pi \mathrm{i} T}{\omega} \lambda \left\{ 1 + \frac{\omega_\mathrm{E}}{2\pi \mathrm{i} T} \left[\psi\left(\tfrac{1}{2} + \tfrac{\omega + \omega_\mathrm{E}}{2\pi \mathrm{i} T}\right) - \psi\left(\tfrac{1}{2} + \tfrac{\omega - \omega_\mathrm{E}}{2\pi \mathrm{i} T}\right) + \psi\left(1 - \tfrac{\omega_\mathrm{E}}{2\pi \mathrm{i} T}\right) - \psi\left(1 + \tfrac{\omega_\mathrm{E}}{2\pi \mathrm{i} T}\right) \right] \right\}.$$

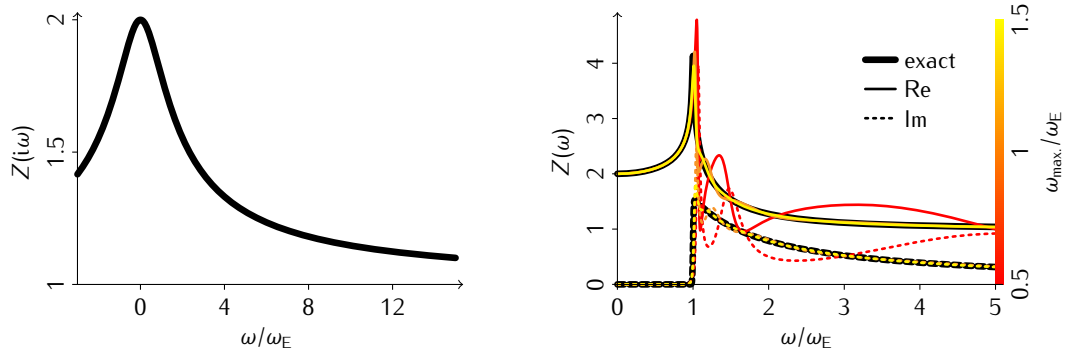

Figure 5.1: Exact normal-state CDOS renormalization together with selected Padé approximants for an electron-phonon coupling strength $\lambda = 1$, a phonon frequency $\omega_\mathrm{E} = 20\,\mathrm{meV}$ and a temperature $T = 1\,\mathrm{K}$.

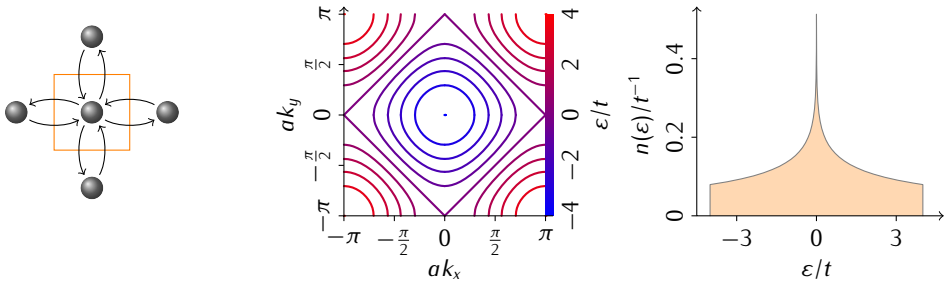

(a) unit cell **(b)** dispersion **(c)** density of states

Figure 5.2: Properties of the square tight-binding lattice.

In Fig. 5.1, $Z(\omega)$ is plotted on both the real and the imaginary axis. In the former case it is complemented with some PADÉ approximants which interpolate the imaginary-axis result $Z(\mathrm{i}\omega_n)$ at all MATSUBARA frequencies $\omega_n \in (0, \omega_{\text{max.}})$. All beyond the respective $\omega_{\text{max.}}$ is discarded.

On the imaginary axis the renormalization is real and bell-shaped with the center at the origin. On the real axis it is more complicated: There is a peak with an imaginary discontinuity at the phonon frequency $\pm\omega_\text{E}$. Below that, the imaginary part vanishes and the real part increases with frequency starting slightly above $1 + \lambda$. Beyond that, real and imaginary parts decay towards unity and zero, respectively.

It turns out that the quality of the PADÉ approximant increases with $\omega_{\text{max.}}$, as expected. Already for small multiples of ω_E the exact and approximate curves coincide to a high degree.

5.1.2 Square lattice

In order to perform calculations beyond the approximation of a constant density of states, some kind of model or experimental data which provides the necessary electronic structure is required. Throughout the present work, a tight-binding model of a square lattice will be applied for this purpose. The unit cell with a single basis atom is depicted in Fig. 5.2a, where arrows represent the allowed electronic transitions. The defining HAMILTON operator in first quantization reads

$$\mathrm{H} = -t \sum_{\boldsymbol{R}} [|\boldsymbol{R} + \boldsymbol{t}_1\rangle + |\boldsymbol{R} - \boldsymbol{t}_1\rangle + |\boldsymbol{R} + \boldsymbol{t}_2\rangle + |\boldsymbol{R} - \boldsymbol{t}_2\rangle]\langle\boldsymbol{R}|,$$

where the sum goes over all lattice sites $\boldsymbol{R} = n_1\boldsymbol{t}_1 + n_2\boldsymbol{t}_2$ with $n_1, n_2 \in \mathbb{Z}$ at which the WANNIER states $|\boldsymbol{R}\rangle$ are localized. t is the nearest-neighbor coupling parameter, $\boldsymbol{t}_1 = [a\ 0]$ and $\boldsymbol{t}_2 = [0\ a]$ are the translation vectors of length a, the lattice constant.

An expansion into BLOCH states $|\boldsymbol{k}\rangle$ with $\boldsymbol{k} = [k_x\ k_y]$ via the FOURIER transform

$$|\boldsymbol{R}\rangle = \int \mathrm{d}\boldsymbol{k}\, \mathrm{e}^{-\mathrm{i}\boldsymbol{k}\boldsymbol{R}} |\boldsymbol{k}\rangle,$$

where the integration is e.g. over the first BRILLOUIN zone, leads to the dispersion relation

$$\varepsilon(\boldsymbol{k}) = -2t\,[\cos(k_x a) + \cos(k_y a)]$$

a contour plot of which is given in Fig. 5.2b.

Finally, the corresponding density of states per spin and unit cell, shown in Fig. 5.2c, reads

$$n(\varepsilon) = \frac{K\left(1 - \left(\frac{\varepsilon}{4t}\right)^2\right)}{2\pi^2 t} \quad \text{where} \quad K(x) = \int_0^{\frac{\pi}{2}} \mathrm{d}\varphi \left[1 - x \sin^2(\varphi)\right]^{-\frac{1}{2}}$$

is the complete elliptic integral of the first kind [10, Eq. 4.146 and 4.147]. It features a VAN HOVE singularity at the FERMI level $\varepsilon = 0$ at half-filling, at which it diverges logarithmically [51, Eq. 7]. Since the density of states at the chemical potential of the non-interacting system enters in the definition of the coupling strengths in Eq. 4.4, which have to be finite, well-defined quantities, a reduced particle number, namely quarter-filling, is chosen in the following.

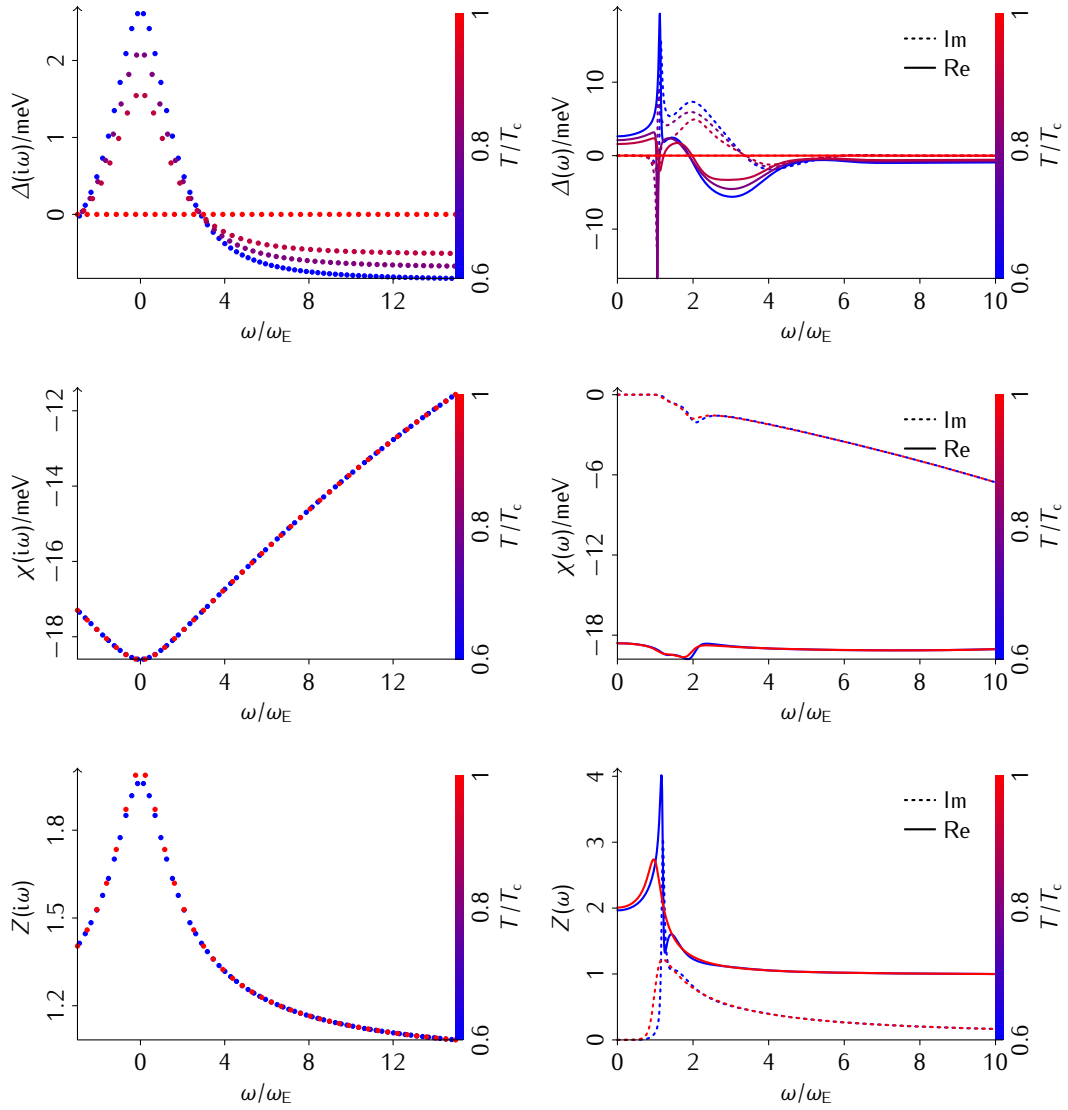

Figure 5.3: Imaginary- and real-axis self-energy components at different temperatures for a square-lattice density of states with an electronic bandwidth of 2 eV at quarter-filling, a phonon frequency $\omega_E = 20\,\text{meV}$, an electron-phonon coupling strength $\lambda = 1$, a Coulomb pseudo-potential $\mu^* = 0.1$ and a cutoff frequency $\omega_N = 100\,\omega_E$. Note that the displayed frequency ranges do not correspond to the cutoff.

5.2 Self-energy on real and imaginary axis

In Fig. 5.3 numerical solutions of the local Eliashberg equations stated in Eqs. 4.7 are shown together with their Padé approximants as presented in Section 4.10, analytically continued to the real axis, for different temperatures. For all parameter sets used in this work, the qualitative appearance of the resulting curves is the same:[1]

On the imaginary-axis not only the renormalization $Z(i\omega_n)$, in accordance with Fig. 5.1, but also the energy gap $\Delta(i\omega_n)$ and shift $\chi(i\omega_n)$ are bell-shaped and centered at the origin. The first-mentioned are always concave functions whereas the sign of the latter may change, resulting in a convex curve as in the example.

Asymptotically, the energy gap approaches the negative or vanishing constant Coulomb contribution given in Eq. 4.16, the renormalization goes to unity and the energy shift vanishes, but much more slowly than the former two.

[1] The imaginary-axis curves resemble those displayed in Refs. 51 and 52.

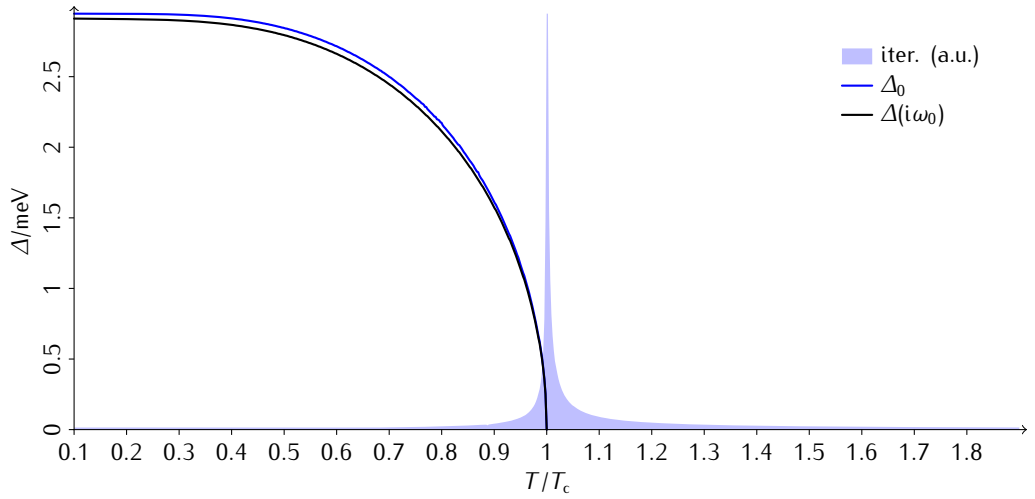

Figure 5.4: Order parameters. The temperature dependence of leading MATSUBARA and measurable gap is shown for the same parameter set as in Fig. 5.3, except for a lower cutoff frequency $\omega_N = 15\,\omega_E$. The phase transition in characterized by a diverging number of iterations needed to reach self-consistency.

The maybe most characteristic property of the energy gap is its temperature dependence, further discussed in the subsequent section, through which it is qualified as an order parameter for the superconducting state. With rising temperature it decreases with increasing speed towards zero, which is reached, by definition, at the critical temperature. In principal, this process affects the magnitude rather than the shape of the curve, resulting in a common zero of the displayed family of curves or, more precisely, of their analytic continuations, since naturally the solution is discrete on the imaginary axis and does not include this very point in general. Over the same temperature range, the other two quantities barely change.

On the real axis the shapes turn out to be more complicated. The renormalization $Z(\omega)$ basically resembles the analytic one, shown in Fig. 5.1, the properties of which have already been discussed. One of them, namely the vanishing imaginary part at frequencies below the renormalized phonon frequency, is recognized in the energy gap $\Delta(\omega)$ and shift $\chi(\omega)$ as well. The former even features the aforementioned peaks, in the vincinity of which the exact behavior of the PADÉ approximants is untrustworthy for being very sensitive to parameter changes. Beyond the peak, the real and imaginary parts of the energy gap describe arches of opposite orientation. The asymptotes of all quantities are the same as on the imaginary-axis, although in the case of the energy shift this does not become apparent from the depicted detail.

5.2.1 Temperature dependence of order parameter

Leaving the invariant shape of the energy gap on the imaginary frequency axis out of account, the temperature dependence of its magnitude, represented by its value at the first MATSUBARA frequency, is shown in Fig. 5.4, supplemented by the corresponding curve for the energy gap which is actually measurable in experiments and defined by the fixed-point equation [6, Eq. 3a]

$$\Delta_0 = \mathrm{Re}[\Delta(\Delta_0)]. \tag{5.1}$$

Both curves turn out to be very similar: Starting at absolute zero, they remain nearly constant at first and subsequently become ever steeper approaching the critical temperature at which they vanish. They resemble the well-known BCS result, exemplified in Fig. 2.1, which changes exponentially and like a square root near $T = 0$ and T_c, respectively [10, Eq. 11.60].

Fig. 5.4 also shows how the number of iterations needed to obtain a self-consistent solution of the ELIASHBERG equations increases drastically at the critical temperature. This is due to the magnitude of the energy gap converging much slower than its shape [6, p. 185]. Enforcing the normal-state property $\Delta = 0$ yields similar convergence rates at all temperatures, T_c included.

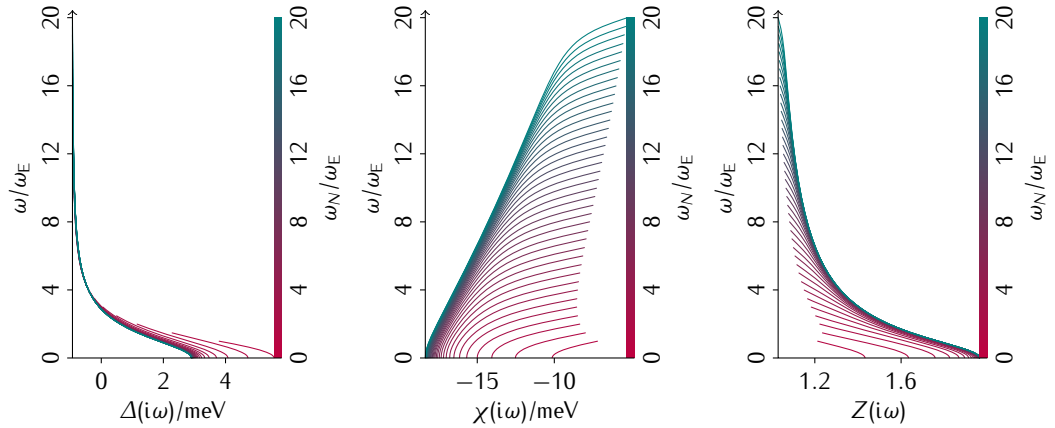

Figure 5.5: Comparison to expose cutoff-induced errors in the components of the self-energy. Except for the cutoff and a temperature $T = 1\,\mathrm{K}$, the settings are as for the results displayed in Figs. 5.3 and 5.4.

5.3 Convergence tests

It is now investigated how the results are influenced by the choices of, first, the cutoff frequency of the Matsubara sums and, secondly, the number of points used for the quadrature of the energy integrals, which are both mandatory for a computational implementation of the Eliashberg equations. This knowledge is necessary to obtain confidence in all subsequent results.

5.3.1 Convergence of self-energy with cutoff frequency

In Fig. 5.5 the self-energy components on the imaginary axis are shown for different cutoff frequencies. Since a low temperature has been chosen, the Matsubara frequencies lie sufficiently close together to use line rather than scatter plots.

It turns out that the sensitivities of different quantities to the cutoff frequency differ. The energy shift proves to be affected most, especially near the cutoff itself where it decays spontaneously. A similar behavior, but much less pronounced, is found for the renormalization, in contrast to the energy gap which exhibits the correct asymptotes. Regarding the magnitude it becomes evident that the energy gap is favored by a low cutoff whereas renormalization and energy shift are suppressed.

With the above results in mind one could argue that an application of the imaginary-axis Eliashberg equations at low frequencies, where the computational workload is small, is pointless, at least being interested in more than qualitative tendencies. Nevertheless, when determining the critical temperature, the artifacts of the cutoff in the frequency dependence of the self-energy will be of minor importance.

5.3.2 Convergence of T_c with cutoff frequency

The quantity to be handled with most care regarding the cutoff is the Coulomb pseudo-potential already discussed in Section 4.6.1, which led to the introduction of a rescaled quantity. In order to point out the benefits of the latter, in Fig. 5.6 the critical temperature is shown as a function of the cutoff frequency for both a constant and a rescaled Coulomb pseudo-potential.

Depending on whether the density of states is assumed to be constant or not, different rescaling prescriptions have to be used. For the CDOS approximation, Eq. 4.20 can be directly applied. Otherwise one has to resort to Eq. 4.17 which unfortunately involves the original coupling constant μ_C rather than McMillan's Coulomb pseudo-potential μ^*. Hence, in order to obtain roughly comparable results in both cases, whenever the density of states is taken into account the first step is to estimate μ_C from μ^* which is done via Eq. 4.14, where E_B is assumed to be half the electronic bandwidth.

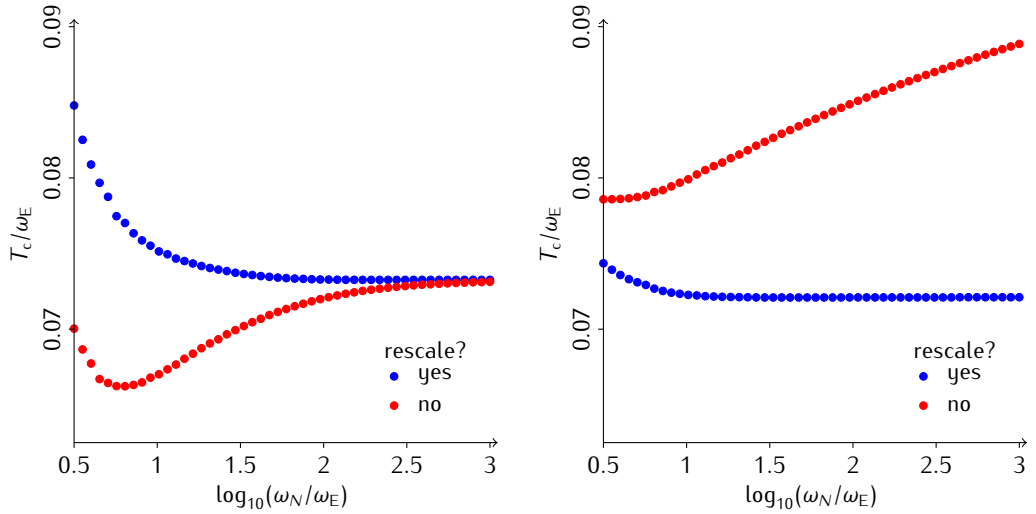

(a) square lattice at quarter-filling **(b)** constant density of states

Figure 5.6: Convergence with cutoff for a phonon frequency $\omega_E = 20\,\text{meV}$, an electron-phonon coupling strength $\lambda = 1$ and a Coulomb pseudo-potential $\mu^* = 0.1$. In each panel, the latter is rescaled differently.

It is confirmed that within the CDOS approximation the rescaling is required in order to yield convergent results. This does not apply to the Eliashberg equations in general since within nothing but the local approximation one has convergence in any case; it is just considerably faster if an appropriate rescaling is performed. The CDOS convergence rate is not reached though.

An enhancement of the critical temperature with increasing cutoff frequency for a constant Coulomb pseudo-potential is in accordance with the fact that an appropriately rescaled Coulomb pseudo-potential behaves similarly, since the Coulomb interaction opposes superconductivity [53, p. 1038]. Having performed the rescaling, one is left with a decreasing curve which may be ascribed to results for the order parameter presented in Fig. 5.5.

Until now is has been taken for granted that the cutoff is defined in terms of frequency rather than a specific number of Matsubara frequencies. The latter is thus defined by the cutoff frequency and the temperature together. Hence, in Fig. 5.6 it varies both along the horizontal and the vertical axis. The reason for this definition of the cutoff is that, as stated above, the shape of the self-energy as a function of frequency does not change much with temperature.

5.3.3 Convergence of T_c with energy resolution

The remaining quantity by which the accuracy of numerical solutions is limited, is the number of points used for discretizing the integrands in Eqs. 4.7. The quadrature is performed using the trapezoidal rule and the energy points chosen equally spaced.

As can be seen in Fig. 5.7, the occurring errors are not as predictable as in Fig. 5.6, where the critical temperature was shown to converge with the cutoff frequency following continuous curves. Instead, the resulting critical temperatures are scattered apparently at random (of cause each calculation alone is deterministic) around the correct value, loosely bounded by radii which shrink with increasing resolution.

As already anticipated in the caption of Fig. 4.1b, the errors are larger for lower phonon frequencies, which correspond to lower temperatures at which the Lorentz functions to be integrated over are sharper and thus only resolved accurately if neighboring sample points are very close. Theoretically, it is also possible to guarantee the same precision for all temperatures with a constant number of points. But this requires an intelligent, non-equidistant sampling.

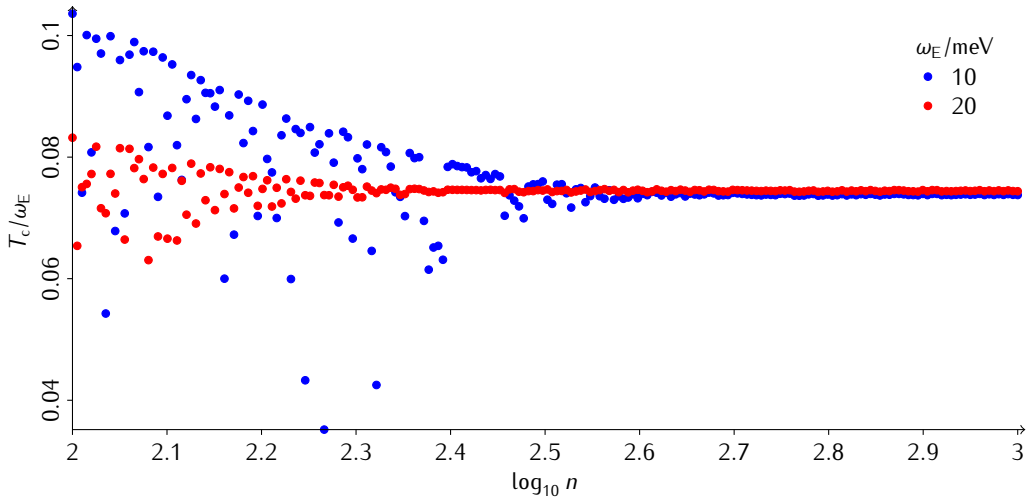

Figure 5.7: Convergence with the number of integration points for two different phonon frequencies. Constants are defined as in Fig. 5.4.

5.4 McMillan's equation for Einstein spectra

Having shown that the numerical results are stable and satisfy the qualitative expectations, the next step is a direct comparison with a well-established result, namely McMillan's equation for the critical temperature. It was derived starting from the CDOS Eliashberg theory, so that the latter should reproduce the results of the former at least approximately.

If there is any justifiable discrepancy between the original and the present work it is due to the electron-phonon spectral function or, more precisely, the phonon density of states. Whereas McMillan performed his calculations for niobium, now a simple Einstein spectrum is assumed. Interestingly, in place of the peak at the Einstein frequency in the real-axis self-energy displayed in Fig. 5.3, the analogous result of McMillan [1, Fig. 4] features two peaks which also appear in the phonon density of states of niobium.

Back on topic, the aim of this section is to derive an alternative T_c formula which differs from McMillan's only by the three fit parameters which are adjusted to an Einstein spectrum, i.e. a single phonon frequency, $\omega_E = 20\,\text{meV}$ in this case.

To that end, the first step is to determine critical temperatures for different electron-phonon coupling strengths and Coulomb pseudo-potentials. (McMillan calculated λ for different T_c and μ^*.) The results are listed in Table 5.1. The second step is to perform the linear regressions for Eqs. 4.15 applying the usual least-squares method. This is visualized in Fig. 5.8. The fit parameters turn out to be $A = 0.94 \pm 0.03$, $B = 1.11 \pm 0.01$ and $C = 0.74 \pm 0.01$. Hence,

$$T_c^E = \frac{\omega_E}{0.94} \exp\left[-\frac{1.11\,(1+\lambda)}{\lambda - 0.74\lambda\mu^* - \mu^*}\right].$$

λ \ μ^*	0.000	0.050	0.100	0.150	0.200	0.250
0.6	12.995	8.735	5.235	2.648	1.028	0.253
0.8	20.255	15.420	11.024	7.238	4.220	2.067
1.0	26.602	21.537	16.746	12.344	8.474	5.283
1.2	32.122	26.922	21.934	17.215	12.867	9.021
1.4	37.005	31.684	26.548	21.641	17.013	12.762
1.6	41.401	35.950	30.680	25.621	20.807	16.295

Table 5.1: $T_c \pm 0.001\,\text{K}$ for different λ and μ^* with $\omega_E = 20\,\text{meV}$.

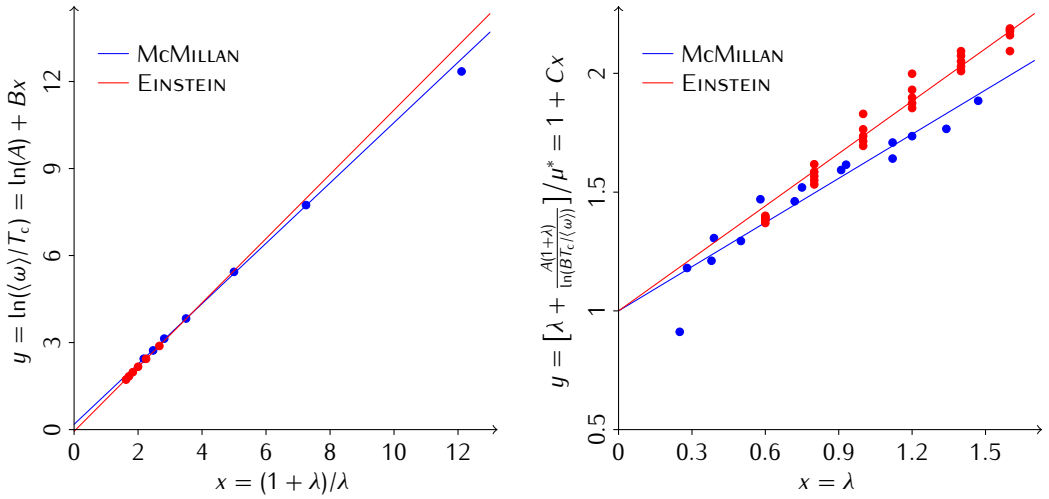

(a) $\mu^* = 0$ **(b)** $\mu^* > 0$

Figure 5.8: Combined representation of McMillan's original data and lines of best fit together with their newly calculated counterparts for an Einstein phonon spectrum.

5.5 Critical-temperature benchmarks

At this point a comparison of local and CDOS Eliashberg theory as well as McMillan's formula, both original and adjusted, can be performed. Therefor, T_c is calculated for different ω_E, λ and μ^* whereby only one parameter is varied at a time and the others are held constant. The results are presented in Fig. 5.9.

Altogether, a very good agreement can be reported. As expected, the adjusted version of McMillan's formula does best in reproducing the critical temperature according to CDOS Eliashberg theory for Einstein spectra. The original formula works comparably good but it slightly underestimates the dependence on the Coulomb pseudo-potential and already fails at lower electron-phonon coupling strengths. However, it is well known that McMillan's formula intrinsically underestimates T_c for large λ [2]. It predicts the upper bound

$$\lim_{\lambda\to\infty} T_c = \frac{\langle\omega\rangle}{A} \exp\left[-\frac{B}{1 - C\mu^*}\right],$$

whereas Eliashberg theory states an asymptotic behavior proportional to $\sqrt{\lambda}$ [35, Eq. 3.56].

The differences between the results of the Eliashberg theory for constant and square-lattice densities of states are acceptable, especially if the heuristic mapping from μ^* to μ_C is taken into account. There is no general solution to resolve this ambiguity. Nevertheless, it still remains unclear to what extend the critical temperature is determined by the shape of the density of states in the vicinity of the chemical potential, since the square lattice at quarter filling, which has only been analyzed so far, is rather benign in this regard. This question is further investigated in the following section.

Apart from the comparison of the different theories, Fig. 5.9 gives a good overview of the general dependence of the critical temperature on the characteristic variables. Large values of λ and ω_E favor superconductivity, while μ^* opposes it. Concerning ω_E, the proportionality which is immanent in McMillan's formula is perfectly confirmed. It is responsible for the isotope effect and may be explained by the fact that ω_E enters the Eliashberg equations only through $\lambda(n)$ or the phononic Green function, the *'broadening'* of which is determined by T/ω_E.

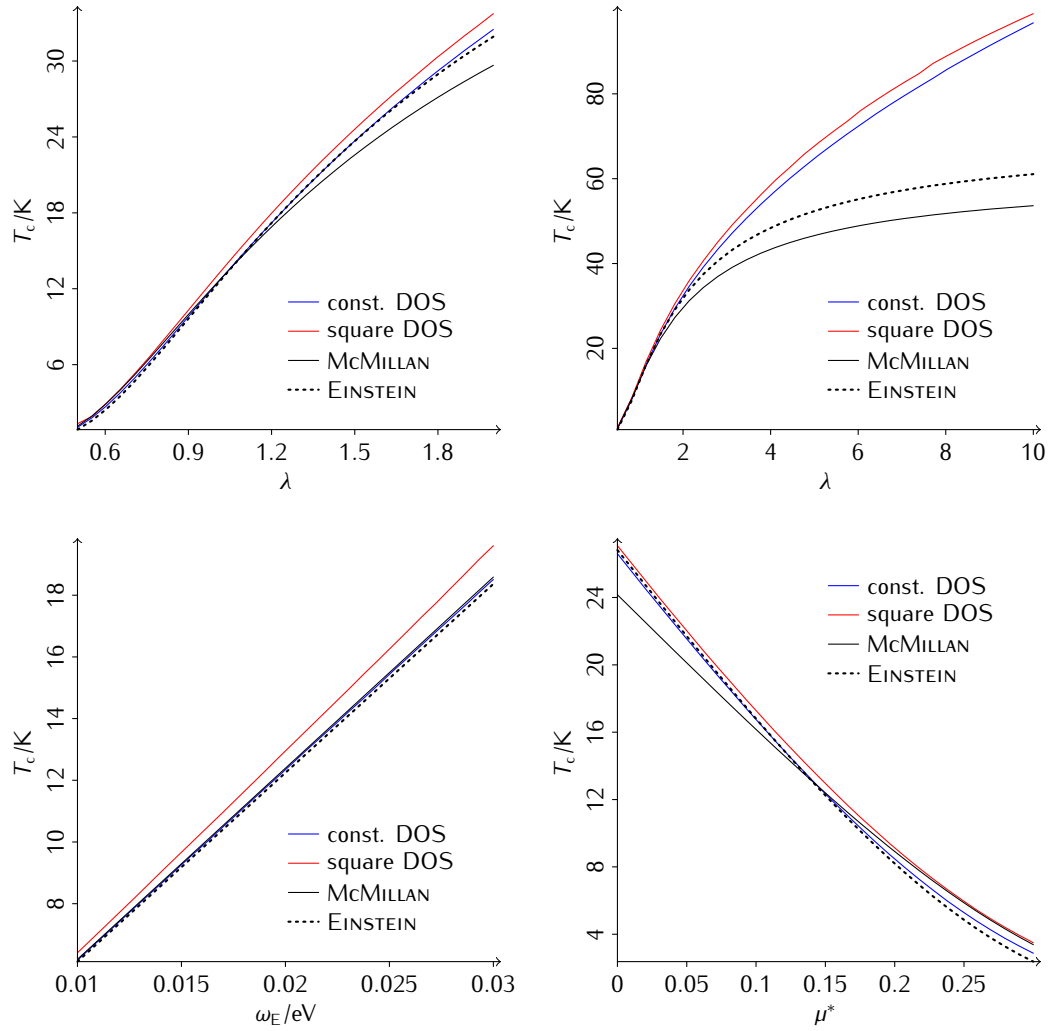

Figure 5.9: Comparison of the critical temperatures according to McMillan's formula in its original form and with its constants adjusted to an Einstein phonon spectrum as well as the local Eliashberg equations, either within the approximation of a constant density of states or for a square lattice with an electronic bandwidth of 2 eV at quarter-filling. As constants, an Einstein frequency $\omega_E = 20\,\text{meV}$, an electron-phonon coupling $\lambda = 1$ and a Coulomb pseudo-potential $\mu^* = 0.15$ are chosen. The Matsubara sum is cut off at $\omega_N = 15\,\omega_E$. 2001 points were used for the numerical solution of the energy integral.

5.6 Energy dependence

The final survey regarding the single-band Eliashberg theory is concerned with the dependence of the critical temperature on the shape of the density of states near the chemical potential, where the superconducting pairing takes place.

This is done by *'scanning'* the entire domain of the density of states of the square lattice by varying the chemical potential of the non-interacting system with respect to which the coupling strengths are defined. In addition to the critical temperature the change in the chemical potential (in order to conserve the particle number) and the leading value of the energy shift are determined. The results are shown in Fig. 5.10 together with a plot of the density of states. Note that the magnitude of the density of states only enters through the coupling strengths which are held constant.

The following interpretation is guided by the observations that a high density of states is generally favorable for superconductivity and that not only its value at one exact energy

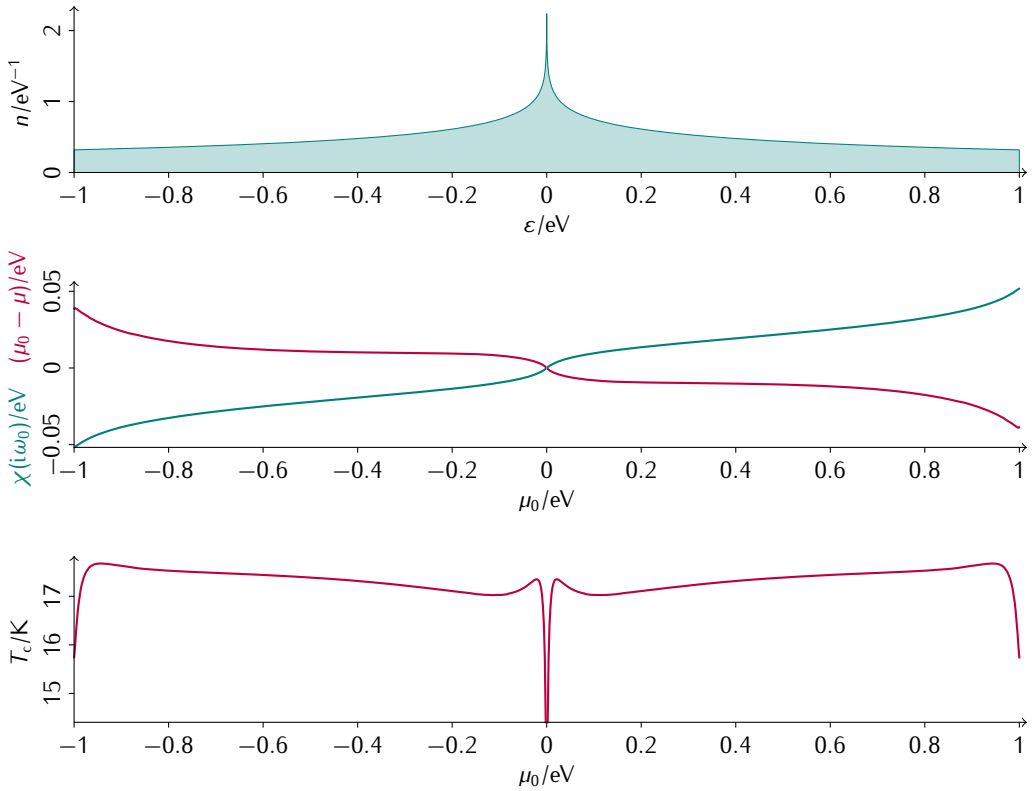

Figure 5.10: Energy dependence. It is shown how the critical temperature, the self-consistent chemical potential and the leading energy shift change with the chemical potential of the non-interacting system. Again, the parameters are the same as in Fig. 5.4.

contributes, but rather floating averages with respect to bell-shaped weight functions which are centered at $\mu - \chi(\mathrm{i}\omega_n)$, which can be directly deduced from Eq. 4.7.

Although $\chi(\mathrm{i}\omega_n)$ is partially compensated by the change of the chemical potential $\mu_0 - \mu$ [34, p. 80], as can be seen in the central panel of Fig. 5.10, it still determines the direction of the effective energy shift. More precisely, only for small MATSUBARA frequencies $\chi(\mathrm{i}\omega_n)$ exceeds the constant $\mu_0 - \mu$ in magnitude, but these are the ones with the dominant contribution. Hence, the focus is on $\chi(\mathrm{i}\omega_n)$, which always shifts the center of the floating average towards a higher density of states.

Very close to the VAN HOVE singularity and the band edges the critical temperature is lower than expected because the density of states entering the coupling constant does not represent the average density of states in the vicinity, which is less. At the singularity itself the matrix elements of the electron-phonon and COULOMB interaction must vanish in order to justify the definition of finite coupling constants. If a critical temperature shall be ascribed to this case at all, it must be zero.

In between these extremes the situation is different: Approaching the VAN HOVE singularity from one of the sides, the center of the floating average is continuously shifted towards more favorable energies, albeit with decreasing magnitude, hence the slow decrease of the critical temperature. However, in the proximity of the VAN HOVE singularity the steep slope of the density of states overcompensates this effect, which leads to a boost of the critical temperature shortly before it drops towards zero.

To conclude, the shape of the density of states may affect the critical temperature considerably, especially where changes with energy are strong, e.g. at VAN HOVE singularities. This is a problem inherent in the definition of the coupling strengths, which should give a reliable measure of the real coupling. A possible solution is to use intensive coupling strengths which are defined with respect to wave functions rather than the density of states [54].

Chapter 6

Multi-band results

In the previous chapter it has been confirmed that McMillan's equation can very well be used to predict critical temperatures of local Eliashberg theory if only one electronic band is considered. The question remains, whether it may also be applied if the coupling strengths are matrices rather than scalars, which is equivalent to the problem of finding single-band systems which resemble multi-band systems with respect to the critical temperature – self-energies etc. will certainly differ. Having three degrees of freedom at hand, namely the phonon frequency ω_E, the electron-phonon coupling λ and the Coulomb pseudo-potential μ^*, there are of course innumerable possibilities to accomplish this. However, since an unphysical redistribution of influences shall be avoided, the further shall not be modified and, if the latter vanishes, one is left with determining a single parameter λ without ambiguities. This is what the present chapter is dedicated to, for the special case of a two-band system and within the CDOS approximation.

To begin with, the temperature dependence of the order parameters of the different bands is investigated in analogy to Section 5.2.1. Next, it presented how intra- and inter-band coupling strengths can be varied independently without altering the critical temperature. Based on this, the approximate mappings onto scalar coupling constants proposed in Section 4.9.2 are visualized using the example of inter-band coupling alone. Finally, the same approximations are tested with respect to the critical temperature itself.

6.1 Temperature dependence of order parameters

In the multi-band formalism a different self-energy, and thus a different energy gap, may be associated with each band. In Fig. 6.1 the two gaps of the considered two-band systems are shown as functions of temperature, i.e. in their role as order parameters, for different strengths of the inter-band coupling. The latter is chosen equally spaced on a logarithmic scale, which leads to a higher resolution on the side of small couplings. In the upper panel both inter-band coupling strengths are varied simultaneously, in the lower panels either of them is zero in order to point out its specific influence. Actually the latter situations are unphysical, since they may only be realized if either of the band densities of states, which also enter the diagonal coupling strengths, is zero or infinite (see Section 4.8). The diagonal elements, however, are chosen to be finite constants which differ by a factor of two.

In the case of intra-band coupling alone, which is not displayed in Fig. 6.1, one finds two curves which exactly resemble those for the single-band systems corresponding to the separate bands – because that is what they are. Each band has its own critical temperature; the upper one is associated with the system as a whole. Also, the number of iterations needed to reach convergence is found to be enhanced at both critical temperatures.

As soon as the influence of the band with the higher critical temperature on the other band is switched on – it is important to note that this coupling is not bidirectional –, the end of the lower curve is extended towards the end of the upper one resulting in a common critical temperature,[1] which retains the exact value determined by the greater intra-band coupling

[1] Within the BCS theory, a similar behavior has been observed by Suhl, Matthias and Walker [55, Fig. 2].

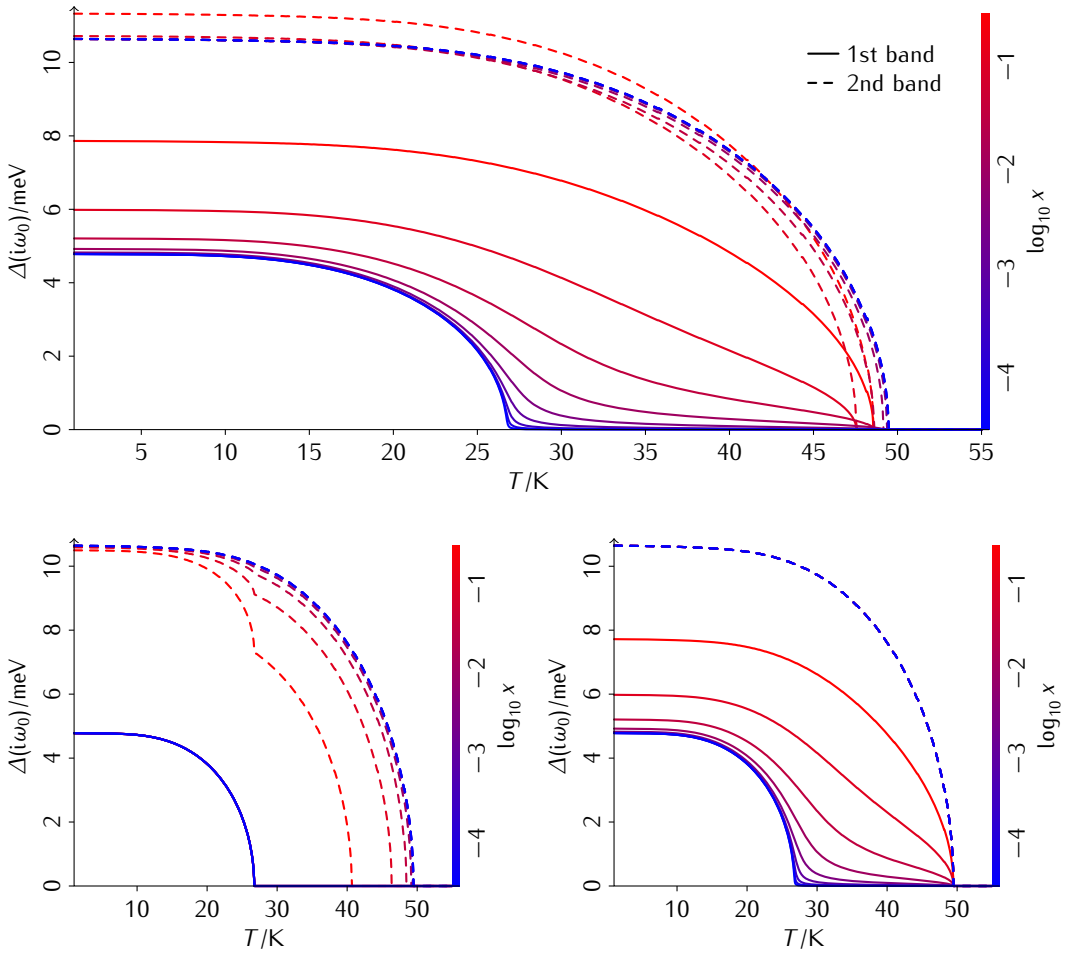

Figure 6.1: Incrementally switching on inter-band coupling. In analogy to Fig. 11 of Ref. 47, the temperature dependence of the leading MATSUBARA gaps of a two-band system with a phonon frequency $\omega_E = 20\,\text{meV}$ and no explicit COULOMB interaction is shown for different electron-phonon coupling matrices

$$\boldsymbol{\lambda}_{\text{top}} = \begin{bmatrix} 1 & x \\ x & 2 \end{bmatrix}, \quad \boldsymbol{\lambda}_{\text{left}} = \begin{bmatrix} 1 & 0 \\ x & 2 \end{bmatrix} \quad \text{and} \quad \boldsymbol{\lambda}_{\text{right}} = \begin{bmatrix} 1 & x \\ 0 & 2 \end{bmatrix}.$$

The density of states is assumed to be constant and the cutoff frequency chosen to be $\omega_N = 15\,\omega_E$.

strength (right panel). For this to happen, the strength of the switched-on coupling is irrelevant and only influences the magnitude along the newly formed tail.

In the case of a reversed influence, the upper critical temperature approaches the lower one, which in turn remains constant (left panel). At the same time, the lower curve becomes apparent in the shape of the upper curve at corresponding temperatures, resulting in a sharp bend at the lower critical temperature.

When both effects are combined, i.e. when the inter-band couplings are switched on simultaneously, there is a common critical temperature which depends on the common coupling strength (upper panel). At all other non-zero temperatures both curves are differentiable because the lower curve is softened by the way it reaches for the end of the upper curve, the shape of which it still has influence on.

Notably, the critical temperature is not always enhanced if an element of the electron-phonon coupling matrix increases. The possibility of an inhibiting influence is disregarded when taking the maximum eigenvalue of the coupling matrix as an effective scalar coupling strength, as described in Section 4.9.2, since it increases monotonically as a function of any element, just like the resulting critical temperature.

6.2 Critical isotherms

The influence of the individual elements of the electron-phonon coupling matrix on the critical temperature requires a more detailed analysis. Making a start, this section is dedicated to the search for *different* coupling matrices which yield the *same* critical temperature, i.e. for *'critical isotherms'* in the space of the matrix elements.

6.2.1 Hyperbolas of constant T_c

To divide the problem into manageable parts the following question is proposed: How must either the intra- or the inter-band coupling strengths change *simultaneously*, with the respective other pair of elements held constant, so that the corresponding critical temperature is conserved?

The outcome for some representative parameter sets is displayed in Fig. 6.2. The numerical results, illustrated as scatter plots, immediately suggest the following dependency: The matching intra- and inter-band coupling strengths lie on convex and concave sections of hyperbolas, respectively. This assumption is confirmed by comparison with a guess for the analytic dependence, which will be developed subsequently.

Let x represent the variable and y the dependent element of the electron-phonon coupling matrix. The most simple equation defining a hyperbola through $x = y = \lambda$ reads

$$y = \frac{\lambda^2}{x}.$$

However, the asymptotes would coincide with the x- and y-axes which is definitely not always the case in Fig. 6.2. The hyperbola is thus compressed by the factors α and β in x- and y-direction, respectively, with $x = y = \lambda$ defining the fixed point. This yields

$$y = \frac{\frac{\lambda^2}{\alpha(x-\lambda)+\lambda} - \lambda}{\beta} + \lambda = \frac{1}{\beta}\frac{\lambda^2 - \lambda[\alpha(x-\lambda)+\lambda]}{\alpha(x-\lambda)+\lambda} + \lambda = \lambda - \frac{\alpha}{\beta}\frac{\lambda(x-\lambda)}{\alpha(x-\lambda)+\lambda} = \lambda - \frac{\alpha}{\beta}\frac{\lambda}{\alpha + \frac{\lambda}{x-\lambda}}.$$

The new asymptotes are at $x = x_\infty = \lambda(1-\alpha^{-1})$ and $y = y_\infty = \lambda(1-\beta^{-1})$. Thus

$$y = \lambda - \frac{\lambda - y_\infty}{\lambda - x_\infty}\frac{\lambda}{\frac{\lambda}{\lambda - x_\infty} + \frac{\lambda}{x-\lambda}} = \lambda - \frac{\lambda - y_\infty}{x - x_\infty}(x-\lambda).$$

This formula describes the desired relation between the intra-band coupling strengths for x_∞ and y_∞ greater than or equal to λ. In contrast, x_∞ and y_∞ less than or equal to λ are required for the description of the inter-band coupling. The asymptotes may also be expressed in terms of the x- and y-intercepts x_0 and y_0:

$$x_0 = \lambda\Big[1 - \frac{\lambda - x_\infty}{y_\infty}\Big], \qquad x_\infty = \frac{\lambda^2 x_0}{\lambda(x_0+y_0) - x_0 y_0},$$
$$y_0 = \lambda\Big[1 - \frac{\lambda - y_\infty}{x_\infty}\Big], \qquad y_\infty = \frac{\lambda^2 y_0}{\lambda(x_0+y_0) - x_0 y_0}.$$

For each parameter set the asymptotes are determined numerically. For the inter-band coupling, x_∞ and y_∞ are calculated directly by assigning a very large value, 10^{10} say, to either λ_{12} or λ_{21} and solving for the other element. In the intra-band case the asymptotes are excluded from the domain of possible values. Hence, the intercepts are calculated with either λ_{11} or λ_{22} zero. The position of the asymptotes is then concluded by means of the above equations.

The determined hyperbolas are plotted together with the numerical data points, which reveals a very good agreement. The choice of the correct asymptotes depends not only on λ but also on the two matrix elements which are held constant. If an analytic expression of these dependencies were known, a closed set of equations would be obtained which could be solved for the scalar equivalent of the whole coupling matrix. This task is not accomplished within the present work, but in the following section some predictions of the proposed approximate mappings regarding this matter are presented.

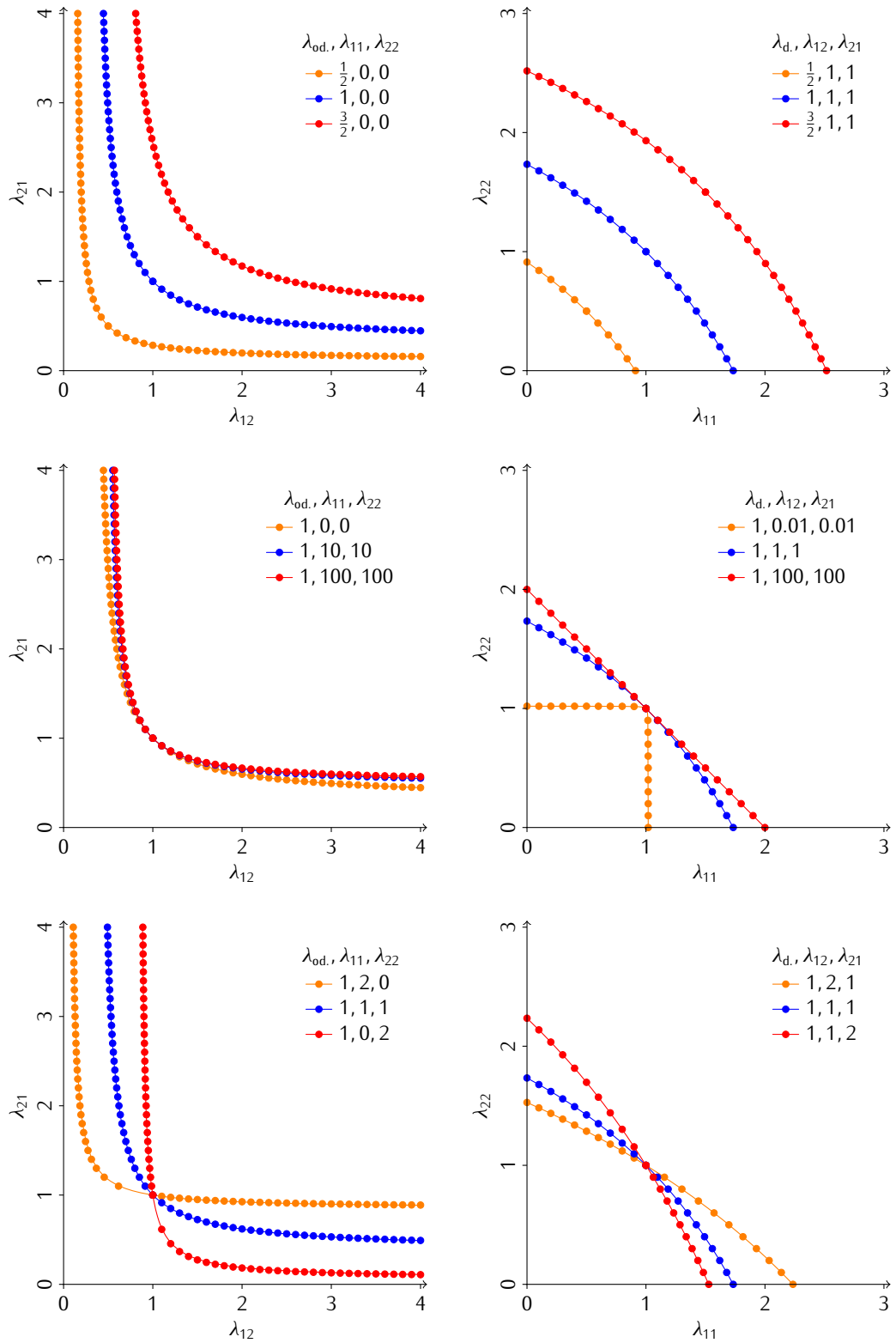

Figure 6.2: Hyperbolas of constant T_c. For the parameters $\omega_E = 20\,\text{meV}$, $\omega_N = 25\,\omega_E$ and $\mu^* = 0$, hyperbolas are shown, along which either intra- or inter-band electron-phonon coupling strengths in a two-band system may be jointly varied without changing the critical temperature. They intersect the bisector of the quadrant at $\lambda_{d.} = \lambda_{11} = \lambda_{22}$ and $\lambda_{od.} = \lambda_{12} = \lambda_{21}$, respectively. It shall be noted that the matrix $\boldsymbol{\lambda} = \lambda_{d.}\boldsymbol{\sigma}_0 + \lambda_{od.}\boldsymbol{\sigma}_1$ and the scalar $\lambda = \lambda_{d.} + \lambda_{od.}$ yield the same critical temperature.

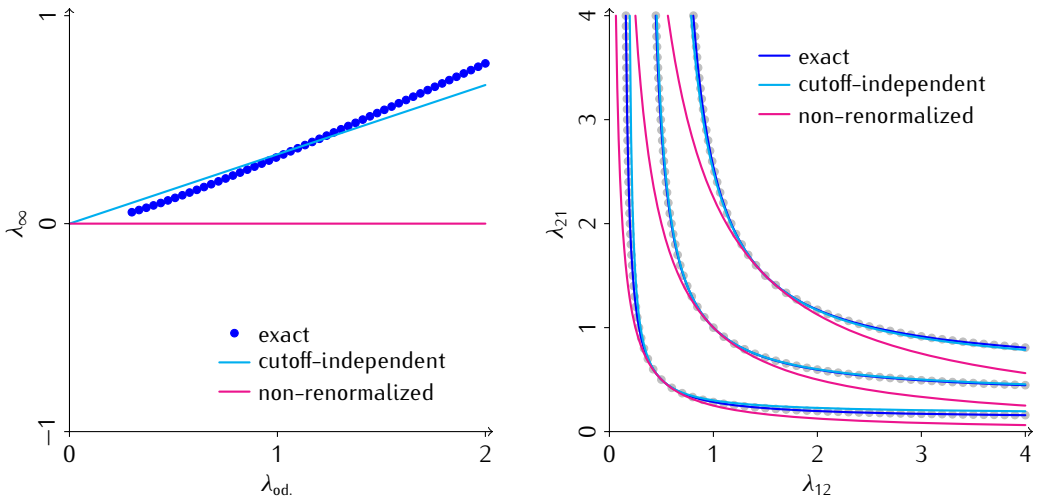

Figure 6.3: Position of the asymptotes λ_∞ of the hyperbolas of constant T_c for inter-band coupling only, i.e. $\lambda_{11} = \lambda_{22} = 0$, as a function of the coupling strengh λ. Not only exact results of the CDOS Eliashberg theory but also the behavior within the approximations of a cutoff-independent mapping onto effective scalar coupling constants (Section 4.9.2) and a renormalization of unity (Section 4.9.2) are presented. Phonon and cutoff frequency are chosen to be $\omega_E = 20\,\text{meV}$ and $\omega_N = 15\,\omega_E$, respectively.

6.2.2 Asymptotes for inter-band coupling

In this section the approximate mappings onto effective scalar coupling strengths which were introduced in Section 4.9.2 are visualized for the special case of inter-band coupling alone, i.e. $\lambda_{11} = \lambda_{22} = 0$. Because of the symmetry implied herein, λ_{12} as a function of λ_{21} is an involution, i.e. its own inverse. Subsequently, both asymptotes have the same distance to their corresponding axes.

The latter is determined both numerically and analytically according to Eqs. 4.9.2 and 4.9.2. In the case studied, the latter reduce to the hyperbola equations

$$\lambda = \sqrt{\lambda_{12}\lambda_{21}} \quad \text{and} \quad \lambda = -\frac{1}{2}\Big[\lambda_{12} + \lambda_{21} + \sqrt{(\lambda_{12}+\lambda_{21})^2 + 12\lambda_{12}\lambda_{21}}\Big].$$

Solving for λ_{21} and taking the limit $\lambda_{12} \to \infty$ yields the respective asymptotes:

$$\lambda_{21} = \frac{\lambda^2}{\lambda_{12}} \to 0 \quad \text{and} \quad \lambda_{21} = \frac{\lambda + \lambda_{12}}{3\lambda_{12} - \lambda}\lambda \to \frac{\lambda}{3}.$$

The results are presented in Fig. 6.3. For all values of λ, the approximation of a cutoff-independent mapping yields better results than the assumption of a renormalization of unity. Especially for $\lambda \approx 1$, the agreement is satisfactory; for larger λ it worsens continuously.

6.3 Effective scalar coupling strengths

Finally, the two mappings shall also be tested with respect to the critical temperatures they predict. To that end a sample of 500 electron-phonon coupling matrices is generated, the elements of which are random samples from a uniform distribution over $[0, 1)$, preselected by the criterion that their maximum eigenvalue is not less then $\frac{1}{2}$ in order to circumvent very low temperatures which are accompanied by a high computational workload caused by considering many Matsubara frequencies. For each matrix and their corresponding scalar couplings strengths, critical temperatures are calculated and plotted against each other. The resulting scatter plots are given in Fig. 6.4. It shall be noted that, on average, random coupling matrices may not represent those describing real materials very well.

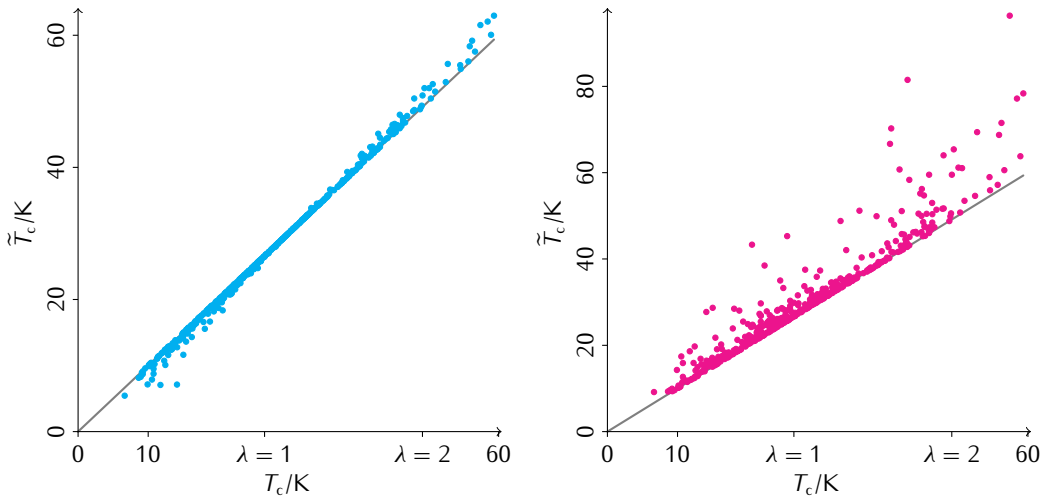

(a) cutoff-independent **(b)** non-renormalized

Figure 6.4: Visualization of the quality of the introduced approximate mappings onto effective scalar coupling strengths. For a random sample of electron-phonon coupling matrices and their corresponding scalar couplings strengths, critical temperatures are calculated and plotted against each other. The temperatures corresponding to integer scalar coupling strengths are marked for a better orientation. The continuous line is the quadrant bisector. Again, $\omega_E = 20\,\text{meV}$ and $\omega_N = 15\,\omega_E$.

The approximation of a cutoff-independent mapping turns out to be considerably more accurate than the assumption of a renormalization of unity, in accordance with the results of the previous section. Again, the former approach yields best results for coupling strengths in the vicinity of unity. Below and above it tends to under- and overestimate the critical temperature. The average absolute error is found to be 0.3 K. Also, the statement made at the end of Section 6.1 is confirmed: Neglecting the renormalization does never lead to an underestimate of the critical temperature – on the contrary in most of the cases. Here, the average absolute error is 2.2 K.

Chapter 7

Conclusion

Principally, the results of the present work are consistent with the critical temperatures obtained from McMillan's formula. In the only case where a direct comparison is possible, i.e. for scalar coupling strengths and within the CDOS approximation, the agreement is satisfactory except for large electron-phonon coupling strengths, a limitation which is well-known though. To some degree, the conformity may even be enhanced by adjusting the fit parameters to the considered phonon spectrum. Beyond this, there no one-to-one correspondence between either the Coulomb pseudo-potentials entering McMillan's formula and the Eliashberg equations considering a real density of states or the coupling matrices and effective scalars in the multi-band case.

Regarding the Coulomb pseudo-potential, several observations have been made: First, the CODS Eliashberg equations require a cutoff of the Matsubara sums. If the original strength of the Coulomb interaction is used without any rescaling, the critical temperature does not converge with an increasing cutoff as it would be the case without the CDOS approximation. Instead, it is known that the correct results are obtained at a cutoff frequency similar to the electronic bandwidth. There is, however, a fairly well justified relation between the parameter for McMillan's equation and the rescaled one to be used at a certain cutoff. Unfortunately this fails for real densities of states, where a heuristic mapping has to be applied. As derived and tested in this work, the actual rescaling may subsequently be performed in consideration of the specific density of states, which yields an improved the rate of convergence.

The Coulomb interaction apart, the predictions of McMillan's formula are also quite accurate beyond the CDOS approach, as long as the density of states near the chemical potential varies slowly. Both at van Hove singularities and band edges is has been observed that the effective contribution of the density of states is less than the one with respect to which the coupling strengths are defined, which leads to overestimated critical temperatures.

Taking multi-band interactions into account, testing the validity of McMillan's formula is equivalent to searching appropriate mappings from coupling matrices onto effective scalars which yield the same critical temperature. Hereof, no exact solution may be reported but two approximations which yield acceptable results. One of them neglects the energy renormalization and tends to overestimate the coupling strength, the other has been derived at the lowest cutoff frequency possible but astonishingly maintains most of its accuracy up to reasonable cutoffs.

Furthermore, for a two-band system it has been found that either the diagonal or off-diagonal elements of the electron-phonon coupling matrix may be varied along specific hyperbolas without altering the corresponding critical temperature. An exact mapping would have been found if the position of the asymptotes as a function of the other matrix elements were known. This has not been accomplished and is thus a possible object of further research. The two approximate mappings only give some qualitative results on that score.

Besides questions concerning the critical temperature, the thesis endeavors to give a useful overview of the Eliashberg theory of superconductivity, including its derivation from the fundamental interactions as well as discussions of the variety of special cases and approximations such as the CDOS approach. Moreover, software has been developed which is yet to be applied in a more physical context such as the description of realistic materials.

Appendix A

Fourier analysis

Whenever there is translational symmetry, no matter if with respect to space or time, it is instructive to explore the space of the corresponding conserved quantity, momentum or energy. This applies especially to solid state physics, where one often has spatial periodicity in addition to conservation of energy.

The mathematical tools to switch between such related representations are given by the Fourier analysis. Despite its prominence, the different transformations for the possible combinations of discrete and continuous domains shall be briefly presented, together with the underlying orthogonality relations.

A.1 Discrete Fourier transform

The *discrete Fourier transform* and its inverse read

$$\hat{y}_\nu = \frac{1}{\sqrt{N}} \sum_{n=n_0}^{n_0+N-1} \mathrm{e}^{2\pi \mathrm{i} n\nu/N} y_n = \hat{y}_{\nu+N},$$
$$y_n = \frac{1}{\sqrt{N}} \sum_{\nu=\nu_0}^{\nu_0+N-1} \mathrm{e}^{-2\pi \mathrm{i} n\nu/N} \hat{y}_\nu = y_{n+N},$$

where $\hat{y}_\nu$ and $y_n \in \mathbb{C}$ are defined for all ν and $n \in \mathbb{Z}$ and recur with period $N \in \mathbb{N}^+$ making the lower bounds ν_0 and $n_0 \in \mathbb{Z}$ arbitrary. Invertibility is ensured by the orthogonality relation

$$\sum_{n=n_0}^{n_0+N-1} \mathrm{e}^{2\pi \mathrm{i} n\nu/N} = N \sum_{n\in\mathbb{Z}} \delta_\nu^{nN}, \tag{A.1}$$

which is proved recognizing the partial sum of a geometrical series:

$$\sum_{n=0}^{N-1} \mathrm{e}^{2\pi \mathrm{i} n\nu/N} = \begin{cases} \sum_{n=0}^{N-1} 1 = N & \text{for } \frac{\nu}{N} \in \mathbb{Z}, \\ \frac{\mathrm{e}^{2\pi \mathrm{i}\nu}-1}{\mathrm{e}^{2\pi \mathrm{i} n\nu/N}-1} = 0 & \text{otherwise.} \end{cases}$$

A.2 Fourier series

The *Fourier series* and its coefficients read

$$y(t) = \sum_{n\in\mathbb{Z}} \mathrm{e}^{2\pi \mathrm{i} nt/T} y_n = y(t+T),$$
$$y_n = \frac{1}{T} \int \mathrm{d}t\, \mathrm{e}^{-2\pi \mathrm{i} nt/T} y(t),$$

where $y(t) \in \mathbb{C}$ is defined for all $t \in \mathbb{R}$ and periodic with period $T \in \mathbb{R}^+$ making the lower limit $t_0 \in \mathbb{R}$ arbitrary and $y_n \in \mathbb{C}$ is defined for all $n \in \mathbb{Z}$. There are two orthogonality relations,

$$\int_{t_0}^{t_0+T} \mathrm{d}t\, \mathrm{e}^{2\pi \mathrm{i} n t T} = T\delta_n^0, \tag{A.2a}$$

$$\sum_{n\in\mathbb{Z}} \mathrm{e}^{2\pi \mathrm{i} n t/T} = T \sum_{n\in\mathbb{Z}} \delta(t - nT). \tag{A.2b}$$

The second equation is just mentioned for completeness since the left-hand side is the FOURIER series of the right-hand side. The first equation is proved by simply carrying out the integral:

$$\int_0^T \mathrm{d}t\, \mathrm{e}^{2\pi \mathrm{i} n t/T} = \begin{cases} \int_0^T \mathrm{d}t = T & \text{for } n = 0, \\ \frac{\mathrm{e}^{2\pi \mathrm{i} n t/T}}{2\pi \mathrm{i} n/T}\Big|_{t=0}^{T} = 0 & \text{otherwise.} \end{cases}$$

A.3 FOURIER transform

The *FOURIER transform* and its inverse read

$$\hat{y}(f) = \int_{-\infty}^{\infty} \mathrm{d}t\, \mathrm{e}^{2\pi \mathrm{i} f t} y(t),$$

$$y(t) = \int_{-\infty}^{\infty} \mathrm{d}f\, \mathrm{e}^{-2\pi \mathrm{i} f t} \hat{y}(f),$$

where $\hat{y}(f)$ and $y(t) \in \mathbb{C}$ are defined for all f and $t \in \mathbb{R}$. The orthogonality relation is

$$\int_{-\infty}^{\infty} \mathrm{d}t\, \mathrm{e}^{2\pi \mathrm{i} f t} = \delta(f).$$

With $\omega = 2\pi f$ and $\eta \in \mathbb{R}$ introduced to generate convergence it is proved in three steps:

$$\int_0^{\infty} \mathrm{d}t\, \mathrm{e}^{\mathrm{i}\omega t} = \lim_{\eta\to 0} \int_0^{\infty} \mathrm{d}t\, \mathrm{e}^{\mathrm{i}\omega t} \mathrm{e}^{-\eta t} = \lim_{\eta\to 0} \frac{\mathrm{e}^{\mathrm{i}\omega t} \mathrm{e}^{-\eta t}}{\mathrm{i}\omega - \eta}\Big|_{\omega=0}^{\infty} = \lim_{\eta\to 0} \frac{1}{\eta - \mathrm{i}\omega}, = \frac{\mathrm{i}}{\omega + \mathrm{i}0^+}, \tag{A.3a}$$

$$\int_{-\infty}^{0} \mathrm{d}t\, \mathrm{e}^{\mathrm{i}\omega t} = \lim_{\eta\to 0} \int_{-\infty}^{0} \mathrm{d}t\, \mathrm{e}^{\mathrm{i}\omega t} \mathrm{e}^{\eta t} = \lim_{\eta\to 0} \frac{\mathrm{e}^{\mathrm{i}\omega t} \mathrm{e}^{\eta t}}{\mathrm{i}\omega - \eta}\Big|_{\omega=-\infty}^{0} = \lim_{\eta\to 0} \frac{1}{\eta + \mathrm{i}\omega} = \frac{-\mathrm{i}}{\omega - \mathrm{i}0^+}, \tag{A.3b}$$

$$\int_{-\infty}^{\infty} \mathrm{d}t\, \mathrm{e}^{\mathrm{i}\omega t} = \lim_{\eta\to 0} \left[\frac{1}{\eta - \mathrm{i}\omega} + \frac{1}{\eta + \mathrm{i}\omega} \right] = \lim_{\eta\to 0} \frac{2\eta}{\eta^2 + \omega^2} = 2\pi\delta(\omega). \tag{A.3c}$$

Appendix B

Source code

On the following pages the complete source code of the Eliashberg solvers developed as part of this thesis is exposed. This may be considered out of place in a written work as the present one, but for the sake of completeness and a verifiability of the presented results it is done nonetheless.

The software consists of three programs, all written in conformance with a recent standard of the programming language *Fortran*, which serve different purposes: `ebmb` provides electronic self-energies on both the real and imaginary frequency axis, `critical` determines critical parameter sets by varying a parameter of choice while holding the others constant and `tc` may be used to find critical temperatures for all electronic bands separately.

The programs may be run via the command line, where all parameters are given as arguments (except for densities of states which must be provided in text files) and the results are either formatted and prompted to standard output or written to disk using their internal representation, the latter being lossless but also platform-dependent. Alternatively, an interface for the popular high-level language *Python* may be used, which is presented first.

B.1 Python interface

The following Python module provides wrapper functions for the different Eliashberg solvers. Parameters are directly passed to the calling functions and the results returned as (dictionaries of) *NumPy* arrays. In addition, there are two functions to generate electronic densities of states, either from an analytic expression in the special case of a square tight-binding lattice or by sampling an arbitrary dispersion relation, the domain of which may be divided into different subdomains in order to obtain separate densities of states for each of them.

```
#!/usr/bin/env python

"""Wrapper and auxiliary functions for Eliashberg solver ebmb"""

import itertools
import numpy as np
from os import path
import subprocess

try:
    from scipy.special import ellipk
except ImportError:
    print 'square_dos not available'

def get(program='ebmb', file='~temporary.dat', replace=True, **parameters):
    """Run 'ebmb', 'tc' or 'critical' and load results.

    Parameters
```

```
    ----------
    program : str
        Name of or path to executable.
    file : str
        Path to output file.
    replace : bool
        Overwrite existing output file?
    **parameters
        Program parameters.

    Returns
    -------
    dict
        Returned if `program` corresponds to 'ebmb'.
        Self-energy components etc.
    ndarray
        Returned otherwise.
        Critical parameter(s).
    """
    if replace or not path.exists(file):
        run(program, file=file, **parameters)

    if program.endswith('ebmb'):
        return load(file)
    else:
        return load_floats(file)

def run(program='ebmb', **parameters):
    """Run 'ebmb', 'tc' or 'critical'.

    Parameters
    ----------
    program : str
        Name of or path to executable.
    **parameters
        Program parameters.
    """
    command = [program]

    for key, value in parameters.items():
        command.append('='.join([key, ','.join(map(str, np.ravel(value)))]))

    subprocess.call(command)

def load(file):
    """Load output file of 'ebmb'.

    Parameters
    ----------
    file : str
        Path to output file.

    Returns
    -------
    dict
        Self-energy components etc.
    """
    data = {}

    with open(file, 'rb') as file:
        while True:
```

```
            name = ''.join(iter(lambda: file.read(1) or ':', ':'))

            if name == 'REAL':
                dtype = np.float64

            elif name == 'INT':
                dtype = np.int32

            elif name == 'DIM':
                shape = np.fromfile(file, np.int32,
                    *np.fromfile(file, np.int32, 1))

            elif name:
                data[name] = np.fromfile(file, dtype,
                    shape.prod()).reshape(shape)
            else:
                return data

def load_floats(file):
    """Load output file of 'tc' or 'critical'.

    Parameters
    ----------
    file : str
        Path to output file.

    Returns
    -------
    ndarray
        Critical parameter(s).
    """
    with open(file, 'rb') as file:
        data = np.fromfile(file, np.float64)

    return data if data.size > 1 else data[0]

def dos(file, epsilon, domain, filters=[], resolution=101, replace=True):
    """Calculate subdomain-resolved density of states and save it to file.

    Parameters
    ----------
    file : str
        Path to output file.
    epsilon : function
        Band structure.
    domain : list of ndarray
        Discretized domains of arguments of `epsilon`.
    filters : list of function
        N filters defining N + 1 subdomains.
    resolution : int
        Resolution of density of states.
    replace : bool
        Overwrite existing output file?

    Returns
    -------
    ndarray
        Energy.
    ndarray
        Subdomain-resolved density of states.
    """
```

```
    if not replace and path.exists(file):
        return

    points = np.prod(map(len, domain))

    energy = np.empty(points)
    pocket = np.empty(points, dtype=int)

    for i, x in enumerate(itertools.product(*domain)):
        energy[i] = epsilon(*x)
        pocket[i] = 0

        for element in filters:
            if element(*x): break
            pocket[i] += 1

    emin = energy.min()
    emax = energy.max()

    binned = ((resolution - 1)
        * (energy - emin) / (emax - emin)).round().astype(int)

    pockets = len(filters) + 1

    count = np.zeros((resolution, pockets), dtype=int)

    for i in range(points):
        count[binned[i], pocket[i]] += 1

    e, de = np.linspace(emin, emax, resolution, retstep=True)

    dos = count / (de * count.sum())
    dos[(0, -1), :] *= 2

    with open(file, 'w') as out:
        for i in range(resolution):
            out.write('% .10f' % e[i])

            for j in range(pockets):
                out.write(' %.10f' % dos[i, j])

            out.write('\n')

    return e, dos if pockets > 1 else dos[:, 0]

def square_dos(file='dos.in', resolution=401, t=0.25, replace=True):
    """Calculate density of states of square lattice and save it to file.

    Parameters
    ----------
    file : str
        Path to output file.
    resolution : int
        Resolution of density of states.
    t : float
        Hopping parameter.
    replace : bool
        Overwrite existing output file?

    Returns
    -------
```

```
    ndarray
        Energy.
    ndarray
        Density of states.
    """
    if not replace and path.exists(file):
        return

    e, de = np.linspace(-4 * t, 4 * t, resolution, retstep=True)

    mid = resolution // 2

    dos = np.empty(resolution)

    dos[:mid] = ellipk(1 - (e[:mid] / (4 * t)) ** 2) / (2 * np.pi ** 2 * t)
    dos[-mid:] = dos[mid - 1::-1]

    if resolution % 2:
        dos[mid] = 0.0
        dos[mid] = 1 / de - dos[0] / 2 - sum(dos[1:-1]) - dos[-1] / 2

    with open(file, 'w') as out:
        for i in range(resolution):
            out.write('% .10f %.10f\n' % (e[i], dos[i]))

    return e, dos

if __name__ == '__main__':
    np.set_printoptions(threshold=9, edgeitems=1)

    square_dos('dos.in')

    for item in sorted(get(dos='dos.in', n=0.5, tell=False).items()):
        print ('%9s = %s' % item).replace('\n', '\n' + ' ' * 12)
```

B.2 Universal modules

This section combines Fortran modules which are either used globally, i.e. in nearly all subsequent subroutines, or applicable universally, i.e. not only in the context of solving the Eliashberg equations.

B.2.1 global.f90

The following module provides information which must be globally accessible. This includes the desired accuracy of floating-point numbers, mathematical and physical constants as well as container data types which are used to pass around parameters and results without the need for endless argument lists at functions calls or, more troublesome, global variables. Additionally, a operator is defined which compares floating point numbers for approximate equality. It decides, for example, whether numerical self-consistency has been reached or an iteration has to continue. In all calculations performed, the default negligible float difference 10^{-15} has been chosen.

```
module global
   implicit none

   integer, parameter :: dp = selected_real_kind(15) ! double precision (8 B)
   integer, parameter :: qp = selected_real_kind(30) ! quad precision (16 B)
   integer, parameter :: i4 = selected_int_kind(9)   ! signed integer (4 B)

```

```
8     real(dp), parameter :: pi = 4 * atan(1.0_dp) ! 3.14159...
9     real(dp), parameter :: kB = 8.61733e-5_dp    ! Boltzmann constant (meV/K)
10
11    integer, parameter :: unit = 11 ! file unit number
12
13    type parameters
14       character(99) :: file = 'none'   ! name of output file
15       character(50) :: form = 'F16.12' ! number format
16
17       logical :: tell = .true. ! use standard output?
18
19       real(dp) :: T = 10.0_dp ! temperature (K)
20
21       real(dp) :: omegaE  = 0.02_dp ! Einstein frequency (eV)
22       real(dp) :: cutoff  = 15.0_dp ! overall cutoff frequency (omegaE)
23       real(dp) :: cutoffC = -1.0_dp ! Coulomb cutoff frequency (omegaE)
24
25       integer(i4) :: bands = 1 ! number of electronic bands
26
27       real(dp), allocatable :: lambda(:, :) ! electron-phonon coupling
28       real(dp), allocatable :: muStar(:, :) ! Coulomb pseudo-potential
29
30       real(dp), allocatable :: energy(:) ! free-electron energy (eV)
31       real(dp), allocatable :: dos(:, :) ! density of Bloch states (a.u.)
32
33       real(dp) ::  n = 0.0_dp ! initial occupancy number
34       real(dp) :: mu = 0.0_dp ! initial chemical potential (eV)
35
36       logical :: conserve = .true. ! conserve particle number?
37
38       logical :: chi = .false. ! find energy shift?
39
40       integer(i4) :: limit = 250000 ! maximum number of iterations
41
42       real(dp) :: error = 1e-05_dp ! bisection error (a.u.)
43       real(dp) ::  zero = 1e-10_dp ! negligible gap at critical temperature (eV)
44       real(dp) ::  rate = 1e-01_dp ! growth rate for bound search
45
46       real(dp) :: clip = 15.0_dp ! maximum real-axis frequency (omegaE)
47
48       integer(i4) :: resolution = 0       ! real-axis resolution
49       logical     :: measurable = .false. ! find measurable gap?
50
51       logical :: rescale = .true.  ! rescale Coulomb pseudo-potential?
52       logical :: imitate = .false. ! cut off renormalization function?
53
54       logical :: normal = .false. ! enforce normal state?
55
56       logical :: power = .true. ! use power method for single band?
57    end type parameters
58
59    type matsubara
60       real(dp), allocatable :: omega(:)    ! frequency (eV)
61       real(dp), allocatable :: Z    (:, :) ! renormalization
62       real(dp), allocatable :: chi  (:, :) ! energy shift (eV)
63       real(dp), allocatable :: Delta(:, :) ! gap (eV)
64       real(dp), allocatable :: phi  (:, :) ! order parameter (eV)
65       real(dp), allocatable :: phiC (:)    ! constant Coulomb contribution (eV)
66
67       integer(i4) :: status ! convergence status
68    end type matsubara
```

```
69
70    type continued
71       real   (dp), allocatable :: omega (:)    ! frequency (eV)
72       complex(dp), allocatable :: Z     (:, :) ! renormalization
73       complex(dp), allocatable :: chi   (:, :) ! energy shift (eV)
74       complex(dp), allocatable :: Delta (:, :) ! gap (eV)
75       real   (dp), allocatable :: Delta0(:)    ! measurable gap (eV)
76
77       integer(i4), allocatable :: status(:) ! convergence status
78    end type continued
79
80    type occupancy
81       real(dp) :: n0, n   ! initial and final occupancy number
82       real(dp) :: mu0, mu ! initial and final chemical potential (eV)
83    end type occupancy
84
85    real(dp) :: epsilon = 1e-15_dp ! negligible float difference (a.u.)
86
87    interface operator(.ap.)
88       module procedure ap
89    end interface
90
91 contains
92
93    elemental function ap(lhs, rhs)
94       logical :: ap
95       real(dp), intent(in) :: lhs, rhs
96
97       ap = abs(lhs - rhs) .le. epsilon
98    end function ap
99 end module global
```

B.2.2 eigenvalues.f90

When testing for superconductivity via the linearized Eliashberg equations, the quantity of interest is the greatest eigenvalue of the kernel given e.g. in Eq. 4.27, which is a non-symmetric matrix with real eigenvalues. It is determined either using the corresponding routine from the well-established linear-algebra package *LAPACK* [56] or via the power method. The latter has the advantage that an eigenvalue of a prior calculation can be used as an initial guess if the parameter set has only changed slightly. However, it requires that the eigenvalue searched for notably exceeds the rest of the spectrum in magnitude. If an interfering eigenvalue is of opposite sign, the situation is still unproblematic since the spectrum can be shifted by adding or subtracting a lower or upper bound to the diagonal of the matrix, respectively.[1] Otherwise, the iteration will oscillate rather than converge and the method must be abandoned.

```
1  module eigenvalues
2     use global
3     use tools, only: bound
4     implicit none
5     private
6
7     public :: spectrum, power_method
8
9     interface
10       subroutine dgeev(jobvl, jobvr, n, a, lda, wr, wi, vl, ldvl, vr, ldvr, &
11          work, lwork, info)
12
```

[1] A suitable eigenvalue bound is given by a function presented in the next section.

```
13          use global
14
15          character, intent(in) :: jobvl, jobvr
16
17          integer, intent(in) :: n, lda, ldvl, ldvr, lwork
18          integer, intent(out) :: info
19
20          real(dp), intent(inout) :: a(lda, *)
21          real(dp), intent(out) :: wr(*), wi(*), vl(lda, *), vr(lda, *), work(*)
22       end subroutine dgeev
23    end interface
24
25 contains
26
27    function spectrum(matrix, error)
28       real(dp), intent(in) :: matrix(:, :)
29       integer, intent(out), optional :: error
30
31       complex(dp) :: spectrum(size(matrix, 1))
32
33       integer :: n, info
34
35       real(dp) :: a(size(matrix, 1), size(matrix, 2))
36       real(dp) :: wr(size(matrix, 1)), wi(size(matrix, 1))
37       real(dp) :: v(1, 1), work(3 * size(matrix, 1))
38
39       a(:, :) = matrix
40
41       n = size(matrix, 1)
42
43       call dgeev(           &
44          & jobvl = 'N',     &
45          & jobvr = 'N',     &
46          &     n = n,       &
47          &     a = a(1, 1), &
48          &   lda = n,       &
49          &    wr = wr(1),   &
50          &    wi = wi(1),   &
51          &    vl = v(1, 1), &
52          &  ldvl = n,       &
53          &    vr = v(1, 1), &
54          &  ldvr = n,       &
55          &  work = work(1), &
56          & lwork = 3 * n,   &
57          &  info = info     )
58
59       spectrum = cmplx(wr, wi, dp)
60
61       if (present(error)) error = info
62    end function spectrum
63
64    subroutine power_method(matrix, vector, value)
65       real(dp), intent(inout) :: matrix(:, :), vector(:)
66       real(dp), intent(out) :: value
67
68       real(dp) :: shift, value0
69
70       integer :: i
71
72       shift = bound(matrix)
73
```

```
74          do i = 1, size(matrix, 1)
75             matrix(i, i) = matrix(i, i) + shift
76          end do
77
78          value0 = -1
79
80          do
81             vector(:) = matmul(matrix, vector)
82
83             value = sqrt(sum(vector ** 2))
84             vector(:) = vector / value
85
86             if (value .ap. value0) exit
87
88             value0 = value
89          end do
90
91          value = value - shift
92       end subroutine power_method
93    end module eigenvalues
```

B.2.3 tools.f90

In the following, five succinct functions or subroutines are presented which each serve a very specific purpose and may be used in a variety of occasions.

- `argument(n)` returns the value of the `n`-th command-line argument as a string of the corresponding length.
- `bound(matrix)` returns a bound for the magnitude of the eigenvalues of the given `matrix` in terms of the minimum of the maximum row and column sums [57, Eqs. 1.1, 1.2].
- `differential(x, dx)` calculates a list of weights or *'differentials'* `dx` from a list of sample points `x` to be used for numerical integration with the trapezoidal rule.
- `interval(x, a, b, lower, upper)` discretizes the interval from `a` to `b` (returned as `x`), where `lower` and `upper` decide which bounds are to be included.
- `matches(str, char)` counts the occurrences of a character in a string.

```
1   module tools
2      use global
3      implicit none
4
5      private
6      public :: argument, bound, differential, interval, matches
7
8   contains
9
10     function argument(n)
11        character(:), allocatable :: argument
12        integer, intent(in) :: n
13
14        integer :: size
15
16        call get_command_argument(n, length=size)
17
18        allocate(character(size) :: argument)
19
20        call get_command_argument(n, value=argument)
```

```
21    end function argument
22
23    real(dp) function bound(matrix)
24       real(dp), intent(in) :: matrix(:, :)
25
26       real(dp) :: R, C, S
27
28       integer :: i
29
30       R = 0
31       do i = 1, size(matrix, 1)
32          S = sum(abs(matrix(i, :)))
33          if (S .gt. R) R = S
34       end do
35
36       C = 0
37       do i = 1, size(matrix, 2)
38          S = sum(abs(matrix(:, i)))
39          if (S .gt. C) C = S
40       end do
41
42       bound = min(R, C)
43    end function bound
44
45    subroutine differential(x, dx)
46       real(dp), intent(in) :: x(:)
47       real(dp), intent(out) :: dx(:)
48
49       integer :: n
50       n = size(x)
51
52       dx(1) = x(2) - x(1)
53       dx(2:n - 1) = x(3:n) - x(1:n - 2)
54       dx(n) = x(n) - x(n - 1)
55
56       dx(:) = dx / 2
57    end subroutine differential
58
59    subroutine interval(x, a, b, lower, upper)
60       real(dp), intent(out) :: x(:)
61       real(dp), intent(in) :: a, b
62       logical, intent(in), optional :: lower, upper
63
64       integer :: i, j, k
65
66       i = size(x)
67       j = 1
68
69       if (present(lower)) then
70          if (lower) j = j - 1
71       end if
72
73       if (present(upper)) then
74          if (upper) i = i - 1
75       end if
76
77       do k = 1, size(x)
78          x(k) = i * a + j * b
79          i = i - 1
80          j = j + 1
81       end do
```

```
82
83          x = x / (i + j)
84       end subroutine interval
85
86       integer function matches(str, char)
87          character(*), intent(in) :: str
88          character(1), intent(in) :: char
89
90          integer :: c
91
92          matches = 0
93
94          do c = 1, len(str)
95             if (str(c:c) .eq. char) matches = matches + 1
96          end do
97       end function matches
98    end module tools
```

B.2.4 formatting.f90

In Fortran, the formatting of floating point numbers is controlled via so-called *edit descriptors*. Since the desired format shall be left to the user, such edit descriptors must be generated at run time. The following module makes this issue a little more comfortable.

```
1     module formatting
2        use global
3        implicit none
4
5        private
6        public :: measure, edit, rule
7
8        integer :: width
9        character(:), allocatable :: w, x
10
11    contains
12
13       subroutine measure(form)
14          character(*), intent(in) :: form
15
16          character(100) :: test
17
18          x = trim(form)
19
20          write (test, "(" // x // ", '|')") pi
21          width = index(test, '|') - 1
22
23          write (test, '(I0)') width
24          w = trim(test)
25       end subroutine measure
26
27       function edit(descriptor)
28          character(:), allocatable :: edit
29          character(*), intent(in) :: descriptor
30
31          integer :: n
32
33          edit = descriptor
34
35          do
```

```
         n = scan(edit, 'wx')
         if (n .eq. 0) return

         select case (edit(n:n))
            case ('w'); edit = edit(:n - 1) // w // edit(n + 1:)
            case ('x'); edit = edit(:n - 1) // x // edit(n + 1:)
         end select
      end do
   end function edit

   function rule(n)
      character(:), allocatable :: rule
      integer, intent(in) :: n

      rule = "('" // repeat('_', n * width) // "')"
   end function rule
end module formatting
```

B.3 Eliashberg solvers

In this section four modules are presented which constitute the physical core of the software, namely the solvers for the multi-band Eliashberg equations. They are subdivided on the one hand into solvers for the self-energy on the imaginary axis or for the maximum eigenvalue of the kernel of the linearized equations and on the other hand according to whether the density of states is taken into account or not.

B.3.1 self_energy.f90

This lengthy module calculates the self-energy taking the density of states into account, i.e. solves Eqs. 4.23, in the course of which not only particle numbers or chemical potentials according to Section 4.7 have to be calculated but also the rescaled Coulomb pseudo-potential defined in Eq. 4.17. Repeatedly, energy integrals are performed numerically using the trapezoidal rule. Since all necessary quantities are already present, the calculation of the kernel in Eq. 4.29 is also performed at the end of the process.

```
module eliashberg_self_energy
   use global
   use tools, only: differential
   implicit none

   private
   public :: self_energy, initialize

   logical :: initial = .true.

   real(dp) :: states
   real(dp), allocatable :: weight(:, :), trapezia(:), matsum(:)

contains

   subroutine self_energy(x, im, oc, kernel)
      type(parameters), intent(in) :: x
      type(matsubara), intent(out) :: im
      type(occupancy), intent(out) :: oc

      real(dp), allocatable, intent(out), optional :: kernel(:, :)

      real(dp) :: nE, Z, phi, chi, mu, domega, A0, B0, residue
```

```
24
25        real(dp), allocatable :: g(:, :, :), U(:, :, :)
26        real(dp), allocatable :: muStar(:, :), A(:, :), B(:, :)
27
28        real(dp), allocatable :: integral_Z  (:, :)
29        real(dp), allocatable :: integral_phi(:, :)
30        real(dp), allocatable :: integral_chi(:, :)
31
32        integer :: step, i, j, n, m, p, q, no, nC, f
33        logical :: done
34
35        if (initial) call initialize(x)
36
37        if (0 .lt. x%n .and. x%n .lt. 2) then
38           oc%n = x%n
39
40           oc%mu &
41              = (x%energy(1) * (2 - oc%n) + x%energy(size(x%energy)) * oc%n) / 2
42
43           done = .false.
44
45           do while (.not. done)
46              where (x%energy .ap. oc%mu)
47                 matsum = 1 / (2 * kB * x%T)
48              elsewhere
49                 matsum = x%energy - oc%mu
50                 matsum = tanh(matsum / (2 * kB * x%T)) / matsum
51              end where
52
53              A0 = 0
54              B0 = 0
55
56              do i = 1, x%bands
57                 trapezia(:) = weight(:, i) * matsum
58
59                 A0 = A0 + sum(trapezia)
60                 B0 = B0 + sum(trapezia * x%energy)
61              end do
62
63              mu = (oc%n - 1 + B0) / A0
64
65              if (oc%mu .ap. mu) done = .true.
66
67              oc%mu = mu
68           end do
69        else
70           oc%mu = x%mu
71
72           oc%n = 1
73
74           matsum(:) = tanh((x%energy - x%mu) / (2 * kB * x%T))
75
76           do i = 1, x%bands
77              oc%n = oc%n - sum(weight(:, i) * matsum)
78           end do
79        end if
80
81        oc%n0  = oc%n
82        oc%mu0 = oc%mu
83
84        f = minloc(abs(x%energy - oc%mu), 1)
```

```
85
86       domega = 2 * pi * kB * x%T
87
88       nE = x%omegaE / domega
89
90       no = ceiling(x%cutoff  * nE - 0.5_dp)
91       nC = ceiling(x%cutoffC * nE - 0.5_dp)
92
93       allocate(im%omega(0:no - 1))
94
95       do n = 0, no - 1
96          im%omega(n) = domega * (n + 0.5_dp)
97       end do
98
99       allocate(g(1 - no:2 * no - 1, x%bands, x%bands))
100
101      do n = 1 - no, 2 * no - 1
102         g(n, :, :) = x%lambda / (1 + (n / nE) ** 2)
103
104         do i = 1, x%bands
105            g(n, :, i) = g(n, :, i) * states / x%dos(f, :)
106         end do
107      end do
108
109      allocate(muStar(x%bands, x%bands))
110
111      muStar(:, :) = x%muStar / (1 + x%muStar &
112         * log(2 * x%omegaE / (x%energy(size(x%energy)) - x%energy(1))))
113
114      if (x%rescale) then
115         where (x%energy .ap. oc%mu)
116            matsum = 1 / (domega * (nC + 0.5_dp))
117         elsewhere
118            matsum = x%energy - oc%mu
119            matsum = atan(matsum / (domega * (nC + 0.5_dp))) / matsum
120         end where
121
122         residue = 0
123
124         do i = 1, x%bands
125            residue = residue + sum(weight(:, i) / x%dos(f, i) * matsum)
126         end do
127
128         residue = residue * states / pi
129
130         muStar(:, :) = muStar / (1 + muStar * residue)
131      end if
132
133      allocate(U(0:no - 1, x%bands, x%bands))
134
135      do n = 0, nC - 1
136         U(n, :, :) = -2 * muStar
137
138         do i = 1, x%bands
139            U(n, :, i) = U(n, :, i) * states / x%dos(f, :)
140         end do
141      end do
142
143      U(nC:, :, :) = 0
144
145      allocate(im%Z(0:no - 1, x%bands))
```

```
146
147         im%Z(:, :) = 1
148
149         allocate(im%phi(0:no - 1, x%bands))
150
151         im%phi(:, :) = 0
152
153         if (.not. (x%normal .or. present(kernel))) im%phi(0, :) = 1
154
155         allocate(im%chi(0:no - 1, x%bands))
156
157         im%chi(:, :) = 0
158
159         allocate(A(0:no - 1, x%bands))
160         allocate(B(0:no - 1, x%bands))
161
162         allocate(integral_Z  (0:no - 1, x%bands))
163         allocate(integral_phi(0:no - 1, x%bands))
164         allocate(integral_chi(0:no - 1, x%bands))
165
166         do i = 1, x%bands
167            do n = 0, no - 1
168               call integrate(n, i)
169            end do
170         end do
171
172         im%status = -1
173
174         do step = 1, x%limit
175            done = .true.
176
177            do i = 1, x%bands
178               do n = 0, no - 1
179                  Z = 0
180                  phi = 0
181                  chi = 0
182
183                  do j = 1, x%bands
184                     do m = 0, no - 1
185                        Z = Z + integral_Z(m, j) &
186                           * (g(n - m, j, i) - g(n + m + 1, j, i))
187
188                        phi = phi + integral_phi(m, j) &
189                           * (g(n - m, j, i) + g(n + m + 1, j, i) + U(m, j, i))
190
191                        chi = chi - integral_chi(m, j) &
192                           * (g(n - m, j, i) + g(n + m + 1, j, i))
193                     end do
194                  end do
195
196                  Z = 1 + Z * kB * x%T / im%omega(n)
197                  phi = phi * kB * x%T
198                  chi = chi * kB * x%T
199
200                  done = done &
201                     .and. (im%Z  (n, i) .ap. Z) &
202                     .and. (im%phi(n, i) .ap. phi) &
203                     .and. (im%chi(n, i) .ap. chi)
204
205                  im%Z  (n, i) = Z
206                  im%phi(n, i) = phi
```

```
207                im%chi(n, i) = chi
208
209                call integrate(n, i)
210             end do
211          end do
212
213          if (x%conserve) then
214             matsum(:) = atan((x%energy - oc%mu) / (domega * (no + 0.5_dp))) &
215                / domega
216
217             residue = 0
218
219             do i = 1, x%bands
220                residue = residue + sum(weight(:, i) * matsum)
221             end do
222
223             mu = ((oc%n - 1) / (4 * kB * x%T) + sum(A * im%chi + B) + residue) &
224                / sum(A)
225
226             done = done .and. (oc%mu .ap. mu)
227
228             oc%mu = mu
229          end if
230
231          if (done) then
232             im%status = step
233             exit
234          end if
235       end do
236
237       allocate(im%Delta(0:no - 1, x%bands))
238
239       im%Delta(:, :) = im%phi / im%Z
240
241       allocate(im%phiC(x%bands))
242
243       do i = 1, x%bands
244          im%phiC(i) = kB * x%T * sum(integral_phi * U(:, :, i))
245       end do
246
247       oc%n = 1 - 4 * kB * x%T * (sum(integral_chi) + residue)
248
249       if (present(kernel)) then
250          allocate(kernel(x%bands * no, x%bands * no))
251
252          do i = 1, x%bands
253             p = i * no
254             do j = 1, x%bands
255                q = j * no
256                do n = 0, no - 1
257                   do m = 0, no - 1
258                      kernel(q - m, p - n) = kB * x%T * A(m, j) &
259                         * (g(n - m, j, i) + g(n + m + 1, j, i) + U(m, j, i))
260                   end do
261                end do
262             end do
263          end do
264       end if
265
266    contains
267
```

```
268         subroutine integrate(n, i)
269            integer, intent(in) :: n, i
270
271            trapezia(:) = weight(:, i) / ((im%omega(n) * im%Z(n, i)) ** 2 &
272               + (x%energy - oc%mu + im%chi(n, i)) ** 2 + im%phi(n, i) ** 2)
273
274            A(n, i) = sum(trapezia)
275            B(n, i) = sum(trapezia * x%energy)
276
277            integral_Z  (n, i) = A(n, i) *  im%Z  (n, i) * im%omega(n)
278            integral_phi(n, i) = A(n, i) *  im%phi(n, i)
279            integral_chi(n, i) = A(n, i) * (im%chi(n, i) - oc%mu) + B(n, i)
280         end subroutine integrate
281
282      end subroutine self_energy
283
284      subroutine initialize(x)
285         type(parameters), intent(in) :: x
286
287         integer :: i
288
289         initial = .false.
290
291         if (allocated(weight)) deallocate(weight)
292         allocate(weight(size(x%energy), x%bands))
293
294         if (allocated(trapezia)) deallocate(trapezia)
295         allocate(trapezia(size(x%energy)))
296
297         if (allocated(matsum)) deallocate(matsum)
298         allocate(matsum(size(x%energy)))
299
300         call differential(x%energy, weight(:, 1))
301
302         do i = 2, x%bands
303            weight(:, i) = weight(:, 1)
304         end do
305
306         weight(:, :) = weight * x%dos
307
308         states = sum(weight)
309
310         weight(:, :) = weight / states
311      end subroutine initialize
312   end module eliashberg_self_energy
```

B.3.2 self_energy_cdos.f90

Just as the preceding one, this module calculates the self-energy, but within the CDOS approximation defined in Eq. 4.9. Accordingly, the Coulomb pseudo-potential is rescaled following Eq. 4.20.

```
1   module eliashberg_self_energy_cdos
2      use global
3      implicit none
4
5      private
6      public :: self_energy_cdos
7
```

```
contains

   subroutine self_energy_cdos(x, im)
      type(parameters), intent(in) :: x
      type(matsubara), intent(out) :: im

      real(dp) :: nE, Z, Delta

      real(dp), allocatable :: lambda(:, :, :), mu(:, :, :)
      real(dp), allocatable :: muStar(:, :), A(:, :)

      integer :: step, i, j, n, m, no, nC
      logical :: done

      nE = x%omegaE / (2 * pi * kB * x%T)

      no = ceiling(x%cutoff  * nE - 0.5_dp)
      nC = ceiling(x%cutoffC * nE - 0.5_dp)

      allocate(im%omega(0:no - 1))

      do n = 0, no - 1
         im%omega(n) = (2 * n + 1) * pi * kB * x%T
      end do

      allocate(lambda(1 - no:2 * no - 1, x%bands, x%bands))

      do n = 1 - no, 2 * no - 1
         lambda(n, :, :) = x%lambda / (1 + (n / nE) ** 2)
      end do

      allocate(muStar(x%bands, x%bands))

      if (x%rescale) then
         muStar(:, :) = x%muStar / (1 + x%muStar * log(nE / (nC + 0.5_dp)))
      else
         muStar(:, :) = x%muStar
      end if

      allocate(mu(0:no - 1, x%bands, x%bands))

      do n = 0, nC - 1
         mu(n, :, :) = -2 * muStar
      end do

      mu(nC:, :, :) = 0

      allocate(im%Z(0:no - 1, x%bands))

      im%Z(:, :) = 1

      allocate(im%Delta(0:no - 1, x%bands))

      im%Delta(:, :) = 0

      if (.not. x%normal) im%Delta(0, :) = 1

      allocate(A(0:no - 1, x%bands))

      do i = 1, x%bands
         A(:, i) = 1 / sqrt(im%omega ** 2 + im%Delta(:, i) ** 2)
```

```
69        end do
70
71        im%status = -1
72
73        do step = 1, x%limit
74           done = .true.
75
76           do i = 1, x%bands
77              do n = 0, no - 1
78                 Z = 0
79                 Delta = 0
80
81                 do j = 1, x%bands
82                    do m = 0, no - 1
83                       Z = Z + im%omega(m) * A(m, j) &
84                          * (lambda(n - m, j, i) - lambda(n + m + 1, j, i))
85
86                       Delta = Delta + im%Delta(m, j) * A(m, j) * (mu(m, j, i) &
87                          +  lambda(n - m, j, i) + lambda(n + m + 1, j, i))
88                    end do
89                 end do
90
91                 Z = 1 + pi * kB * x%T * Z / im%omega(n)
92                 Delta = pi * kB * x%T * Delta / Z
93
94                 done = done &
95                    .and. (im%Z    (n, i) .ap. Z) &
96                    .and. (im%Delta(n, i) .ap. Delta)
97
98                 im%Z    (n, i) = Z
99                 im%Delta(n, i) = Delta
100
101                A(n, i) = 1 / sqrt(im%omega(n) ** 2 + Delta ** 2)
102             end do
103          end do
104
105          if (done) then
106             im%status = step
107             exit
108          end if
109       end do
110
111       allocate(im%phiC(x%bands))
112
113       do i = 1, x%bands
114          im%phiC(i) = pi * kB * x%T * sum(im%Delta * A * mu(:, :, i))
115       end do
116    end subroutine self_energy_cdos
117 end module eliashberg_self_energy_cdos
```

B.3.3 eigenvalue.f90

This module determines the maximum eigenvalue of the Eliashberg kernel which takes the density of states into account. Since the kernel, defined in Eq. 4.29, is returned by the self-energy solver presented in Section B.3.1, all that has to be done is call the eigenvalue solvers and optionally cache the eigenvector to be reused as initial guess if the number of Matsubara frequencies remains constant.

```
1  module eliashberg_eigenvalue
```

```
   use eigenvalues
   use eliashberg_self_energy
   use global
   implicit none

   private
   public :: eigenvalue

contains

   subroutine eigenvalue(status, x)
      type(parameters), intent(in) :: x

      real(dp), intent(out) :: status ! greatest eigenvalue

      real(dp), allocatable :: kernel(:, :) ! Eliashberg kernel
      real(dp), allocatable, save :: phi(:) ! order parameter

      type(matsubara) :: im
      type(occupancy) :: oc

      call self_energy(x, im, oc, kernel)

      if (x%power .and. x%bands .eq. 1) then
         if (allocated(phi)) then
            if (size(phi) .ne. size(kernel, 2)) deallocate(phi)
         end if

         if (.not. allocated(phi)) then
            allocate(phi(size(kernel, 2)))

            phi(:) = 0
            phi(1) = 1
         end if

         call power_method(kernel, phi, status)
      else
         status = maxval(real(spectrum(kernel), dp))
      end if
   end subroutine eigenvalue
end module eliashberg_eigenvalue
```

B.3.4 eigenvalue_cods.f90

Again, a procedure analogous to the preceding one is reimplemented for the CDOS approximation, Eq. 4.27. In this case, however, an exact analytic expression for the renormalization is known which saves the expenses of calling the self-energy solver. For convenience, not only the respective eigenvector but also the memory allocation of all non-scalar quantities is saved where possible, i.e. if the number of MATSUBARA frequencies is not altered.

```
module eliashberg_eigenvalue_cdos
   use eigenvalues
   use global
   implicit none

   private
   public :: eigenvalue_cdos

contains
```

```
10
11    subroutine eigenvalue_cdos(status, x)
12       type(parameters), intent(in) :: x
13
14       real(dp), intent(out) :: status ! greatest eigenvalue
15
16       real(dp), allocatable, save :: &
17          lambda(:, :, :), & ! adjusted phonon Green function
18          muStar(:, :),    & ! Coulomb pseudo-potential
19          matrix(:, :),    & ! Eliashberg kernel
20          vector(:),       & ! order parameter
21          values(:),       & ! all eigenvalues
22          diag  (:)          ! diagonal renormalization contribution
23
24       integer :: no ! index of overall cutoff frequency
25       integer :: nC ! index of Coulomb cutoff frequency
26
27       integer, save :: no0 = -1 ! 'no' from previous subroutine call
28
29       integer :: i, j ! band indices
30       integer :: n, m ! frequency indices
31       integer :: p, q ! index offsets
32
33       real(dp) :: nE ! 'index' defining omegaE as bosonic Matsubara frequency
34
35       nE = x%omegaE / (2 * pi * kB * x%T)
36
37       no = ceiling(x%cutoff  * nE - 0.5_dp)
38       nC = ceiling(x%cutoffC * nE - 0.5_dp)
39
40       if (no .ne. no0) then
41          if (no0 .ne. -1) then
42             deallocate(lambda)
43             deallocate(muStar)
44             deallocate(matrix)
45             deallocate(vector)
46             deallocate(values)
47             deallocate(diag)
48          end if
49
50          allocate(lambda(1 - no:2 * no - 1, 0:x%bands - 1, 0:x%bands - 1))
51          allocate(muStar(                   0:x%bands - 1, 0:x%bands - 1))
52
53          allocate(matrix(0:x%bands * no - 1, 0:x%bands * no - 1))
54          allocate(vector(0:x%bands * no - 1))
55          allocate(values(0:x%bands * no - 1))
56
57          allocate(diag(0:x%bands * no - 1))
58
59          vector(:) = 0
60          vector(0) = 1
61
62          no0 = no
63       end if
64
65       do n = 1 - no, 2 * no - 1
66          lambda(n, :, :) = x%lambda / (1 + (n / nE) ** 2)
67       end do
68
69       if (x%rescale) then
70          muStar(:, :) = x%muStar / (1 + x%muStar * log(nE / (nC + 0.5_dp)))
```

```
71        else
72           muStar(:, :) = x%muStar
73        end if
74
75        do i = 0, x%bands - 1
76           p = i * no
77
78           do j = 0, x%bands - 1
79              q = j * no
80
81              do n = 0, no - 1
82                 do m = 0, no - 1
83                    matrix(q + m, p + n) &
84                       = lambda(n - m, j, i) + lambda(n + m + 1, j, i)
85                 end do
86              end do
87
88              matrix(q:q + nC - 1, p:p + no - 1) = &
89              matrix(q:q + nC - 1, p:p + no - 1) - 2 * muStar(j, i)
90           end do
91        end do
92
93        do i = 0, x%bands - 1
94           p = i * no
95
96           if (x%imitate) then
97              do n = 0, no - 1
98                 diag(p + n) = sum &
99                    (lambda(n:n - no + 1:-1, :, i) - lambda(n + 1:n + no, :, i))
100             end do
101          else
102             diag(p) = sum(lambda(0, :, i))
103
104             do n = 1, no - 1
105                diag(p + n) = diag(p + n - 1) + 2 * sum(lambda(n, :, i))
106             end do
107          end if
108       end do
109
110       do i = 0, x%bands * no - 1
111          matrix(i, i) = matrix(i, i) - diag(i)
112       end do
113
114       do m = 0, no - 1
115          matrix(m::no, :) = matrix(m::no, :) / (2 * m + 1)
116       end do
117
118       if (x%power .and. x%bands .eq. 1) then
119          call power_method(matrix, vector, status)
120       else
121          values(:) = real(spectrum(matrix), dp)
122          status = maxval(values)
123       end if
124    end subroutine eigenvalue_cdos
125 end module eliashberg_eigenvalue_cdos
```

B.4 Continuation to the real axis

The following two modules are concerned with the analytic continuation of the imaginary-axis results to the real axis by means of Padé approximants. The first provides the approximant, the second applies it to the results.

B.4.1 pade.f90

This is the actual implementation of the algorithm given in Section 4.10. Since there is no interest in the intermediate approximants, the backward-recurrence method is used. For each set of values on the imaginary axis, the coefficients are calculated only once; thereafter arbitrary real-axis values can be requested until the module is reinitialized with a new data set.

```
module real_axis_pade
   use global
   implicit none

   private
   public :: coefficients, continuation

   integer :: n
   complex(qp), allocatable :: c(:, :)

contains

   subroutine coefficients(z, u)
      real(dp), intent(in) :: z(:), u(:)

      complex(dp), parameter :: i = (0, 1)
      integer :: p

      n = size(z)

      if (allocated(c)) deallocate(c)
      allocate(c(n, n))

      if (all(u .ap. 0.0_dp)) then
         c(:, :) = 0
         return
      end if

      c(1, :) = u

      do p = 2, n
         c(p, p:) = (c(p - 1, p - 1) - c(p - 1, p:)) &
            / (i * (z(p:) - z(p - 1)) * c(p - 1, p:))

         c(p, p - 1) = -i * z(p - 1) * c(p, p)
      end do
   end subroutine coefficients

   elemental function continuation(x)
      complex(dp) :: continuation
      real(dp), intent(in) :: x

      complex(qp) :: frac
      integer :: p

      frac = 1

```

```
      do p = n, 2, -1
         frac = 1 + (c(p, p) * x + c(p, p - 1)) / frac
      end do

      frac = c(1, 1) / frac

      continuation = cmplx(frac, kind=dp)
   end function continuation
end module real_axis_pade
```

B.4.2 real_axis.f90

This subroutine applies the above algorithm to the previously calculated self-energy. It may calculate both the measurable gap defined in Eq. 5.1 via a fixed-point iteration and the real-axis self-energy on an equidistantly discretized interval.

```
module real_axis
   use global
   use real_axis_pade
   use tools, only: interval
   implicit none

   private
   public :: realize

contains

   subroutine realize(x, im, re)
      type(parameters), intent(in) :: x
      type(matsubara), intent(in) :: im
      type(continued), intent(out) :: re

      integer :: i, n
      real(dp) :: Delta0

      if (x%measurable) then
         allocate(re%Delta0(x%bands))
         allocate(re%status(x%bands))
      end if

      if (x%resolution .gt. 0) then
         allocate(re%omega(x%resolution))
         allocate(re%Delta(x%resolution, x%bands))
         allocate(re%Z(x%resolution, x%bands))

         if (x%chi) allocate(re%chi(x%resolution, x%bands))
      end if

      if (x%measurable .or. x%resolution .gt. 0) then
         do i = 1, x%bands
            call coefficients(im%omega, im%Delta(:, i))

            if (x%measurable) then
               re%Delta0(i) = 1
               re%status(i) = -1

               do n = 1, x%limit
                  Delta0 = real(continuation(re%Delta0(i)))

```

```
                  if (re%Delta0(i) .ap. Delta0) re%status(i) = n

                  re%Delta0(i) = Delta0

                  if (n .eq. re%status(i)) exit
               end do
            end if

            if (x%resolution .gt. 0) then
               call interval(re%omega, 0.0_dp, x%clip * x%omegaE, &
                  lower=.true., upper=.true.)

               re%Delta(:, i) = continuation(re%omega)

               call coefficients(im%omega, im%Z(:, i))
               re%Z(:, i) = continuation(re%omega)

               if (x%chi) then
                  call coefficients(im%omega, im%chi(:, i))
                  re%chi(:, i) = continuation(re%omega)
               end if
            end if
         end do
      end if
   end subroutine realize
end module real_axis
```

B.5 I/O

Subsequently, the input and output routines are presented. As stated at the beginning of the chapter, the input is always via the command-line, whereas the output is directed towards either the standard output or disk.

B.5.1 load.f90

This module is responsible for loading the command-line arguments, initializing the coupling matrices and, possibly, reading the density of states from a given file.

```
module io_load
   use global
   use tools, only: argument, matches
   implicit none

   private
   public :: load

contains

   subroutine load(x)
      type(parameters), intent(out) :: x

      character(:), allocatable :: setting ! command-line argument
      character(:), allocatable :: lhs, rhs ! left- and right-hand side

      character(:), allocatable :: lambda ! string defining lambda
      character(:), allocatable :: muStar ! string defining muStar

      integer :: equals ! position of '='
```

```
21
22       integer :: i ! band index
23       integer :: n ! argument number
24
25       character(99) :: dos_file = 'none' ! file with density of states
26
27       real(dp) :: elements ! number of elements in lambda and muStar
28
29       elements = x%bands ** 2
30
31       do n = 1, command_argument_count()
32          setting = argument(n)
33
34          equals = index(setting, '=')
35
36          lhs = setting(:equals - 1)
37          rhs = setting(equals + 1:)
38
39          select case (lhs)
40             case ('file'); read (rhs, '(A)') x%file
41             case ('form'); read (rhs, '(A)') x%form
42
43             case ('tell'); read (rhs, *) x%tell
44
45             case ('T'); read (rhs, *) x%T
46
47             case ('omegaE');  read (rhs, *) x%omegaE
48             case ('cutoff');  read (rhs, *) x%cutoff
49             case ('cutoffC'); read (rhs, *) x%cutoffC
50
51             case ('lambda', 'lamda')
52                lambda = rhs
53                elements = matches(rhs, ',') + 1
54
55             case ('muStar', 'mu*')
56                muStar = rhs
57                elements = matches(rhs, ',') + 1
58
59             case ('dos'); read (rhs, *) dos_file
60
61             case ('n');  read (rhs, *) x%n
62             case ('mu'); read (rhs, *) x%mu
63
64             case ('conserve'); read (rhs, *) x%conserve
65
66             case ('limit'); read (rhs, *) x%limit
67
68             case ('epsilon'); read (rhs, *) epsilon
69             case ('error');   read (rhs, *) x%error
70             case ('zero');    read (rhs, *) x%zero
71             case ('rate');    read (rhs, *) x%rate
72
73             case ('clip'); read (rhs, *) x%clip
74
75             case ('resolution'); read (rhs, *) x%resolution
76             case ('measurable'); read (rhs, *) x%measurable
77
78             case ('rescale'); read (rhs, *) x%rescale
79             case ('imitate'); read (rhs, *) x%imitate
80
81             case ('normal'); read (rhs, *) x%normal
```

```
82
83              case ('power'); read (rhs, *) x%power
84
85              case default
86                 print "('Ignored unknown parameter ''', A, ''')", lhs
87           end select
88        end do
89
90        x%bands = nint(sqrt(elements))
91
92        allocate(x%lambda(x%bands, x%bands))
93        allocate(x%muStar(x%bands, x%bands))
94
95        if (allocated(lambda)) then
96           read (lambda, *) x%lambda
97        else
98           x%lambda(:, :) = 0
99
100          do i = 1, x%bands
101             x%lambda(i, i) = 1
102          end do
103       end if
104
105       if (allocated(muStar)) then
106          read (muStar, *) x%muStar
107       else
108          x%muStar(:, :) = 0
109       end if
110
111       if (dos_file .ne. 'none') then
112          x%chi = .true.
113          call load_dos(dos_file, x)
114       end if
115
116       if (x%cutoffC .lt. 0) x%cutoffC = x%cutoff
117    end subroutine load
118
119    subroutine load_dos(file, x)
120       character(*), intent(in) :: file
121       type(parameters), intent(inout) :: x
122
123       integer :: n, m
124
125       real(dp) :: test
126       integer :: error
127
128       open (unit, file=file, action='read', status='old')
129
130       n = 0 ! density-of-states resolution
131
132       do
133          read (unit, *, iostat=error) test
134          if (error .ne. 0) exit
135          n = n + 1
136       end do
137
138       rewind unit
139
140       allocate(x%energy(n)) ! free-electron energy (eV)
141       allocate(x%dos(n, x%bands)) ! density of states (a.u.)
142
```

```
143       do m = 1, n
144          read(unit, *) x%energy(m), x%dos(m, :)
145       end do
146
147       close (unit)
148    end subroutine load_dos
149 end module io_load
```

B.5.2 store.f90

If the results shall be processed further with the help of other programs, it is desirable that no information is lost during the transfer process. Hence, the unformatted output of the data in their internal representation is provided by the following routine. It creates binary files which are structured by textual statements which define the identifier, dimension and type of the following data. This file format is understood by the Python interface module described in Section B.1.

```
1  module io_store
2     use global
3     implicit none
4
5     private
6     public :: store
7
8  contains
9
10    subroutine store(x, im, re, oc)
11       type(parameters), intent(in) :: x
12       type(matsubara), intent(in) :: im
13       type(continued), intent(in) :: re
14       type(occupancy), intent(in) :: oc
15
16       open (unit, &
17          file=x%file, action='write', status='replace', access='stream')
18
19       write (unit) 'INT:DIM:', 0_i4
20       write (unit) 'status:', im%status
21
22       write (unit) 'REAL:DIM:', 1_i4, size(im%omega, kind=i4)
23       write (unit) 'iomega:', im%omega
24
25       if (x%bands .gt. 1) &
26          write (unit) 'DIM:', 2_i4, x%bands, size(im%omega, kind=i4)
27
28       write (unit) 'Z:', im%Z
29       write (unit) 'Delta:', im%Delta
30
31       if (x%chi) then
32          write (unit) 'chi:', im%chi
33
34          write (unit) 'DIM:', 0_i4
35
36          write (unit) 'n0:', oc%n0
37          write (unit) "n:", oc%n
38
39          write (unit) 'mu0:', oc%mu0
40          write (unit) "mu:", oc%mu
41       end if
42
```

```
43        write (unit) 'DIM:'
44
45        if (x%bands .gt. 1) then
46           write (unit) 1_i4, x%bands
47        else
48           write (unit) 0_i4
49        end if
50
51        write (unit) 'phiC:', im%phiC
52
53        if (x%measurable) then
54           write (unit) 'INT:status0:', re%status
55           write (unit) 'REAL:Delta0:', re%Delta0
56        end if
57
58        if (x%resolution .gt. 0) then
59           write (unit) 'DIM:', 1_i4, x%resolution
60
61           write (unit) 'omega:', re%omega
62
63           if (x%bands .gt. 1) write (unit) 'DIM:', 2_i4, x%bands, x%resolution
64
65           write (unit) 'Re[Z]:', real(re%Z)
66           write (unit) 'Im[Z]:', aimag(re%Z)
67
68           write (unit) 'Re[Delta]:', real(re%Delta)
69           write (unit) 'Im[Delta]:', aimag(re%Delta)
70
71           if (x%chi) then
72              write (unit) 'Re[chi]:', real(re%chi)
73              write (unit) 'Im[chi]:', aimag(re%chi)
74           end if
75        end if
76
77        close (unit)
78     end subroutine store
79  end module io_store
```

B.5.3 tell.f90

If the results shall be displayed in a human-readable fashion, the following module comes into play. It formats the results considering a possibly defined edit descriptor and prints them to the standard output. If the storage on disk is preferred, the output can be redirected via the command line like this:

```
$ ebmb T=10 lambda=1 muStar=0.1 > self-energy.txt
```

```
1   module io_tell
2      use formatting
3      use global
4      implicit none
5
6      private
7      public :: tell
8
9   contains
10
11     subroutine tell(x, im, re, oc)
12        type(parameters), intent(in) :: x
```

```
13        type(matsubara), intent(in) :: im
14        type(continued), intent(in) :: re
15        type(occupancy), intent(in) :: oc
16
17        integer :: i, n ! band and Matsubara indices
18
19        character(:), allocatable :: head, body, form ! edit descriptors
20
21        call measure(x%form)
22
23        head = edit('(7Aw)')
24        body = edit('(7x)')
25
26        print "('imaginary-axis solution [', I0, ']:', /)", im%status
27
28        if (x%chi) then
29           print head, 'omega/eV', 'Z', 'Delta/eV', 'chi/eV'
30
31           do i = 1, x%bands
32              print rule(4)
33
34              do n = 0, size(im%omega) - 1
35                 print body, im%omega(n), im%Z(n, i), im%Delta(n, i), im%chi(n, i)
36              end do
37           end do
38        else
39           print head, 'omega/eV', 'Z', 'Delta/eV'
40
41           do i = 1, x%bands
42              print rule(3)
43
44              do n = 0, size(im%omega) - 1
45                 print body, im%omega(n), im%Z(n, i), im%Delta(n, i)
46              end do
47           end do
48        end if
49
50        form = edit('(x)')
51
52        if (x%chi) then
53           print "(/, 'initial and final occupancy number:', /)"
54           print edit(form), oc%n0, oc%n
55
56           print "(/, 'initial and final chemical potential (eV):', /)"
57           print edit(form), oc%mu0, oc%mu
58        end if
59
60        print "(/, 'constant Coulomb contribution (eV):', /)"
61        print edit(form), im%phiC
62
63        if (x%measurable) then
64           print "(/, 'measurable gap (eV):', /)"
65
66           form = edit("(x, ' [', I0, ']')")
67
68           do i = 1, x%bands
69              print form, re%Delta0(i), re%status(i)
70           end do
71        end if
72
73        if (x%resolution .gt. 0) then
```

```
74          print "(/, 'real-axis solution:', /)"
75
76          if (x%chi) then
77             print head, 'omega/eV', 'Re[Z]', 'Im[Z]', &
78                'Re[Delta]/eV', 'Im[Delta]/eV', 'Re[chi]', 'Im[chi]'
79
80             do i = 1, x%bands
81                print rule(7)
82
83                do n = 1, x%resolution
84                   print body, re%omega(n), re%Z(n, i), &
85                      re%Delta(n, i), re%chi(n, i)
86                end do
87             end do
88          else
89             print head, &
90                'omega/eV', 'Re[Z]', 'Im[Z]', 'Re[Delta]/eV', 'Im[Delta]/eV'
91
92             do i = 1, x%bands
93                print rule(5)
94
95                do n = 1, x%resolution
96                   print body, re%omega(n), re%Z(n, i), re%Delta(n, i)
97                end do
98             end do
99          end if
100      end if
101   end subroutine tell
102end module io_tell
```

B.6 Programs

At this point all modules and their corresponding subroutines and functions have been presented. Yet to be discussed are the actual executable programs by which they are used, namely `ebmb`, `critical` and `tc`.

B.6.1 ebmb.f90

The workflow of `ebmb` is simple: load the parameters, call the desired self-energy solver, optionally continue the results to the real axis and output them via the desired channels.

```
1  program ebmb
2     use eliashberg_self_energy
3     use eliashberg_self_energy_cdos
4     use global
5     use io_load
6     use io_store
7     use io_tell
8     use real_axis
9     implicit none
10
11    type(parameters) :: x
12    type(matsubara) :: im
13    type(continued) :: re
14    type(occupancy) :: oc
15
16    call load(x)
17
```

```
18    if (x%chi) then
19       call self_energy(x, im, oc)
20    else
21       call self_energy_cdos(x, im)
22    end if
23
24    call realize(x, im, re)
25
26    if (x%file .ne. 'none') call store(x, im, re, oc)
27
28    if (x%tell) call tell(x, im, re, oc)
29 end program ebmb
```

Example of application

Below, the usage of `ebmb` on the command line is exemplified:

```
$ ebmb T=10 lambda=1 muStar=0.1 resolution=300
imaginary-axis solution [66]:

        omega/eV               Z        Delta/eV
-------------------------------------------------
  0.002707214062  1.967226661541  0.002590550215
  0.008121642186  1.927225217112  0.002403912680
  0.013536070311  1.861850034908  0.002090211042
   . . .           . . .           . . .
  0.284257476526  1.072524734721 -0.000838949545
  0.289671904651  1.064021558735 -0.000840387592
  0.295086332775  1.054374032052 -0.000841668334

constant Coulomb contribution (eV):

 -0.000868488361

real-axis solution:

        omega/eV           Re[Z]           Im[Z]    Re[Delta]/eV    Im[Delta]/eV
-------------------------------------------------------------------------------
  0.000000000000  1.972750967345  0.000000000000  0.002615530353  0.000000000000
  0.001003344482  1.973490139549  0.000055160511  0.002619009158 -0.000000029469
  0.002006688963  1.975724185412  0.000092322544  0.002629488374 -0.000000045184
   . . .           . . .           . . .           . . .           . . .
  0.297993311037  1.002267219390  0.105412692473 -0.000896723088 -0.000007474029
  0.298996655518  1.002244792387  0.105059048188 -0.000896528744 -0.000007407687
  0.300000000000  1.002222640329  0.104707774935 -0.000896336488 -0.000007342091
```

B.6.2 critical.f90

`critical` does not only call the appropriate Eliashberg eigenvalue solver but also performs individual tasks, namely the identification of the variable parameter and its optimization via the bisection method.

```
1  program critical
2     use eliashberg_eigenvalue
3     use eliashberg_eigenvalue_cdos
4     use global
5     use io_load
```

```
6     implicit none
7
8     type(parameters), target :: x
9
10    real(dp), pointer :: variable => null() ! parameter to be optimized
11
12    procedure(eigenvalue), pointer :: solver => null() ! solver to be used
13
14    real(dp) :: bound(2) ! bisection bounds
15
16    real(dp) :: status  ! greatest eigenvalue
17    real(dp) :: status0 ! ... in previous step
18
19    logical :: sc1 ! bound(1) within superconducting phase?
20    logical :: try ! still trying out direction?
21
22    integer :: i, j ! band indices
23
24    call load(x)
25
26    variable => x%T
27
28    if (x%T .lt. 0) then
29       variable => x%T
30       variable = -variable
31    end if
32
33    if (x%omegaE .lt. 0) then
34       variable => x%omegaE
35       variable = -variable
36    end if
37
38    do i = 1, x%bands
39       do j = 1, x%bands
40          if (x%lambda(j, i) .lt. 0) then
41             variable => x%lambda(j, i)
42             variable = -variable
43          end if
44
45          if (x%muStar(j, i) .lt. 0) then
46             variable => x%muStar(j, i)
47             variable = -variable
48          end if
49       end do
50    end do
51
52    if (x%chi) then
53       solver => eigenvalue
54    else
55       solver => eigenvalue_cdos
56    end if
57
58    call solver(status, x)
59
60    status0 = status
61
62    sc1 = status .ge. 1
63    try = .true.
64
65    do
66       bound(1) = variable
```

```
67          variable = variable * (1 + x%rate)
68
69          call solver(status, x)
70
71          if (status .eq. status0) stop 'stationary point'
72
73          if (sc1 .neqv. status .ge. 1) exit
74
75          if (sc1 .eqv. status .gt. status0) then
76             if (try) then
77                variable = bound(1)
78                x%rate = -x%rate
79                try = .false.
80                cycle
81             end if
82
83             stop 'local extremum'
84          end if
85
86          status0 = status
87       end do
88
89       bound(2) = variable
90
91       do
92          variable = sum(bound) / 2
93
94          if (abs(variable - bound(1)) .le. x%error) exit
95
96          call solver(status, x)
97
98          if (sc1 .eqv. status .ge. 1) then
99             bound(1) = variable
100         else
101            bound(2) = variable
102         end if
103      end do
104
105      if (x%tell) print '(' // trim(x%form) // ')', variable
106
107      if (x%file .ne. 'none') then
108         open (unit, &
109            file=x%file, action='write', status='replace', access='stream')
110         write (unit) variable
111         close (unit)
112      end if
113   end program critical
```

Examples of application

By default, the critical temperature is determined:

```
$ critical lambda=2,0.1,0.1,1
47.261724151225
```

In a second step one could determine an effective scalar coupling constant:

```
$ critical T=47.261724151225 lambda=-1
1.897134874960
```

B.6.3 tc.f90

Finally, a program is presented which determines the critical temperatures for all bands separately via the bisection method. Since this requires the calculation of the full self-energy at each step of the iteration, the use of `critical` should be preferred, if possible.

```
program tc
   use eliashberg_self_energy
   use eliashberg_self_energy_cdos
   use formatting
   use global
   use io_load
   implicit none

   type(parameters) :: x
   type(matsubara) :: im
   type(occupancy) :: oc

   integer :: i, j ! band indices

   real(dp), allocatable :: upper(:), lower(:), T(:) ! bounds and Tc's

   character(:), allocatable :: head, body ! edit descriptors

   call load(x)

   if (x%tell) then
      call measure(x%form)

      head = edit('(Aw)')
      body = edit('(x)')

      print head, 'T/K'
      print rule(1)
   end if

   allocate(T(x%bands))

   allocate(upper(x%bands))
   allocate(lower(x%bands))

   lower(:) = -1
   upper(:) = -1

   call bounds

   BANDS: do i = 1, x%bands
      x%T = upper(i)

      do while (lower(i) .lt. 0)
         if (x%T .le. x%error) then
            T(i) = 0
            cycle BANDS
         end if

         x%T = x%T * (1 - x%rate)
         call bounds
      end do

      x%T = lower(i)

```

```
56          do while (upper(i) .lt. 0)
57             x%T = x%T * (1 + x%rate)
58             call bounds
59          end do
60
61          do
62             x%T = (lower(i) + upper(i)) / 2
63
64             if (upper(i) - lower(i) .le. 2 * x%error) then
65                T(i) = x%T
66                cycle BANDS
67             end if
68
69             call bounds
70          end do
71       end do BANDS
72
73       if (x%tell) then
74          print *
75          print head, 'Tc/K'
76          print rule(1)
77          print body, T
78       end if
79
80       if (x%file .ne. 'none') then
81          open (unit, &
82             file=x%file, action='write', status='replace', access='stream')
83          write (unit) T
84          close (unit)
85       end if
86
87    contains
88
89       subroutine bounds
90          if (x%tell) print body, x%T
91
92          if (x%chi) then
93             call self_energy(x, im, oc)
94          else
95             call self_energy_cDOS(x, im)
96          end if
97
98          do j = 1, x%bands
99             if (abs(im%Delta(0, j)) .le. x%zero) then
100               if (upper(j) .gt. x%T .or. upper(j) .lt. 0) upper(j) = x%T
101            else
102               if (lower(j) .lt. x%T .or. lower(j) .lt. 0) lower(j) = x%T
103            end if
104         end do
105      end subroutine bounds
106   end program tc
```

B.7 User manual

On the following pages, the user manual for the software package is displayed.

ebmb

Solve multiband Eliashberg equations

Outline

This software provides three programs:

1. ebmb itself solves the multiband Eliashberg equations (Eqs. 1 or 2) on a cut-off imaginary axis and optionally continues the results to the real axis via Padé approximants.

   A material is defined by nothing but an Einstein phonon frequency, intra- and interband electron-phonon couplings and Coulomb pseudo-potentials and, if desired, the band densities of Bloch states, otherwise assumed to be constant.

2. `tc` finds the critical temperature for each band separately via the bisection method. Superconductivity is defined by the order parameter exceeding a certain threshold.

3. `critical` finds the critical point via the bisection method varying a parameter of choice. Superconductivity is defined by the kernel of the linearized gap equation (Eq. 3) having an eigenvalue greater than or equal to unity. The shape of the density of states cannot be taken into account.

Installation

The makefile is designed for the *GNU* or *Intel* Fortran compiler and may be run in optimization or validation mode:

```
$ make compiler=gfortran mode=optimize   (default)
          ...   ifort   ...   validate
```

I/O

- Parameters are defined on the command line:

  $ ⟨program⟩ ⟨key 1⟩=⟨value 1⟩ ⟨key 2⟩=⟨value 2⟩ ...

  The available keys and default values are listed in Table 1.

- Unless `tell=false`, the results are printed to standard output.

- Unless `file=none`, a binary output file is created. For `critical` and `tc` it simply contains one or more double precision floating point numbers, for ebmb the format defined in Tables 2 and 3 is used.

- The provided *Python* wrapper functions load the results into *NumPy* arrays:

  ```
  import ebmb
  results = ebmb.get(⟨program⟩, ⟨file⟩, ⟨replace⟩,
      ⟨key 1⟩=⟨value 1⟩, ⟨key 2⟩=⟨value 2⟩, ...)
  ```

  ⟨replace⟩ decides whether an existing ⟨file⟩ is used or overwritten.

  Given a band structure, its discretized domain and $n - 1$ filters, an input file with the density of states resolved for n subdomains is generated like this:

  ```
  from numpy import cos, dot, linspace, pi
  DOSfile('dos.in', epsilon=lambda *k: -cos(k).sum() / 2,
      domain=[linspace(-pi, pi, 1000, endpoint=False)] * 2,
      filters=[lambda *k: pi ** 2 / 2 <= dot(k, k) <= pi ** 2])
  ```

Eliashberg theory

Let $\hbar = k_B = 1$. Fermionic and bosonic Matsubara frequencies are defined as $\omega_n = (2n+1)\pi T$ and $\nu_n = 2n\pi T$, respectively. The quantity of interest is the Nambu self-energy matrix[1]

$$\boldsymbol{\Sigma}_i(n) = \mathrm{i}\omega_n[1 - Z_i(n)]\mathbf{1} + \underbrace{Z_i(n)\,\Delta_i(n)}_{\phi_i(n)}\boldsymbol{\sigma}_1 + \chi_i(n)\boldsymbol{\sigma}_3,$$

where the Pauli matrices are defined as usual and i is a band index. Renormalization $Z_i(n)$, order parameter $\phi_i(n)$ and energy shift $\chi_i(n)$ are determined by the Eliashberg equations[2]

$$\begin{aligned}
Z_i(n) &= 1 + \frac{T}{\omega_n}\sum_j\sum_{m=0}^{N-1}\int_{-\infty}^{\infty}\mathrm{d}\varepsilon\frac{n_j(\varepsilon)}{n_j(\mu_0)}\frac{\omega_m Z_j(m)}{\Theta_j(\varepsilon,m)}\Lambda_{ij}^{-}(n,m),\\
\phi_i(n) &= T\sum_j\sum_{m=0}^{N-1}\int_{-\infty}^{\infty}\mathrm{d}\varepsilon\frac{n_j(\varepsilon)}{n_j(\mu_0)}\frac{\phi_j(m)}{\Theta_j(\varepsilon,m)}[\Lambda_{ij}^{+}(n,m) - U_{ij}^{*}(m)],\\
\chi_i(n) &= -T\sum_j\sum_{m=0}^{N-1}\int_{-\infty}^{\infty}\mathrm{d}\varepsilon\frac{n_j(\varepsilon)}{n_j(\mu_0)}\frac{\varepsilon-\mu+\chi_j(m)}{\Theta_j(\varepsilon,m)}\Lambda_{ij}^{+}(n,m),\\
\Theta_i(\varepsilon,n) &= [\omega_n Z_i(n)]^2 + \phi_i^2(n) + [\varepsilon - \mu + \chi_i(n)]^2,
\end{aligned} \tag{1}$$

and may then be analytically continued to the real-axis by means of Padé approximants.[3] The electron-phonon coupling matrices and the rescaled Coulomb pseudo-potential are connected to the corresponding input parameters via

$$\Lambda_{ij}^{\pm}(n,m) = \lambda_{ij}(n-m) \pm \lambda_{ij}(n+m+1), \qquad \lambda_{ij}(n) = \frac{\lambda_{ij}}{1+\left[\frac{\nu_n}{\omega_E}\right]^2},$$

$$U_{ij}^{*}(m) = \begin{cases} 2\mu_{ij}^{*}(N_C) & \text{for } m < N_C,\\ 0 & \text{otherwise,}\end{cases} \qquad \frac{1}{\mu_{ij}^{*}(N_C)} = \frac{1}{\mu_{ij}^{*}} + \ln\frac{\omega_E}{\omega_{N_C}},$$

or, if the band density $n_i(\varepsilon)$ of Bloch states with energy ε per spin, band and unit cell is given,

$$\frac{1}{\mu_{ij}^{*}(N_C)} = \frac{1}{\mu_{ij}^{*}} + \ln\frac{2\omega_E}{D} + \frac{1}{\pi}\sum_i\int_{-\infty}^{\infty}\mathrm{d}\varepsilon\frac{n_i(\varepsilon)}{n_i(\mu_0)}\begin{cases}\frac{1}{\varepsilon-\mu_0}\arctan\frac{\varepsilon-\mu_0}{\omega_{N_C}} & \text{for } \varepsilon \neq \mu_0,\\ \frac{1}{\omega_{N_C}} & \text{otherwise,}\end{cases}$$

where D is the electronic bandwidth. μ_0 and μ are the chemical potentials for free and interacting particles, respectively. The latter ensures that the particle number is conserved:

$$2\sum_i\int_{-\infty}^{\infty}\mathrm{d}\varepsilon\frac{n_i(\varepsilon)}{\mathrm{e}^{(\varepsilon-\mu_0)/T}+1} = n_0 \overset{!}{=} n \approx 1 - 4T\sum_i\int_{-\infty}^{\infty}\mathrm{d}\varepsilon\, n_i(\varepsilon)\left[\sum_{n=0}^{N-1}\frac{\varepsilon-\mu+\chi_i(n)}{\Theta_i(\varepsilon,n)} + \frac{\arctan\frac{\varepsilon-\mu}{\omega_N}}{2\pi T}\right].$$

Approximating $n_i(\varepsilon) \approx n_i(\mu_0)$ yields $\chi_i(n) = 0$ and the constant-DOS Eliashberg equations

$$\begin{aligned}
Z_i(n) &= 1 + \frac{\pi T}{\omega_n}\sum_j\sum_{m=0}^{N-1}\frac{\omega_m}{\sqrt{\omega_m^2+\Delta_j^2(m)}}\Lambda_{ij}^{-}(n,m),\\
\Delta_i(n) &= \frac{\pi T}{Z(n)}\sum_j\sum_{m=0}^{N-1}\frac{\Delta_j(m)}{\sqrt{\omega_m^2+\Delta_j^2(m)}}[\Lambda_{ij}^{+}(n,m) - U_{ij}^{*}(m)].
\end{aligned} \tag{2}$$

[1] Y. Nambu, Phys. Rev. **117**, 648 (1960)

[2] G. M. Eliashberg, Soviet Phys. JETP **11**, 696 (1960).
A comprehensive review is given by P. B. Allen and B. Mitrović in Solid state physics **37** (1982)

[3] H. J. Vidberg and J. W. Serene, J. Low Temp. Phys. **29**, 179 (1977)

At the critical temperature, $\Delta_i(m)$ is infinitesimal and negligible relative to ω_m. This yields

$$\begin{aligned}\Delta_i(n) &= \sum_j \sum_{m=0}^{N-1} K_{ij}(n,m)\,\Delta_j(m),\\ K_{ij}(n,m) &= \frac{1}{2m+1}[\Lambda^+_{ij}(n,m) - \delta_{ij}\delta_{nm} D_i^N(n) - U^*_{ij}(m)],\\ D_i^N(n) &= \sum_j \sum_{m=0}^{N-1} \Lambda^-_{ij}(n,m) \overset{N=\infty}{=} \sum_j \Big[\lambda_{ij} + 2\sum_{m=1}^{n} \lambda_{ij}(m)\Big].\end{aligned} \tag{3}$$

$Z_i(n)$ is not biased by the cutoff if $D_i^\infty(n)$ is used in place of $D_i^N(n)$ in the kernel $K_{ij}(n,m)$.

—— Acknowledgment ——

Parts of the program are inspired by the EPW code[4] and work of Malte Rösner.

—— Contact ——

Any feedback may be directed to jan.berges@uni-bremen.de.

[4] F. Giustino, M. L. Cohen and S. G. Louie, Phys. Rev. B **76**, 165108 (2007) for a methodology review.
Results related to Eliashberg theory are given by E. R. Margine and F. Giustino, Phys. Rev. B **87**, 024505 (2013)

key	default	unit	symbol	description	ebmb	tc	critical	variable
file	none	–	–	output file	+	+	+	−
form	F16.12	–	–	number edit descriptor	+	+	+	−
tell	true	–	–	use standard output?	+	+	+	−
T	10	K	T	temperature	+	+	+	+
omegaE	0.02	eV	ω_E	EINSTEIN frequency	+	+	+	+
cutoff	15	ω_E	ω_N	overall cutoff frequency	+	+	+	−
cutoffC	ω_N	ω_E	ω_{N_C}	COULOMB cutoff frequency	+	+	+	−
lambda	**1**	1	λ_{ij}	electron-phonon coupling	+	+	+	+
muStar	**0**	1	μ^*_{ij}	COULOMB pseudo-potential	+	+	+	+
dos	none	–	–	file with density of states	+	+	+	−
n	–	1	n_0	initial occupancy number	+	+	+	−
mu	0	eV	μ_0	initial chemical potential	+	+	+	−
conserve	true	–	–	conserve particle number?	+	+	+	−
limit	250000	1	–	maximum number of iterations	+	+	+	−
epsilon	10^{-15}	a.u.	–	negligible float difference	+	+	+	−
error	10^{-5}	a.u.	–	bisection error	−	+	+	−
zero	10^{-10}	eV	–	negligible gap at T_c (threshold)	−	+	−	−
rate	10^{-1}	1	–	growth rate for bound search	−	+	+	−
clip	15	ω_E	–	maximum real-axis frequency	+	−	−	−
resolution	0	1	–	resolution of real-axis solution	+	−	−	−
measurable	false	–	–	find measurable gap?	+	−	−	−
imitate	false	–	–	use $Z_i(n)$ biased by cutoff?	−	−	+	−
rescale	true	–	–	use μ^*_{ij} rescaled for cutoff?	+	+	+	−
normal	false	–	–	enforce normal state?	+	−	−	−
power	true	–	–	power method for single band?	−	−	+	−

Table 1: Input parameters.

- The columns ebmb, tc and critical show which keys are used by these programs.
- The rightmost column indicates which parameters may be chosen as variable for critical. The variable is marked with a negative sign; its absolute value is used as initial guess. If no parameter is negative, the critical temperature is searched for.
- lambda and muStar expect flattened square matrices of equal size the elements of which are separated by commas. It is impossible to vary more than one element at once.
- dos has lines ε/eV n_1/a.u. n_2/a.u. ... with ε ascending but not necessarily equidistant.

⟨CHARACTERS key⟩:⟨$n_1 \times \ldots \times n_r$ NUMBERS value⟩
associate key with value

DIM:⟨INTEGER r⟩⟨r INTEGERS $n_1 \ldots n_r$⟩
define shape (column-major)

INT: take NUMBERS as INTEGERS

REAL: take NUMBERS as DOUBLES

Table 2: Statements allowed in binary output. The data types CHARACTER, INTEGER and DOUBLE take 1, 4 and 8 bytes of storage, respectively.

imaginary-axis results		
`iomega`	MATSUBARA frequency (without i)	ω_n
`Delta`	gap	$\Delta_i(n)$
`Z`	renormalization	$Z_i(n)$
`chi`	energy shift	$\chi_i(n)$
`phiC`	constant COULOMB contribution	ϕ_{C_i}
`status`	status (steps till convergence or -1)	–
occupancy results		
`n0`	initial occupancy number	n_0
`n`	final occupancy number	n
`mu0`	initial chemical potential	μ_0
`mu`	final chemical potential	μ
real-axis results		`resolution` > 0
`omega`	frequency	ω
`Re[Delta]`	real gap	$\Delta_i(\omega)$
`Im[Delta]`	imaginary gap	$\Delta_i(\omega)$
`Re[Z]`	real renormalization	$Z_i(\omega)$
`Im[Z]`	imaginary renormalization	$Z_i(\omega)$
`Re[chi]`	real energy shift	$\chi_i(\omega)$
`Im[chi]`	imaginary energy shift	$\chi_i(\omega)$
measurable results		`measurable=true`
`Delta0`	measurable gap	$\Delta_{0i} = \mathrm{Re}[\Delta_i(\Delta_{0i})]$
`status0`	status of measurable gap	–

Table 3: Keys used in binary output.

Acknowledgment

I would like to thank Professor Tim Wehling for the opportunity to write my master's thesis in this interesting field of physics, Professor Gerd Czycholl for offering a second opinion, Malte Rösner, Gunnar Schönhoff, Malte Schüler, Roelof Groenewald and the whole working group for instructive discussions, Miriam Nüß for the final proofreading, especially my parents Brigitte Berges and Ulrich Seevers for continuously supporting my studies and finally all developers of public software and information.

Declarations

Authorship

I hereby declare that I have written the present thesis on my own and that none but the referenced sources and aids were used. All passages that I have taken, literally or not, from other works are identified as such and their respective origins specified.

> ***Urheberrechtliche Erklärung:*** *Hiermit versichere ich gemäß § 10 (11) der allgemeinen MPO vom 27. Oktober 2010, dass ich die vorliegende Arbeit selbstständig verfasst und keine als die angegebenen Quellen und Hilfsmittel verwendet habe. Alle Stellen, die ich wörtlich oder sinngemäß aus anderen Werken entnommen habe, habe ich unter Angabe der Quellen als solche kenntlich gemacht.*

Bremen, October 10, 2016

Jan Berges

Publication

I approve that my thesis may be consulted for research purposes in the university archives.

> ***Erklärung zur Veröffentlichung von Abschlussarbeiten:*** *Ich bin damit einverstanden, dass meine Abschlussarbeit im Universitätsarchiv für wissenschaftliche Zwecke von Dritten eingesehen werden darf.*

Bremen, October 10, 2016

Jan Berges

List of Figures

Bibliography

[1] W. L. McMillan: "Transition temperature of strong-coupled superconductors". In: *Phys. Rev.* **167** (1968), pp. 331–344. DOI: 10.1103/PhysRev.167.331.

[2] P. B. Allen and R. C. Dynes: "Transition temperature of strong-coupled superconductors reanalyzed". In: *Phys. Rev. B* **12** (1975), pp. 905–922. DOI: 10.1103/PhysRevB.12.905.

[3] W. L. McMillan and J. M. Rowell: "Tunneling and strong-coupling superconductivity". InRef.: 58, pp. 561–613.

[4] G. M. Eliashberg: "Interactions between electrons and lattice vibrations in a superconductor". In: *Sov. Phys. JETP* **11** (1960), pp. 696–702.

[5] Y. Nakagawa and A. D. B. Woods: "Lattice dynamics of niobium". In: *Phys. Rev. Lett.* **11** (1963), pp. 271–274. DOI: 10.1103/PhysRevLett.11.271.

[6] H. J. Vidberg and J. W. Serene: "Solving the Eliashberg equations by means of *N*-point Padé approximants". In: *J. Low Temp. Phys.* **29** (1977), pp. 179–192. DOI: 10.1007/BF00655090.

[7] J. Bardeen, L. N. Cooper, and J. R. Schrieffer: "Microscopic theory of superconductivity". In: *Phys. Rev.* **106** (1957), pp. 162–164. DOI: 10.1103/PhysRev.106.162.

[8] J. Bardeen, L. N. Cooper, and J. R. Schrieffer: "Theory of superconductivity". In: *Phys. Rev.* **108** (1957), pp. 1175–1204. DOI: 10.1103/PhysRev.108.1175.

[9] H. Fröhlich: "History of the theory of superconductivity". InRef.: 59, chap. 1, pp. 1–11.

[10] G. Czycholl: *Theoretische Festkörperphysik. Von den klassischen Modellen zu modernen Forschungsthemen*. 3rd ed. (revised). Berlin, Heidelberg: Springer, 2008. DOI: 10.1007/978-3-540-74790-1.

[11] D. van Delft and P. Kes: "The discovery of superconductivity". In: *Phys. Today* **63** (2010), pp. 38–43. DOI: 10.1063/1.3490499.

[12] H. Kamerlingh Onnes: "Further experiments with liquid helium. D. On the change of electrical resistance of pure metals at very low temperatures, etc. V. The disappearance of the resistance of mercury". In: *Proceedings, Koninklijke Akademie van Wetenschappen* **14** (1911), pp. 113–115.

[13] W. Meissner and R. Ochsenfeld: "Ein neuer Effekt bei Eintritt der Supraleitfähigkeit". In: *Naturwissenschaften* **21** (1933), pp. 787–788. DOI: 10.1007/BF01504252.

[14] F. London and H. London: "The electromagnetic equations of the supraconductor". In: *Proc. R. Soc. A* **149** (1935), pp. 71–88. DOI: 10.1098/rspa.1935.0048.

[15] V. L. Ginzburg and L. D. Landau: "On the theory of superconductivity". In: *Zh. Eksp. Teor. Fiz.* **20** (1950), pp. 1064–1082. DOI: 10.1007/978-3-540-68008-6_4.

[16] E. Maxwell: "Isotope effect in the superconductivity of mercury". In: *Phys. Rev.* **78** (1950), pp. 477–477. DOI: 10.1103/PhysRev.78.477.

[17] C. A. Reynolds et al.: "Superconductivity of isotopes of mercury". In: *Phys. Rev.* **78** (1950), pp. 487–487. DOI: 10.1103/PhysRev.78.487.

[18] H. Fröhlich: "Interaction of electrons with lattice vibrations". In: *Proc. R. Soc. A* **215** (1952), pp. 291–298. DOI: 10.1098/rspa.1952.0212.

[19] W. Nolting: *Grundkurs Theoretische Physik 7. Viel-Teilchen-Theorie*. Berlin, Heidelberg: Springer, 2015. doi: 10.1007/978-3-642-25808-4.

[20] N. N. Bogoliubov: "A new method in the theory of superconductivity. I". In: *Sov. Phys. JETP* **7** (1958), pp. 41–46.

[21] F. J. Dyson: "The radiation theories of Tomonaga, Schwinger, and Feynman". In: *Phys. Rev.* **75** (1949), pp. 486–502. doi: 10.1103/PhysRev.75.486.

[22] T. Matsubara: "A new approach to quantum-statistical mechanics". In: *Progr. Theoret. Phys.* **14** (1955), pp. 351–378. doi: 10.1143/PTP.14.351.

[23] G. D. Mahan: *Many-particle physics*. 3rd ed. New York: Kluwer Academic/Plenum Publishers, 2000.

[24] P. A. M. Dirac: *The principles of quantum mechanics*. 4th ed. (revised). The International Series of Monographs on Physics 27. Oxford: Clarendon Press, 1958.

[25] F. J. Dyson: "The *S* matrix in quantum electrodynamics". In: *Phys. Rev.* **75** (1949), pp. 1736–1755. doi: 10.1103/PhysRev.75.1736.

[26] G.-C. Wick: "The evaluation of the collision matrix". In: *Phys. Rev.* **80** (1950), pp. 268–272. doi: 10.1103/PhysRev.80.268.

[27] D. J. Thouless: "Use of field theory techniques in quantum statistical mechanics". In: *Phys. Rev.* **107** (1957), pp. 1162–1163. doi: 10.1103/PhysRev.107.1162.

[28] M. Gaudin: "Une démonstration simplifiée du théorème de Wick en mécanique statistique". In: *Nucl. Phys.* **15** (1960), pp. 89–91. doi: 10.1016/0029-5582(60)90285-6.

[29] L. P. Gor'kov: "On the energy spectrum of superconductors". In: *Sov. Phys. JETP* **7** (1958), pp. 505–508.

[30] W. von der Linden, E. Berger, and P. Valášek: "The Hubbard-Holstein model". In: *J. Low Temp. Phys.* **99** (1995), pp. 517–525. doi: 10.1007/BF00752333.

[31] L. Hedin: "New method for calculating the one-particle Green's function with application to the electron-gas problem". In: *Phys. Rev.* **139** (1965), pp. A796–A823. doi: 10.1103/PhysRev.139.A796.

[32] L. Hedin and S. Lundqvist: "Effects of electron-electron and electron-phonon interactions on the one-electron states of solids". InRef.: 60, pp. 1–181. doi: 10.1016/S0081-1947(08)60615-3.

[33] Y. Nambu: "Quasi-particles and gauge invariance in the theory of superconductivity". In: *Phys. Rev.* **117** (1960), pp. 648–663. doi: 10.1103/PhysRev.117.648.

[34] P. B. Allen and B. Mitrović: "Theory of superconducting T_c". InRef.: 61, pp. 1–92. doi: 10.1016/S0081-1947(08)60665-7.

[35] S. Galasso: "Generalization of the Eliashberg equations and density functional theory applied to the analysis of the fundamental properties of iron-based superconductors". PhD thesis. Politecnico di Torino, 2015. doi: 10.6092/polito/porto/2596360.

[36] E. R. Margine and F. Giustino: "Anisotropic Migdal-Eliashberg theory using Wannier functions". In: *Phys. Rev. B* **87** (2013), p. 024505. doi: 10.1103/PhysRevB.87.024505.

[37] A. B. Migdal: "Interaction between electrons and lattice vibrations in a normal metal". In: *Sov. Phys. JETP* **7** (1958), pp. 996–1001.

[38] P. B. Allen: "Fermi-surface harmonics: A general method for nonspherical problems. Application to Boltzmann and Eliashberg equations". In: *Phys. Rev. B* **13** (1976), pp. 1416–1427. doi: 10.1103/PhysRevB.13.1416.

[39] D. J. Scalapino, J. R. Schrieffer, and J. W. Wilkins: "Strong-coupling superconductivity. I". In: *Phys. Rev.* **148** (1966), pp. 263–279. doi: 10.1103/PhysRev.148.263.

[40] V. Ambegaokar and L. Tewordt: "Theory of the electronic thermal conductivity of superconductors with strong electron-phonon coupling". In: *Phys. Rev.* **134** (1964), A805–A815. doi: 10.1103/PhysRev.134.A805.

[41] D. J. Scalapino, Y. Wada, and J. C. Swihart: "Strong-coupling superconductor at nonzero temperature". In: *Phys. Rev. Lett.* **14** (1965), pp. 102–105. doi: 10.1103/PhysRevLett.14.102.

[42] R. C. Dynes: "McMillan's equation and the T_c of superconductors". In: *Solid State Commun.* **10** (1972), pp. 615–618. doi: 10.1016/0038-1098(72)90603-5.

[43] J. R. Schrieffer: *Theory of superconductivity*. Revised printing. Advanced Book Program. Westview Press, 1983.

[44] N. N. Bogoliubov, V. V. Tolmachev, and D. V. Shirkov: *A new method in the theory of superconductivity*. New York: Consultants Bureau, 1959.

[45] P. Morel and P. W. Anderson: "Calculation of the superconducting state parameters with retarded electron-phonon interaction". In: *Phys. Rev.* **125** (1962), pp. 1263–1271. doi: 10.1103/PhysRev.125.1263.

[46] S. Schafroth, J. J. Rodríguez-Núñez, and H. Beck: "Some global properties of the attractive Hubbard model in the superconducting phase: the T-matrix approximation in two dimensions". In: *J. Phys. Condens. Matter* **9** (1997), L111—L118. doi: 10.1088/issn.0953-8984.

[47] E. J. Nicol and J. P. Carbotte: "Properties of the superconducting state in a two-band model". In: *Phys. Rev. B* **71** (2005), p. 054501. doi: 10.1103/PhysRevB.71.054501.

[48] P. Entel and M. Peter: "On the influence of Fermi surface anisotropy on H_{c2} of weak and strong coupling superconductors". In: *J. Low Temp. Phys.* **22** (1976), pp. 613–621. doi: 10.1007/BF00659063.

[49] P. Entel: "Anisotropy effects in superconductors with magnetic impurities. I". In: *Z. Phys. B* **23** (1976), pp. 321–330. doi: 10.1007/BF01316542.

[50] W. B. Jones and W. J. Thron: "Numerical stability in evaluating continued fractions". In: *Math. Comp.* **28** (1974), pp. 795–810. doi: 10.1090/S0025-5718-1974-0373265-5.

[51] R. Szczęśniak: "The selected thermodynamic properties of the strong-coupled superconductors in the van Hove scenario". In: *Solid State Commun.* **138** (2006), pp. 347–352. doi: 10.1016/j.ssc.2006.03.012.

[52] R. Szczęśniak: "The numerical solution of the imaginary-axis Eliashberg equations". In: *A. Phys. Pol. A* **109** (2006), pp. 179–186. doi: 10.12693/APhysPolA.109.179.

[53] J. P. Carbotte: "Properties of boson-exchange superconductors". In: *Rev. Mod. Phys.* **62** (1990), pp. 1027–1157. doi: 10.1103/RevModPhys.62.1027.

[54] W. E. Pickett and B. Klein: "Influence of electronic structure on superconducting properties of complex crystals: Theory and application to Nb_3Sn". In: *Solid State Commun.* **38** (1981), pp. 95–98. doi: 10.1016/0038-1098(81)90797-3.

[55] H. Suhl, B. T. Matthias, and L. R. Walker: "Bardeen-Cooper-Schrieffer theory of superconductivity in the case of overlapping bands". In: *Phys. Rev. Lett.* **3** (1959), pp. 552–554. doi: 10.1103/PhysRevLett.3.552.

[56] E. Anderson et al.: *LAPACK users' guide*. 3rd ed. Philadelphia, PA: Society for Industrial and Applied Mathematics, 1999.

[57] H. Wolkowicz and G. P. H. Styan: "Bounds for eigenvalues using traces". In: *Linear Algebra Appl.* **29** (1980), pp. 471–506. doi: 10.1016/0024-3795(80)90258-X.

[58] R. D. Parks, ed.: *Superconductivity*. Vol. 1. New York: Marcel Dekker, 1969.

[59] B. Deaver and J. Ruvalds, eds.: *Advances in superconductivity*. NATO Advanced Science Institute Series 100. New York: Plenum Press, 1982.

[60] F. Seitz, D. Turnbull, and H. Ehrenreich, eds.: *Solid state physics. Advances in research and applications*. Vol. 23. New York, London: Academic Press, 1969.

[61] H. Ehrenreich, F. Seitz, and D. Turnbull, eds.: *Solid state physics. Advances in research and applications*. Vol. 37. New York, London: Academic Press, 1982.